

Bangor University

DOCTOR OF PHILOSOPHY

Intramolecular hydrogen bonding in polyhydroxynaphthoquinone dyes

Maskery, James Samuel

Award date:
2014

Awarding institution:
Bangor University

[Link to publication](#)

General rights

Copyright and moral rights for the publications made accessible in the public portal are retained by the authors and/or other copyright owners and it is a condition of accessing publications that users recognise and abide by the legal requirements associated with these rights.

- Users may download and print one copy of any publication from the public portal for the purpose of private study or research.
- You may not further distribute the material or use it for any profit-making activity or commercial gain
- You may freely distribute the URL identifying the publication in the public portal ?

Take down policy

If you believe that this document breaches copyright please contact us providing details, and we will remove access to the work immediately and investigate your claim.

Download date: 07. Aug. 2024

Intramolecular hydrogen bonding in polyhydroxynaphthoquinone dyes

By James Samuel Maskery



Ysgol Cemeg
School of Chemistry
Rhagoriueth ers 1884 | Excellence since 1884



Acknowledgements

I would like to thank Dr R. A. Davies for his continued support, help and assistance as my supervisor over the past 4 years of the PhD, giving up his time to discuss and evaluate the methods of my study.

I would also like to thank CAST Ltd. for their funding in conjunction with the KESS scholarship scheme, for allowing me the opportunity to undertake this PhD.

My final thanks go to my family and housemates that have given me great encouragement and patience over the years.

Abstract

Intra- and inter-molecular hydrogen bonding greatly affects both physical and chemical properties for a wide variety of important molecules. This study focuses on intramolecular hydrogen bonding in polyhydroxy-1,4-naphthoquinones. The little known “bond counting rule”, dictates that the global minimum will be comprised of a maximum number of highly stabilizing interactions. Hydrogen bonding was chosen for this work as the energy of the bond is typically $20\text{--}40\text{ kJ mol}^{-1}$, which is larger than computational error, allowing statistically significant energy differences between conformers to be determined.

A series of interactions between neighbouring hydroxyl groups and each other, and between hydroxyl groups and neighbouring carbonyl groups were postulated. Quantification of the interaction energies was accomplished using a training set of several hundred unique isomers, allowing a quantitative bond counting rule to be developed. Harmonic vibrational spectroscopic and QTAIM analyses were performed for key interactions to aid in their characterisation as baseline, stabilising or destabilising. The effect of molecular conformation upon the wavelength and absorbance of electronic absorption spectra were also probed, highlighting the need to obtain low-energy conformations.

Potential energy hypersurface (PES) for single and pairs of C-O bond rotation(s) not only indicate the presence of stationary points corresponding to maxima, minima and transition structures, but also any rotational barriers and reaction pathways for rotamer interconversion. To aid PES visualization, a set of custom Python-based tools were designed and constructed allowing creation of both graphic and haptic Web3D virtual models for teaching purposes. Increased topological perception and object manipulation were obtained using 3-D rapid prototyped models.

Contents

Chapter 1	Introduction	
1.1	Topical overview	Page 2
1.2	Bond counting rules	Page 3
1.3	Naphthoquinones	Page 6
1.4	Crystallographic Review	Page 7
1.5	Hydrogen bonding	Page 12
1.6	QTAIM hydrogen bonding studies	Page 15
1.7	Hypotheses and Aims	Page 19
1.7.1	<i>Hypotheses</i>	Page 19
1.7.2	<i>Aims</i>	Page 19
1.7	Summary	Page 20
Chapter 2	Polyhydroxy-1,4-Naphthoquinone Intramolecular Hydrogen Bond Counting Rules	
2.1	Introduction	Page 23
2.1.1	<i>Quantum Chemistry</i>	Page 24
2.2	Training set development	Page 25
2.3	Prototype bond counting rules	Page 28
2.4	Comparison of bond counting rules	Page 41
2.5	Sieving	Page 42
2.6	Summary and future work	Page 44
2.6.1	<i>Consideration for an unknown molecule</i>	Page 44
Chapter 3	Polyhydroxy-1,4-naphthoquinone Vibrational Frequencies	
3.1	Introduction	Page 46
3.2	Methodology	Page 47
3.3	Results and discussion	Page 47
3.3.1	<i>Monosubstitution</i>	Page 47
3.3.2	<i>Dihydroxy (non-interacting)</i>	Page 48
3.3.3	<i>Dihydroxy (interacting)</i>	Page 49
3.4	Summary	Page 50

Chapter 4	Hydrogen Bonding QTAIM Analyses	
4.1	Introduction	Page 52
4.2	Methodology	Page 52
4.3	Terminology	Page 53
4.3.1	<i>Critical Points</i>	Page 53
4.3.2	<i>Bond paths</i>	Page 55
4.3.3	<i>Laplacian</i>	Page 55
4.3.4	<i>Electron density at the BCP</i>	Page 56
4.3.5	<i>Bond ellipticity</i>	Page 56
4.3.6	<i>Other QTAIM features</i>	Page 56
4.3.7	Calculation set-up	Page 57
4.4	Interactions	Page 57
4.5	R6 Interaction	Page 59
4.6	R5 Interaction	Page 60
4.7	C6 Interaction	Page 62
4.8	OH5 Interaction	Page 64
4.9	M4 and OO4 Interactions	Page 66
4.10	OO5 Interaction	Page 67
4.11	Summary	Page 68
Chapter 5	Potential energy surface (PES) visualization	
5.1	Introduction	Page 70
5.2	Design of parser	Page 72
5.2.1	<i>Data Manipulation</i>	Page 72
5.2.2	<i>Colour scaling</i>	Page 74
5.2.3	<i>Output types</i>	Page 74
5.2.3.1	CSV format	Page 75
5.2.3.2	VRML format	Page 76
5.2.3.3	X3D/H3D format	Page 78
5.3	Results and discussion	Page 80
5.3.1	<i>1-D Scans</i>	Page 80
5.3.2	<i>2-D non-interacting results</i>	Page 81
5.3.2.1	2,5- and 2,8-DHNQ	Page 81
5.3.2.2	2,6- and 2,7-DHNQ	Page 83

5.3.2.3	5,7-DHNQ	Page 85
5.3.2.4	5,8-DHNQ	Page 86
5.3.3	<i>2-D interacting results</i>	Page 88
5.3.3.1	2,3-DHNQ	Page 88
5.3.3.2	5,6-DHNQ	Page 90
5.3.3.3	6,7-DHNQ	Page 92
5.3	Summary and future developments	Page 94
Chapter 6	Effect of conformer upon electronic spectra	
6.1	Introduction	Page 97
6.2	Methodology	Page 98
6.3	Results and discussion	Page 99
6.3.1	<i>HF mono-substitution results</i>	Page 99
6.3.2	<i>B3LYP hexa-substituted results</i>	Page 100
6.3.3	<i>Comparison with experimental results</i>	Page 101
6.4	Conclusions	Page 102
Chapter 7 – Conclusions and future work		
7.1	Overview	Page 104
7.2	Underling conclusions	Page 107
7.3	Continuing development	Page 108
Bibliography		Page 110
Appendix I – Python parser		Page 122
Appendix II – PES paper submitted to PCCP journal		Page 134
Appendix III – Draft bond counting rule methodology paper		Page 148

Chapter

I

Chapter 1 - Introduction

1.1 Topical overview

Rules of thumb and empirical rules are used in everyday life to make judgments on activities and actions that are been undertaken. Murphy's Law,^[1] typically stated as "Anything that can go wrong, will go wrong", the five-second rule,^[2] states that food dropped on the ground will not be significantly contaminated with bacteria if it is picked up within five seconds of being dropped, or the two second rule, is a rule of thumb by which a driver may maintain a safe following distance at any speed.

These are examples of rules which are applied in broad ways that do not have to be strictly accurate nor reliable in all situations. These simple rules of thumb are easily taught and can be applied to a variety of situations easily for approximate calculations or for making a determination of some kind.

Most chemists are familiar with the use of simple, empirical rules to aid understanding and learning of complex phenomena. Electronic structure and bonding^[3] can be explained or predicted through the use of electron counting as well as classifying compounds.

There are many rules that rely on electron counting, here is a selection of some of them:

- Octet rule^[4,5] used with Lewis structures for main group elements
- *d*-electron count^[6] (transition metal valence electron configuration)
- Eighteen electron^[7,8] and Tolman's^[9] rules within transition metal chemistry
- Polyhedral skeletal electron pair theory for cluster compounds^[10-15]

Reactivity is often explained *via* empirical rules, *e.g.* (*anti*-)Markownikoff alkene addition,^[16,17] alkene formation *via* elimination^[18-20] or Woodward-Hoffmann rules for pericyclic reactions.^[21-26] Several models for symmetric induction have been developed.^[27-29]

Similarly, valence-shell electron-pair repulsion (VSEPR) theory^[30,31] or the 657^[42] method may be used to predict molecular geometries.^[32] The electronic structures and UV-VIS absorption wavelength maxima of conjugated organic molecules may be predicted using Hückel theory^[33-36] and Woodward-Fieser rules^[37,38] respectively.

1.2 The bond counting rule (BCR)

The term “bond counting rule” can vary significantly between different fields of chemistry. The main areas of use of “bond counting rules” are:

- Electron counting in bonds ^[39-42]
- Surface science diffusion rates ^[43-49]
- Hardness predictions for diamond ^[50]
- System configuration
 - BCN ternary systems ^[51-57]
 - Fullerenes ^[58]
 - Superlattices^[59]

Wang *et al.*^[41] created semiconducting optoelectronic materials which satisfied the two-electron-per-bond counting. Rhim *et al.*^[39,40] also used the two-electron-*per*-bond counting rule with his work on creating superconductors from superlattices.

Righi *et al.*^[43] reported that lattice site occupancies in homoepitaxial SiC growth was found to be compatible with simple bond counting rules. Similarly Lloyd-Williams *et al.*^[44] described graphene epitaxy on Ru(100) and Ir(111) surfaces using bond counting rules. Molecular dynamics simulations of rates of atom hopping to nearest-neighbour positions on flat Cu(100) was undertaken by Frantz *et al.*^[45] which obeyed a different set of simple bond counting rules. Spatial and temporal fluctuations of

step edges was found to obey a bond counting rule.^[46] Further nearest-neighbour work was undertaken by Camarda *et al.*^[47] who examined probability of the Monte Carlo event bond-counting rules. Deposition and the film morphology evolution during epitaxial growth of silicon carbide through the use of similar procedures was performed by Masia *et al.*^[48]. Maximisation of first nearest neighbour pairs of pure copper precipitates by Kulikov *et al.*^[49] can also be classed as work that is similar to a simple bond counting rule approach.

A generic (applicable to most sp^2 and sp^3 carbons) bond counting rule accounting for the roughness of diamond (001) was established by Yang *et al.*^[50], providing a qualitative account of the step energy order without the need for detailed calculations.

The most common form of the bond counting rule is, however, used in several major on BCN and BN systems have heavily been studied and reviewed as they contain the most comprehensive methods for counting bonding systems. The approaches used are both simple and predictive in finding out which structures are most stable. Whilst the method is simply based on common sense, it is still relatively unknown to the vast majority of chemists.

Table 1. Mean bond energy^[60,61] (kJ mol⁻¹) for single bonds observed in ternary BCN systems. C-X values (X= N, O, F, S, Cl) are minimal values as actual values vary widely according to the degree of B-X multiple bonds.

Bond	Bond Energy	Reference
B-N	500	60
C-B	365	60
C-C	347	61
B-B	310	60
C-N	286	61
N-N	158	61

These intramolecular counting methods are currently only used on formal bonding within a set structure. However overall these methods could provide the best counting rule to move forwards with as their main underlying principle is, that a molecule will seek to maximise any strongly stabilising terms whilst reducing the number of destabilising or weakly stabilising terms.

Fan *et al.*^[58] investigated stability and BN-substitution patterns of C₁₂B₆N₆ fullerenes that using bond counting rules in conjunction with density functional theory (DFT) calculations (B3LYP/6-31G*). Low energy configurations followed a continuity pattern for the substitutions of BN units in the fullerene cage. A simple bond counting rule with only the nearest-neighbour terms served as an effective guide to look for low energy configurations. Extension of the bond counting rule by including three-body terms (or greater) was found to be essential for a quantitative description. The methodology of used with in this work, such as conformational enumeration, has a similar flow/methodology that can be see within the Fan *et al.*^[58] paper. A quantitative BCR was employed to study relative energetics of B/N-containing fullerenes.^[58] A code is constructed for a molecular system describing the number and types of bonding present. An error of 20 kJ mol⁻¹ was determined for B/N-doped fullerenes using regression.

The work of Matar *et al.*^[51] on the use of structural geomimetism allows first principles design of new materials based upon binary C₃N₄ and C₁₁N₄ or ternary BC₂N systems, whilst looking at different mechanical properties. Other novel BCN materials^[53-57] can be generated using the bond counting rule, in which C-C and B-N bonds were generally accepted as the strongest whilst B-B and N-N bonds tended to be the weakest. Luo *et al.*^[56] erroneously state that C-B bonds are forbidden, whilst Kar *et al.*^[57] incorrectly states that both C-B and C-N bonds are disfavoured.

Table 1 shows that C-B bonds appear to more stable than C-C, whilst B-B and C-N bond can be seen to have similar energies. There is a difference of energy of *ca.* ~350 kJ mol⁻¹ between the B-N bonds and N-N bonds showing that the preference for B-N bonds and rejection of N-N bonds is justifiable. Monte Carlo simulations of solid solutions^[54] revealed a strong preference for neighbouring B-N and C-C atoms, which is consistent with the bond counting rules mentioned in other works.

The work on promising solar absorbing material, Si_3AlP , by Yang et al.^[59] demonstrates the transferability of bond counting rules, which were applied to a Si_3AlP superlattice, maximising the number of Si-Al and Si-P bonds whilst keeping Al-P and Si-Si bonds to a minimum. No Al-Al bonds or P-P bonds were observed in the Si_3AlP superlattice.

1.3 Naphthoquinone

One of the main approaches in this thesis is the development of a novel bond counting rule to investigate hydrogen bonding^[62] in 1,4-naphthoquinone. Quinones in general are usually found in plants, fungi and bacteria as well as in animals.^[63] Naphthoquinones are an important class of both natural and synthetic organic compounds.^[64,65] Although the 1,4- isomer is generally referred to as naphthoquinone, other isomers such as 1,2-,^[66] 1,5-, 2,3-, and 2,6-naphthoquinone can be formed.

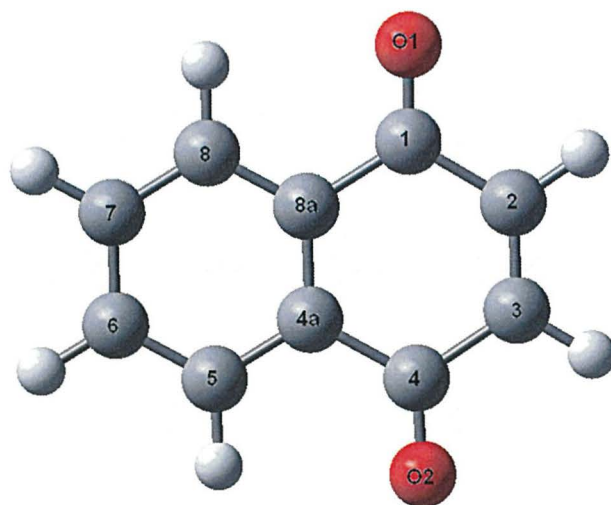


Figure 1. Numbering scheme for parent 1,4-naphthoquinone.

1,4-Naphthoquinone is a planar molecule with a single aromatic ring fused to a quinone subunit, nomenclature for positional changes can be seen in Figure 1. Each of the protons located on the naphthoquinone core can be substituted, e.g. with hydroxyl groups, leading to generation of a series of (poly)substituted naphthoquinones.^[67-69]

Naphthoquinones have uses as both dyes and pharmaceutically active compounds.^[63] One of the most common forms is lawsone^[69-71] / hennotannic acid (2-hydroxy-1,4-naphthoquinone), isolated from the leaves of the henna plant^[70], which has been used for hundreds of years to dye skin/hair as well as other natural and synthetic compounds.^[72] Another common naphthoquinone is juglone^[71,73,74] (5-hydroxy-1,4-naphthoquinone) which has been used as a dye^[63] and as a herbicide / pesticide.^[24] Other uses of these chemicals are as indicators for pH^[69] and acidity/basicity^[75].

Other more highly substituted hydroxy naphthoquinones are the spinochromes:

- B^[76,77] (2,3,5,7-tetrahydroxy-1,4-naphthoquinone)
- D^[77] (2,3,5,6,8-pentahydroxy-1,4-naphthoquinone)
- E^[63,78] (hexahydroxy-1,4-naphthoquinone)

All spinochromes occur naturally as pigments in the shell and spines of sea urchins in Japanese waters and form highly coloured crystalline solids.

1.4 Crystallographic Review

In order to develop general observations for conformer preferences based upon both intra- and intermolecular hydrogen bonding, which affects crystal packing, a review of available structure, stored within the Cambridge Structure Database (CSD) provided by the Chemical Database Service (CDS) was carried out.

As many of the structures were recorded before the development of modern X-ray crystallographic techniques such as Rietveld refinement, certain structures tabulated in Table 2, contain only unit cell parameters, whilst others do not have refined hydrogen atom positions (but contain coordinates for heavier main-group atoms).

Table 2. CSD survey of polyhydroxy-1,4-naphthoquinones containing no known hydrogen atom positions. ^a m = monoclinic, o = orthorhombic, a/t = anorthic/triclinic, N/A = no unit cell information. ^b N/A = no atomic coordinates for any atom.

CSD Code	Unit Cell ^a	Hydroxyl Arrangement ^b	Ref.	CSD Code	Unit Cell ^a	Hydroxyl Arrangement ^b	Ref.
AHMNAQ	a/t	N/A	79	DUMSEJ	N/A	N/A	89
BAKPUY	a/t	2	80	FAHNAE	a/t	2	90
CHNAPQ	m	3	81	FAHAE01	a/t	2	90
DEZXOW	m	2	82	HMNAPQ10	m	3	91
DHNAPH	m	5, 8	83	JUGLON	m	5	92
DHNAPH01	m	5, 8	84	MDXNAQ	a/t	5, 8	93
DHNAPH03	m	5, 8	85	NPOQUN	m	N/A	94
DHNAPH06	m	5, 8	86	PVVAQS	m	N/A	95
DHNAPH07	m	N/A	87	VAXQUH	m	4	96
DHNAPH08	m	N/A	87	ZZZEVW	a/t	N/A	97
DHNAPH09	m	N/A	88	ZZZRWA	o	N/A	97
DHNAPH10	m	N/A	88				

Whilst the above crystal structures help to state hydroxyl substitution positions on the 1,4-naphthoquinone core, it does not help to determine whether any of the molecules possess intra- or intrer-molecular hydrogen bonding to any degree. The above structures require a second crystallographic study using modern Rietveld refinement techniques to determine the position and orientation of the hydrogen atoms.

Relative orientations of known hydroxyl group positions within this work, are described relative to the nearest carbonyl group, with *Z* and *E* indicating *syn-* (*cis-*) or *anti-* (*trans-*) periplanar conformations respectively.

Surveyed 1,4-naphthoquinones were mostly planar with slight deviations from planarity (Tables 3, 4 and 5). Approximately 71% of the structures exhibit 5- (or equivalent 8-) substitution, exclusively forming strong 6-membered intramolecular hydrogen bonds (Tables 4 and 5). 5-membered hydrogen bonds seem to be weaker as only 40% substitute on the 2- (or equivalent 3-) positions (Tables 3 and 5). Only 11% of the structures substitute on the 6- (or equivalent 7-) positions, which are incapable of intramolecular hydrogen bonding. Intermolecular hydrogen bonds may, however, form between any position and another on a neighbouring molecule.

Table 3. CSD survey of polyhydroxy-1,4-naphthoquinones with possible 5-membered hydrogen bonds: ^a m = monoclinic, o = orthorhombic, a/t = anorthic/triclinic, ^b position and orientation relative to nearest carbonyl group, ^c Hydroxyl group, ^d hydrogen bond, ^e relative to nearest carbonyl group, ^g structure stated as 1,4-naphthoquinone, but displayed 1,5-naphthoquinone. (Accurate to 2 d.p. for both ^{c,d} and 1 d.p. for ^e)

CSD Code	Unit Cell ^a	Hydroxyl Arrangement ^b	O-H Hydroxyl Bond length ^c (Å)	O...H Hydrogen bond length ^d (Å)	Dihedral Angle ^e (°)	Ref.
EKEWOH	m	2 Z	0.84	2.31	-15.9	98
IHXNAQ01	o	2 Z	0.80	2.25	-7.1	99
IHXNAQ02	m	2 Z	0.81	2.32	-3.5	99
IHXNAQ03	m	2 Z	0.82	2.22	1.8	99
OBEWAV	a/t	3 Z	0.90	2.23	1.0	100
OBEXOK	a/t	3 Z	0.85	2.21	2.5	100
TELYAK	a/t	2 Z	0.82	2.22	-4.5	101
TELYAK01 ^g	a/t	2 Z	0.89	2.24	-1.5	102
TELYAK02	o	2 Z	0.82	2.22	-7.7	103
TELYAK03	m	2 Z	0.82	2.22	-4.5	103
UHUKAJ	a/t	2 Z	0.80	2.15	4.7	104
UMOMAL	m	2 Z	0.89	2.20	-1.6	105
UMOMAL01	m	2 Z	0.86	2.15	0.9	105
VOHFII	m	2 Z	0.84	2.21	-11.4	106

Table 4. CSD survey of polyhydroxy-1,4-naphthoquinones with possible 6-membered hydrogen bonds. ^a m = monoclinic, o = orthorhombic, a/t = anorthic/triclinic, ^b position and orientation relative to nearest C=O group, ^c Hydroxyl group, ^d hydrogen bond, ^e relative to nearest C=O group, ^f hydrogen missing. (Accurate to 2 d.p. for both ^{c/d} and 1 d.p. for ^e)

Code	Unit Cell ^a	Hydroxyl Arrangement ^b	Interatomic information (5 or 8)			Ref.
			O-H Bond length ^c (Å)	O...H Bond length ^d (Å)	Dihedral Angle ^e (°)	
BADWUA	m	5 Z	0.95	1.66	3.3	110
CIFRIS	m	5 Z, 8 ^f	0.74	1.98	-6.0	111
DAMSIU	m	5 Z	0.90	1.79	-2.4	112
DCDHNQ01	m	5 Z, 8 Z	0.99, 0.98	1.73, 1.76	3.3, 5.1	113
DERKOB	o	5 Z, 6 E	0.84	1.78	0.9	114
DHNAPH04	m	4 Z, 8 Z	1.24, 1.24	1.37, 1.37	2.6, -2.6	115
DHNAPH05	m	4 Z, 8 Z	1.07, 1.07	1.57, 1.57	6.1, -6.1	115
DHNAPH17	m	5 Z, 8 Z	0.99, 0.99	1.77, 1.76	0.6, 1.2	115
FIYLOO	m	5 Z	0.96	1.82	-7.1	117
FUSNOW10	a/t	5 Z, 5 Z, 5 Z	0.82, 0.9, 0.89	1.84, 1.79, 1.81	2.4, 4.4, 3.2	118
GAFSOV	a/t	5 Z	1.08	1.65	6.1	119
IPOJUT	a/t	8 Z	0.86	1.81	-0.6	120
ISOWUJ	m	5 Z	0.84	1.86	-0.2	121
ISOXAQ	m	8 Z	0.84	1.86	-0.2	121
LICKIR	m	5 Z	0.82	1.91	7.8	122
LICKOX	o	5 Z	0.84	1.84	-1.9	122
LICLAK	m	5 Z	0.84	1.89	-3.5	122
NORPEQ	m	5 Z	0.86	1.73	1.8	123
NUDPIM	a/t	8 Z	1.02	1.63	0.3	124
PVVAQS01	m	5 Z	0.89	1.71	9.7	125
ULUHUE	a/t	8 Z	0.91	1.79	-4.8	126
UQOJEQ	o	8 Z	0.84	1.87	0.0	127
YODKAE	m	5 Z	0.89	1.77	2.4	128
ZZZQRS01	o	4 Z 8 Z	1.03, 1.03	1.60, 1.60	0.0, 0.0	129

Table 5. CSD survey of hydroxynaphthoquinone with possible 6- and 5-membered hydrogen bonds. ^a m = monoclinic, o = orthorhombic, a/t = anorthic/triclinic, ^b position and orientation relative to nearest carbonyl group, ^c Hydroxyl group, ^d hydrogen bond, ^e relative to nearest carbonyl group. (Accurate to 2 d.p. for both ^{c/d} and 1 d.p. for ^e)

CSD Code	Unit Cell ^a	Hydroxyl Arrangement ^b	5- or 8- positions			2- or 3- positions			Ref.
			O-H Bond length ^c (Å)	O··H Bond length ^d (Å)	Dihedral Angle ^e (°)	O-H Bond length ^c (Å)	O··H Bond length ^d (Å)	Dihedral Angle ^e (°)	
NEPNTH	a/t	2 Z, 5 Z	0.93	1.67	-1.0	0.78	2.09	-4.6	107
NERLUS	a/t	2 Z, 3 E, 5 Z, 6 Z, 8 Z	1.04, 0.92	1.57, 1.75	-5.3, -3.1	0.89	2.17	11.0	108
YUFMER	o	3 Z, 5 Z	0.92	1.77	0.9	0.97	2.08	5.3	109

The average distance of the strong 6-membered hydrogen bond at the 5- (or equivalent 8-) positions is *ca.* 1.75 Å, whilst the weaker 5-membered hydrogen bond formed at either the 2- or 3- positions have longer hydrogen bond lengths of 2.21 Å. Similarly, the longer hydroxyl O-H bond lengths are exhibited for the 6-membered hydrogen bonds, although the crystallographic O-H bond lengths appear to be much shorter than those obtained from calculations (*c.a.* 0.90 – 1.00 Å depending upon theory, method and basis set). From this survey an interaction that would lead to the hydroxyl groups pointing toward one another, possibly classed as a steric interference due to it having a destabilizing effect on the molecule, is not observed.

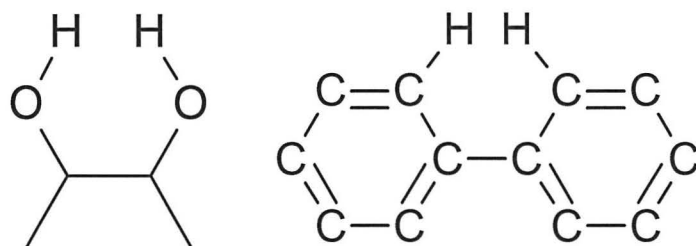


Figure 2. Classically described steric interference where the Hydrogen atoms are so close together that they would overlap.

From looking at the intermolecular structures as a whole, it has shown that the 2 and 5 positions are favoured and retain an intramolecular confirmation. This indicates that the intramolecular stability of these bonding confirmations is stronger than any intermolecular bonding that could have been formed. From this it can also be implied that the bonding strength of these interactions is stronger than intermolecular bonding and therefore significantly different statistically to a none bonded version. This gives rise to an opportunity to use intramolecular bonding in a mathematical approach to working out energy that could benefit both simulations and preliminary crystal structures if the intramolecular bonding is strong.

1.5 hydrogen bonding

Hydrogen bonding has been studied using spectroscopic and diffraction techniques.^[130] Despite the discovery of the hydrogen bond a century ago, the definition of the hydrogen bond is ever changing, with a recent IUPAC redefinition occurring in 2011,^[131] based upon recent theoretical developments, *e.g.* QTAIM (Quantum Theory of Atoms In Molecules).

Symmetric hydrogen bonds are observed in ice and solid phases of many anhydrous acids at high pressures.^[132] The three-centre four-electron bonds, space the hydrogen atom exactly halfway between two identical atoms, resulting in bonds of equal strength. As the bond order is 0.5, its strength is comparable to that of a covalent bond. The “ionic” bond is important as the duet rule for the first shell appears to be violated.

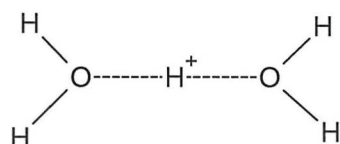


Figure 3. Symmetric Hydrogen bonding found in ice.

Strong, low-barrier hydrogen bonds form when the distance between two heteroatom acceptor and donor atoms is short. The barrier mentioned is the barrier in energy for the hydrogen to move from one heteroatom to the other. For regular hydrogen bonds in which the O \cdots O distance is *ca.* 2.8 Å, the hydrogen is asymmetrically bonded. When the distance decreases to *ca.* 2.55 Å, the proton is able to move between both atoms with no energy barrier. When the distances decreases even further (< 2.29 Å), the bond becomes a short-strong hydrogen bond.^[133] Low-barrier hydrogen bonds within transition states are important for enzyme catalysis.^[134]

The hydrogen bond is characterized by a proton acceptor (typically electronegative pnictogens, chalcogens and halogens, although π -bonds may be loosely included) possessing a lone pair of electrons. Due to the small van der Waals radius of 1.2 Å, hydrogen-hydrogen contact distances less than 2.4 Å are rare. Short (1.8 – 2.0 Å H \cdots H) dihydrogen bonds^[135,136] are observed in NaBH₄·2H₂O where the proton acceptor is a metal hydride. Although the dihydrogen bond has been studied using neutron diffraction,^[137,138] with similar geometries to hydrogen bonds, its relationship to conventional hydrogen, ionic and covalent bonds remains unclear. Dihydrogen bonding stabilises the solid phase of H₃NBH₃^[137] containing both protic (H δ^+) and hydridic (H δ^-) atoms, whilst isoelectronic ethane is a gas. Dihydrogen bond formation is assumed to precede formation of H₂ gas from the reaction of a hydride and a protic acid.^[135,138] The dihydrogen bond should not be confused with:

- H–H bonding from dihydrogen bound to a metal
- agostic interactions (three-centre two-electron bonds between coordinatively-unsaturated transition metals and C–H bonds)^[139,140]
- hydrogen-hydrogen bonds^[141-143] between two neutral non-bonding close-contact hydrogen atoms *e.g.* within (planar) biphenyl, phenanthrene and chrysene. Although the existence of H \cdots H bond paths is not in question, the relative stability of phenanthrene compared to its isomers can also be adequately explained by comparing resonance stabilizations^[142] or more effective π - π overlap.^[143]

Resonance assisted hydrogen bonds (RAHB) are strong intramolecular hydrogen bonds with unusually short distances observed between $O=C-OH\cdots$ or $\cdots O=C-C=C-OH$ for aromatic β -diketones (Figure 4) and β -enaminones^[144] caused by π -delocalization involves the hydrogen which cannot solely be described by a Coulombic model.

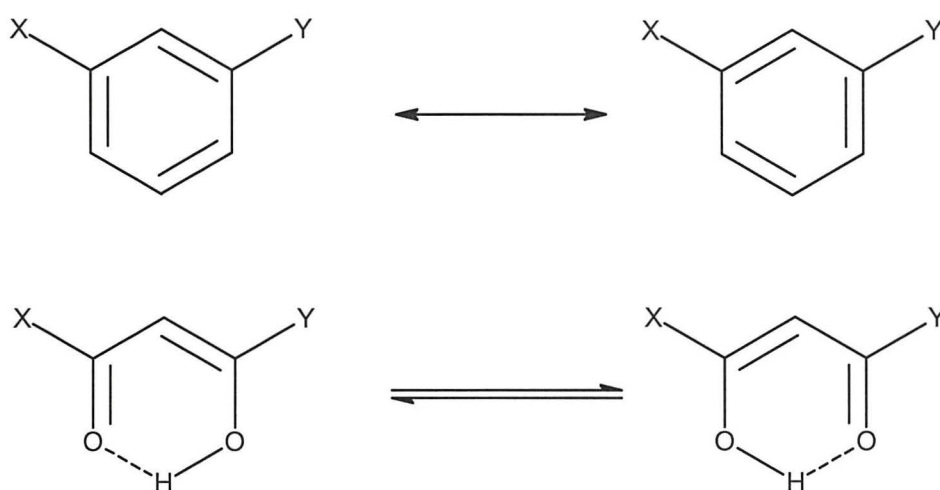


Figure 4. Comparison of resonance forms for meta-substituted benzenes and β -diketone enol tautomers, the latter is similar to R6 interactions described in this work (see Section 2,3).

Relative conformer stabilities were analysed using multiple linear regression with terms derived from a presence/absence matrix consisting of three parameters:

- heteroatom outside the ring
- heteroatom linked to the ring
- presence or absence of a ring double bond

where Boolean flags either describe the absence of a double bond or the presence of an oxygen atom (zero), or the presence of either a double bond or nitrogen atom (one).

1.6 Quantum Theory of Atoms In Molecules

Quantum Theory of atoms in molecules (QTAIM) (for terminology see Section 4.3) has been extensively used to study inter- and intra-molecular hydrogen bonding:

- Protein folding^[145]
- Charge density analysis^[146-191]
- Bond path analysis^[141,152-154]
- Cooperativity analysis^[155]
- Cluster analysis^[156]
- Dimer analysis^[157-161]
- Crystal systems^[162]

In a seminal piece of work, Koch and Popelier^[146] formulated eight necessary hydrogen bonding criteria (later adopted by IUPAC for hydrogen bonding redefinition) based upon QTAIM charge density analyses:

- 1) Topology – Bond critical points and linking both paths must appear between the hydrogen and the acceptor atom. Ring critical points were found to guarantee a consistent topology. If the ring and bond critical points coalesce, annihilation occurs resulting in an abrupt change of topology or structure.^[163] This means that if there are no bonding paths then a bond does not exist and if the ring and bond critical points sit very close together then accurate data can not be obtained.
- 2) Charge density at bond critical point – typically an order of magnitude smaller than those found for a covalent-bond.^[146,164,165] i.e. a hydrogen bond should have less electron density compared to a formal bond.

- 3) Laplacian of the charge density at the bond critical point, $\nabla^2\rho_{\text{BCP}}$ – it is crucial that $\nabla^2\rho_{\text{BCP}}$ is positive, but also the ranges of values are within a reasonable range.^[146] The correlation between $\nabla^2\rho_{\text{BCP}}$ with the interaction energy is also linear. This means that the stronger the density is the stronger the bond and if negative then the electrons are avoiding the area so cannot be a bond.
- 4) Mutual penetration of hydrogen and acceptor - in order to estimate this penetration, the non-bonded radii of these atoms have to be compared to the corresponding bonded radii. This distance is measured in the direction of hydrogen bond formation as seen from the nucleus. i.e. if the atoms are too far apart the electrons cannot be shared between them so is very unlikely a bond has formed.

The following criteria occur from integrated properties which require considerable computational effort than the above local effects.

- 5) Loss of charge of the hydrogen atom - this is obtained by subtracting the electronic population of the hydrogen as a free monomer from the corresponding hydrogen in the complex. i.e. some of the hydrogen's electrons are now been used by the acceptor atom.
- 6) Energetic destabilization of the hydrogen atom – this states that the hydrogen atom must be destabilized in the complex. This effect is measured by the difference in total atomic energy between the complex and the monomer.
- 7) Decrease of dipolar polarization of the hydrogen atom – the magnitude of the dipolar polarization of the hydrogen atomic distribution is decreased upon complex formation.
- 8) Decrease of the hydrogen atom volume – this criterion was shown to have a good trend, however some exceptions were found. Additional work is needed to confirm this.

The work of LaPointe *et al.*^[145] examined protein folding present in a selection of 13 amino acid long α -helical peptides. An investigation of the intramolecular hydrogen bond critical points and bond graphs found two N–H \cdots O and one C–H \cdots O, the former possessing higher energetic stability and electron density at the bond critical points.

Mandado *et al.*^[146] investigated the presence of intramolecular hydrogen bonding in 1,2-ethanediol and 1,2-dihydroxybenzene. In 1,2-dihydroxybenzene, located bond critical points were dismissed as artefacts of the computational level used, which required further investigation.^[149] This is illustrated by Hermida-Ramón *et al.*^[148] on whether small carboxylic acids contained intramolecular hydrogen bonding or not. The investigation yielded different results partially dependent upon the level of computational theory used.^[148]

Fuster *et al.*^[150] showed that correlations between electron localization function (ELF) and QTAIM analyses existed whilst attempting to probe resonance assisted vs conventional hydrogen bonds. No significant differences were found between both types of hydrogen bond, although resonance aided in producing stronger bonds.

Intramolecular N–H \cdots O hydrogen bonds were investigated by Grabowski *et al.*^[151] for 3-(aminomethylene)pyran-2,4-dione, in which RCP characteristics gave a good indication of hydrogen bond strength. Oliveira *et al.*^[161] probed the relationship between imidazolidine derivatives and PEG/PVP polymers, with QTAIM confirming the existence of N–H \cdots O red-shifted hydrogen bonds and C–H \cdots O blue-shifted (“*anti*”-) hydrogen bonds.^[161]

Grabowski *et al.*^[152] analysed the bond paths within a small set of molecules acting as Lewis acid and bases. Reported X–H bond lengths elongated linearly when stronger binding energies were observed.

As described in Section 1.5, Matta *et al.*^[141] reported different types of dihydrogen bonding. Dihydrogen bonding was stated to be stabilizing,^[1814] (confirmed independently by Hernández-Trujillo *et al.*^[153]) which appeared to conflict with the standard explanation of H···H interactions as “non-bonded steric repulsions”.

Cioslowski *et al.*^[154] demonstrated that the existence of an attractor interaction line between a pair of nuclei did not necessarily imply the presence of bonding between those nuclei, with the H···H interaction being controlled by the H···H distance.

Grabowski *et al.*^[155] found that hydrogen bonding interactions were enhanced if the number of hydrogen bonding HF molecules forming the cluster were increased. Bonds lengths elongated and increased density were observed with increased numbers of participating HF molecules.

Huang *et al.*^[156] reported that methanol clusters showed differences in hydrogen bonding strength when the methanol clusters were small, with hydrogen bonds showing partial covalent character and characteristic red-shift.

An investigation of glycine dimers was undertaken to probe possible bonding structures.^[157] A cyclic planar dimer was the most stable since it contained two strong OH···O hydrogen bonds. An investigation into the bonding between halogen containing compounds gave an insight into different intermolecular bonding that could take place,^[158] such as non-covalent hydrogen bonding.

Hermida-Romón *et al.*^[159] reported blue-shift hydrogen bonding within benzene–benzene and benzene–naphthalene complexes. The size of the shift could not be directly correlated against the ability of the donor to reorganize its electronic density.^[159]

Vener *et al.*^[162] investigated strong hydrogen bonding in crystalline materials. A transition region separating shared and closed-shell hydrogen bonded interactions, allowing migration of the hydrogen atom was reported.

1.7 Hypotheses and Aims

1.7.1 Hypotheses

- Changes in the geometric structure of a molecule will affect its physical and chemical properties such as UV adsorption data.
 - This means that if a molecule is in a different conformation i.e. 1,2 and 1,3 there will be differences in the observable chemical properties of the molecules.
- The energy of a molecule can be approximated by the energies of its constituent components and interactions *via* an adaptation of the bond counting rule
 - This states that if you have two conformers of the same molecule you can work out the energy of them by adding the bonding energies and intramolecular forces together.

1.7.2 Aims

- The constituent energies may be quantified and characterised using quantum mechanical methods
- Develop a quantitative bond counting rule *via* the use of multiple linear regression from a training set of rotamers

- Use a qualitative bond counting rule to predict low energy conformers for a large series of possible isomers
- Develop guidelines for the minimal approach to aid computational costs
- Potential energy surfaces will allow rotational barriers to be analysed
- Web3D technology can deliver interactive graphic and haptic representations of potential energy surfaces for teaching purposes as well as improved visualization.
- 3D printing of potential energy surfaces may be employed for possible augmented reality applications.

1.8 Summary

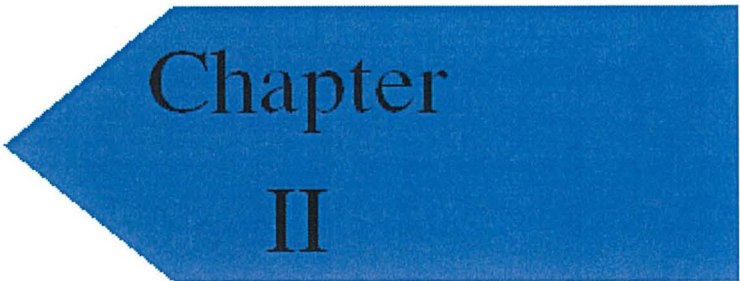
The bond counting rule is a less well known empirical rule which states that a molecule will seek to maximize any stabilizing interactions whilst minimizing the number of destabilizing interactions. The majority of studies have been focused on alloy configurations and conformations, such as the generation of ternary B/C/N superlattices from carbon allotropes.^[51-57] The transferability of bond counting rules have been demonstrated for Si_3AlP .^[59]

A crystallographic survey has hinted at the importance of both 5- and 6-membered intramolecular hydrogen bonds within hydroxy-1,4-naphthoquinone. Although QTAIM produces good descriptions of hydrogen bonding,^[146] additional work is required in order to fully redress whether certain QTAIM features are artefacts of the level of theory.^[147]

To put this all into perspective, the IUPAC definition of a hydrogen bond (including QTAIM criteria) has been updated as of 2011,^[131] indicating the ever evolving description of the common hydrogen bond by the chemistry community. The

definition changed to include computationally derived structures, stating that analysis of the electron density topology of hydrogen-bonded systems should usually shows a bond path connecting hydrogen and acceptor and a Bond Critical point between them (see Section 4.3.1).

This work in the following chapter represents to my knowledge, the first application of a bond counting rule to study hydrogen bonding. As the average energy of an intramolecular hydrogen-bond lies between 2-161 kJ mol⁻¹,^[67,68] differentiation of conformers based upon hydrogen-bond counts should be possible, provided that the energy of each type of hydrogen bond are easily differentiated.



Chapter II

Chapter 2 - Polyhydroxy-1,4-Naphthoquinone

Intramolecular Hydrogen Bond Counting

Rules

2.1 Introduction

As mentioned in chapter 1, the rarely used bond counting rule (BCR) has previously been applied to study relative strengths of bonds and their effect on structure and energetics^[39-59]. For ternary B/C/N systems,^[51-57] with a single use for Si₃AlP^[59]. This chapter will aim to create a similar band counting rule that can be applied to hydrogen bonding environments.

Analysis of variance (ANOVA) was employed within this section of work, ANOVA was chosen as it is a collection of statistical models that are used to analyse the difference between group means. The multiple linear regression statistical model was employed within the ANOVA as this approach the standard way in which a scalar dependent variable (*i.e.* energy) can be compared to one or more explanatory variables (*e.g.* bonding types).

In the case of the ANOVA multiple linear regression the ANOVA's group means for the variables was used and then the multiple linear regression statistical model then tested the results to give a R Squared value (how close the data fits the line of best fit) and standard error (by how much the values deviated from the line of best fit). With both of these values comparisons can be made between different mathematical models for different bond counting rules.

2.1.1 Quantum Chemistry

When solving a quantum chemistry problem the first step is to look at trying to solve the Schrödinger equation with an electronic molecular Hamiltonian operating on the wavefunction. An exact answer to the Schrödinger equation is only possible for a single hydrogen atom, as other systems consist for three or more particles; an approximated solution is therefore required.

One of the most common ways of approximating this solution is the molecular orbital (MO) theory, in which the wavefunction is written as a linear combination of known atomic orbitals (LCAO). The variation principle states a flexible wavefunction will lower the energy and imply that a better wavefunction is obtained. The MO approach to quantum chemistry is the conceptual basis of the Hartree-Fock (HF) and post Hartree-Fock methods.

Basis sets are the way in which the atomic orbitals are generated within the calculation; the most basic of these is the Slater-type atomic orbitals (STOs). STOs are found by fitting analytical exponential functions directly to the atomic wavefunctions. STOs give rise to cusps in electron density at the nuclei; Gaussian functions provide a better approximation. Therefore a basis set can then be specified by listing the exponents for each orbital type used within it.

If only one function is used for each atomic orbital then the basis set is referred to as a minimal basis, If double is used the basis set then becomes of double zeta quality. A split-valence basis set is generated when two basis functions are used for the valence atomic orbitals but only one basis function is used for inner-shell atomic orbitals. Atomic orbitals can become polarised when a molecule is formed so a basis function can be added that increases the maximum number of orbitals allowed for a given atom, leading to a double zeta plus polarization basis set (DPZ). Anions, compounds with lone pairs and hydrogen bonds have significant electron density at long distances, therefore highly diffuse functions are needed. In this respect the 6-311++G(d,p) basis was chosen for this work.

2.2 Development of a training set

A training set of polyhydroxy-1,4-naphthoquinone isomers was used to construct the bond counting rule, as the addition of a hydrogen bond may cause the total energy to differ by *ca.* 20-40 kJ mol⁻¹, allowing statistically significant energy differences. Furthermore, the set fully describes the different intramolecular interactions present.

To generate a complete data set, all possible planar conformers and rotamers were accounted for. The total number of possible rotamers for all substitutions of the base 1,4-naphthoquinone are presented in Table 6. As the parent 1,4-naphthoquinone has C_{2v} symmetry, certain positional and rotational isomers are duplicated. To reduce computational effort, only unique conformers are included within the training set. This mirrors the approach of Fan *et al.*^[58]

Table 6. Table of all possible 1,4-naphthoquinone isomers

# OH groups	Max # planar conformers	Max # positional isomers	Max # rotamers	Distinct positional isomers	Distinct rotamers
0	1	1	1	1	1
1	2	6	12	3	6
2	4	15	60	9	33
3	8	20	160	10	80
4	16	15	240	9	126
5	32	6	192	3	96
6	64	1	64	1	36
Total	127	64	729	36	378

From Table 6, application of molecular symmetry reduced the total number of calculations from 729 to a more manageable 378. The training set was generated by entering each of the 378 structure into the WebMO program and the basic structure then transferred into a text file in the Cartesian coordinate data structure.

For this study, in order to evaluate the average bond counting rule, energetics for all its components are accurately needed, therefore all rotamers were enumerated and analysed to produce a large dataset. It will be demonstrated in Section 2.4, that a minimal subset of 17 isomers, which describe all unique positions, orientations and interactions, generate a single set of unique bond counting rule terms.

Once all possible unique rotamers were enumerated, identification of substitution positions and different types of intramolecular interactions was initially performed on paper. Manual data entry into *Microsoft Excel*, in order to obtain energy terms *via* multiple linear regression was also found to be ineffective, particularly for complex bond counting rules. Both methods were tedious, repetitive and open to error.

In order to alleviate this, in-built IF logical statements, combined with AND and OR Boolean logic as required, with array totalling using the SUM function, allowed efficient data modification using “drag and drop” techniques without need for extensive recalculation (Figure 5). New bond counting rules could be efficiently created and analysed using multiple linear regression.

Preliminary calculations (not included in this thesis for ease of conveyance) were performed using AM1 and HF/6-31G(*d*). Similar trends and results were observed for each bond counting rule. As mentioned previously, the bond counting rule aims to maximize the number of strong bonds present within a system, whilst limiting the number of weak ones, giving an optimized structure.

The use of AM1 and HF/6-31G(*d*) was chosen as while not been as accurate as DFT or post HF methods they are accurate enough to give an indication of if there is a significant change in energy between different molecular conformations to allow this study to take place.

	A	B	C	D	E	F	G	H	I	J	K	L	M	N	O	P	Q	R	S	T	U	V	W	X	Y	Z	AA	AB	AC	AD	AE	
1	molecule		2	3	5	6	7	8		R5 (2)	R5 (3)	R6 (5)	R6 (8)		OH5 (23)	OH5 (56)	OH5 (67)	OH5 (78)		C6 (23)	C6 (56)	C6 (67)	C6 (78)		Number of Hydroxyl	Number of R6	Number of R5	Number of C6	Number of OH	Rel HF	HF	
2																																
3	0_hf									0	0	0	0		0	0	0	0		0	0	0	0		0	0	0	0	0	0	0	-532.0329619
4	2_E_hf	E								0	0	0	0		0	0	0	0		0	0	0	0		1	0	0	0	0	0	-196605.844	-606.9161628
5	2_Z_hf	Z								1	0	0	0		0	0	0	0		0	0	0	0		1	0	1	0	0	0	-196629.6528	-606.9252311
6	23_EE_hf	EE								0	0	0	0		0	0	0	0		1	0	0	0		2	0	0	1	0	0	-393172.841	-681.7845677
7	23_EZ_hf	EZ								0	1	0	0		1	0	0	0		0	0	0	0		2	0	1	0	1	0	-393228.8146	-681.8058869
8	23_ZZ_hf	ZZ								1	1	0	0		0	0	0	0		0	0	0	0		2	0	2	0	0	0	-393237.255	-681.8091017
9	EEE_235_hf	EEE	E							0	0	0	0		0	0	0	0		1	0	0	0		3	0	0	1	0	0	-589751.583	-756.657446
10	EEZ_235_hf	EEZ								0	0	1	0		0	0	0	0		1	0	0	0		3	1	0	1	0	0	-589795.6323	-756.6742235
11	EZE_235_hf	EZE								0	1	0	0		1	0	0	0		0	0	0	0		3	0	1	0	1	0	-589811.3024	-756.6801919
12	EZZ_235_hf	EZZ								0	1	1	0		1	0	0	0		0	0	0	0		3	1	1	0	1	0	-589851.1459	-756.6953675
13	ZEE_235_hf	ZEE	E							1	0	0	0		1	0	0	0		0	0	0	0		3	0	1	0	1	0	-589807.1438	-756.6786608
14	ZEZ_235_hf	ZEZ								1	0	1	0		1	0	0	0		0	0	0	0		3	1	1	0	1	0	-589851.598	-756.6955397
15	ZZE_235_hf	ZZE								1	1	0	0		0	0	0	0		0	0	0	0		3	0	2	0	0	0	-589819.1752	-756.6831905
16	ZZZ_235_hf	ZZZ								1	1	1	0		0	0	0	0		0	0	0	0		3	1	2	0	0	0	-589859.7867	-756.6986586
17	2356_EEEE_hf	EEEE	E							0	0	0	0		0	1	0	0		1	0	0	0		4	0	0	1	1	0	-786361.9163	-831.5423568
18	2356_EEEZ_hf	EEEZ								0	0	0	0		0	0	0	0		1	1	0	0		4	0	0	2	0	0	-786327.0552	-831.5290789
19	2356_EEEZ_hf	EEEZ								0	0	1	0		0	0	0	0		1	0	0	0		4	1	0	1	0	0	-786385.346	-831.5512807
20	2356_EEZZ_hf	EEZZ								0	0	1	0		0	1	0	0		1	0	0	0		4	1	0	1	1	0	-786408.379	-831.5600535
21	2356_EZEE_hf	EZEE								0	1	0	0		1	1	0	0		0	0	0	0		4	0	1	0	2	0	-786421.4122	-831.5650176
22	2356_EZEZ_hf	EZEZ								0	1	0	0		1	0	0	0		0	1	0	0		4	0	1	1	1	0	-786385.765	-831.5514403
23	2356_EZZE_hf	EZZE								0	1	1	0		1	0	0	0		0	0	0	0		4	1	1	0	1	0	-786440.775	-831.5723925
24	2356_EZZZ_hf	EZZZ								0	1	1	0		1	1	0	0		0	0	0	0		4	1	1	0	2	0	-786462.2842	-831.5805849
25	2356_ZEEE_hf	ZEEE	E							1	0	0	0		1	1	0	0		0	0	0	0		4	0	1	0	2	0	-786418.3278	-831.5638428
26	2356_ZEEZ_hf	ZEEZ								1	0	0	0		1	0	0	0		0	1	0	0		4	0	1	1	1	0	-786383.3522	-831.5505213
27	2356_ZEZE_hf	ZEZE								1	0	1	0		1	0	0	0		0	0	0	0		4	1	1	0	1	0	-786442.5974	-831.5730866
28	2356_ZEZZ_hf	ZEZZ								1	0	1	0		1	1	0	0		0	0	0	0		4	1	1	0	2	0	-786466.0203	-831.5820079
29	2356_ZZEE_hf	ZZEE								1	1	0	0		0	1	0	0		0	0	0	0		4	0	2	0	1	0	-786429.9743	-831.5682787
30	2356_ZZEZ_hf	ZZEZ								1	1	0	0		0	0	0	0		0	1	0	0		4	0	2	1	0	0	-786394.4192	-831.5547365
31	2356_ZZZE_hf	ZZZE								1	1	1	0		0	0	0	0		0	0	0	0		4	1	2	0	0	0	-786450.3101	-831.5760242
32	2356_ZZZZ_hf	ZZZZ								1	1	1	0		0	1	0	0		0	0	0	0		4	1	2	0	1	0	-786472.306	-831.584402
33	EEEE_23567_hf	EEEE	E							0	0	0	0		0	1	0	0		1	0	1	0		5	0	0	2	1	0	-982941.1913	-906.4154381
34	EEEE_23567_hf	EEEE	E							0	0	0	0		0	1	1	0		1	0	0	0		5	0	0	1	2	0	-982977.4502	-906.4292484
35	EEEE_23567_hf	EEEE	E							0	0	0	0		0	0	1	0		1	1	0	0		5	0	0	2	1	0	-982939.0441	-906.4146203
36	EEEE_23567_hf	EEEE	E							0	0	0	0		0	0	0	0		1	1	0	0		5	0	0	2	0	0	-982923.8651	-906.4088389

Figure 5. Excel spreadsheet for the bond counting rule, the first set of columns indicates the position and orientation. The next 3 sets of 4 indicate the locations where there specific types of bonding can take place. The last section contains the interaction counts and structural energies for each conformation.

As a hydrogen bond is fairly long and polarizable, Gaussian^[169] calculations reported in this chapter were run at HF/6-311++G(*d,p*) for all polyhydroxy-1,4-naphthoquinone unique isomers. HF/6-311++G(*d,p*) was chosen as the calculation method of choice as it gave good accuracy due to the polarization and diffuse functions which help with energies of long bonds. It also was not as computationally intensive as B3LYP as mentioned previously all 378 structures needed to be evaluated in order for the ANOVA multiple linear regression to have a full set of data to work over. However if B3LYP was employed the same trends would also be visible within the results.

Ultrafine geometry optimisation convergence criteria ensure accuracy of vibrational spectra (Chapter 3). Ultrafine SCF convergence criteria in conjunction with 6*d* and 10*f* Cartesian (rather than pure 5*d* and 7*f*) *d*- and *f*-function basis sets are necessary for QTAIM analysis (Chapter 4). Energies relative to the lowest energy of each subgroup, e.g. 2,3,5-trihydroxy-1,4-naphthoquinone were derived. A series of custom Python parsers were employed for the text searching of output files. A similar approach using batch files containing Linux “grep” commands could also have been employed.

2.3 Prototype bond counting rule

The first approach undertaken whilst attempting to adapt the bond counting rule for intramolecular hydrogen bonding systems, was to simply count the number of hydrogen bonds present in the molecule, plotting this directly against the calculated energy. There was very little correlation between the relative energy of each set of molecules and the corresponding hydrogen bond count (Figure 6). It was therefore deemed that the number of hydroxy substituted groups could be influencing the results. To try and eliminate this problem, a new method was attempted.

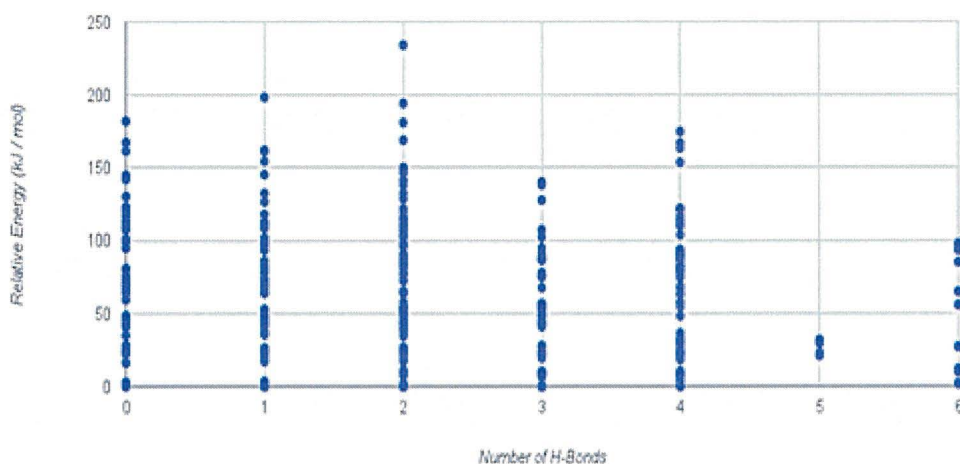


Figure 6. Relative energy of the structures plotted against the number of hydrogen bond present. (Each point is an individual conformations energy)

The next attempt at eliminating this error possibly produced by the different number of hydroxyl groups was to only examine trihydroxy-1,4-naphthoquinones. This gave a subset of values to work with. The general methodology, however, did not change, albeit with a constant number of OH groups. This smaller test data set was made to have a relative energy to the lowest energy structure within the set.

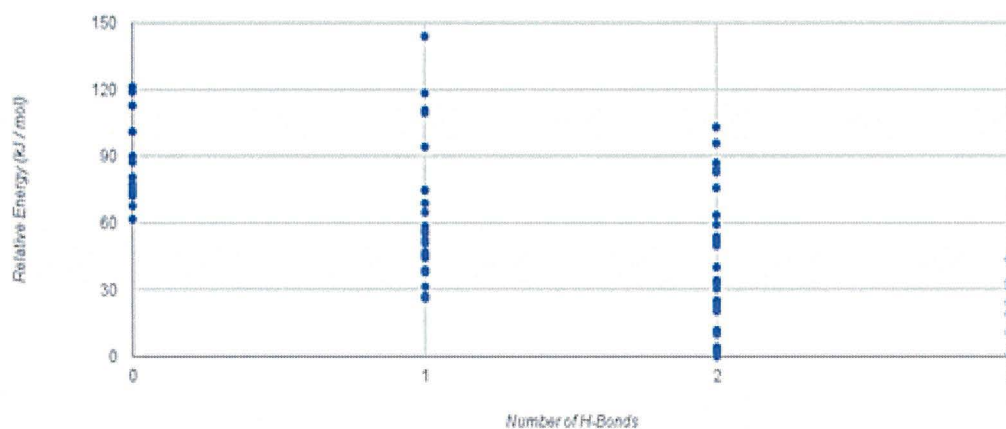


Figure 7. Global relative energy of trihydroxy-1,4-naphthoquinone plotted against the number of hydrogen bonds. (Each point is an individual conformations energy)

Statistical improvement was achieved in Figure 7, with low energy molecules exhibiting higher hydrogen bond counts. Although higher energy structures had lower hydrogen bond counts, the method could still not be used as a prediction tool. This methodology of grouping the different number of hydroxy substituted groups as a base line improved the method as a whole.

It was decided to take this method a step further so that it could be applied to the data set as a whole. The number of hydroxyl groups added to the system would also be taken into account so that all of the data could be set against a single relative energy of the base 1,4-naphthoquinone molecule.

To work out the energy of the addition of each hydroxyl group to the base structure, hydroxy-1,4-naphthoquinone molecules as a whole would be examined. The energy of the molecule relative to the base was plotted against the total number of hydroxyl groups present (Figure 8). The average energy for addition of a single hydroxyl group was found to be $-196597 \text{ kJ mol}^{-1}$.

A prototype bond counting rule of the form :

$$E = E_0 + N_b E_b + N_h E_h$$

Rule 1. BCR with number of hydrogen bonds (N_b) with energy (E_b) and number of hydroxyl groups (N_h) with energy (E_h).

where E is the total energy of the molecule, E_0 is the energy of the parent (in this case 1,4-naphthoquinone), plus the average energy (E_b) of the number of hydrogen bonds (N_b), and the average energy (E_h) and number of hydroxyl groups (N_h). This new methodology was then tested against the data set as a whole to see if this would improve the statistics of the adapted bond counting rule.

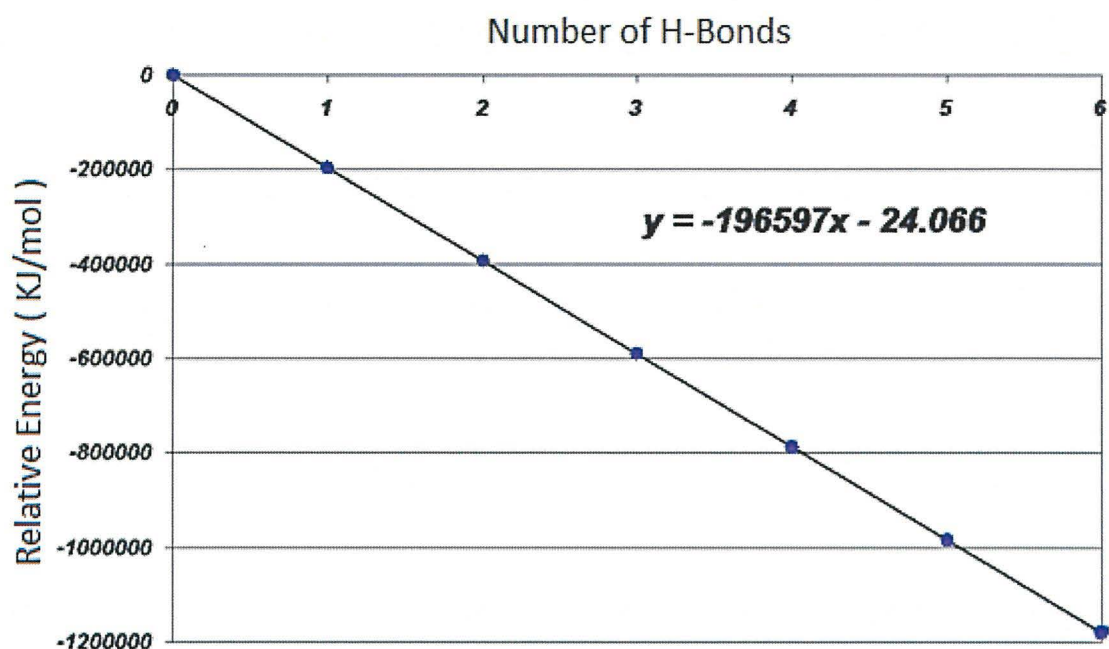


Figure 8. Global relative energies plotted against the number of hydroxyl groups present. As $m \gg \sigma$, the plot appear to be perfect. (m = gradient and σ = deviation)

To do this, the *Excel* spreadsheet of data mentioned previously was modified to include the number of hydroxyl groups as well as the number of hydrogen bonds present. This still did not greatly improve the statistics, although the spread in the energies appeared to reflect strengths of different hydrogen bonds (Figure 9).

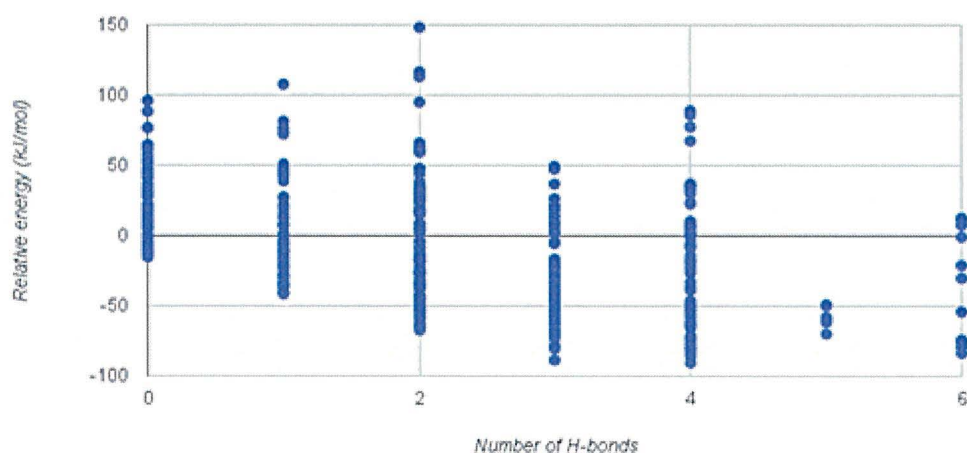


Figure 9. Plot of energy vs. the number of hydrogen bonds with the number of hydroxyl groups removed. (Each point is an individual conformations energy)

A significant difference in the strength of the hydrogen bond present in 2- and 5-monohydroxy-1,4-naphthoquinones was noted from specific output files, confirming crystallographic trends (Section 1.4). Examining relative energy differences, the 5- and 6- membered hydrogen bonds had respective energies of 24 and 44 kJ mol⁻¹, confirming the presence of different hydrogen bonding environments and energies.

Table 7. Energy differences between hydroxy-1,4-naphthoquinone. Difference taken relative to highest energy of each position.

Position	Orientation	Difference in energies (kJ mol ⁻¹)
2	Z	-24
2	E	0
5	Z	-44
5	E	0
6	Z	-3
6	E	0

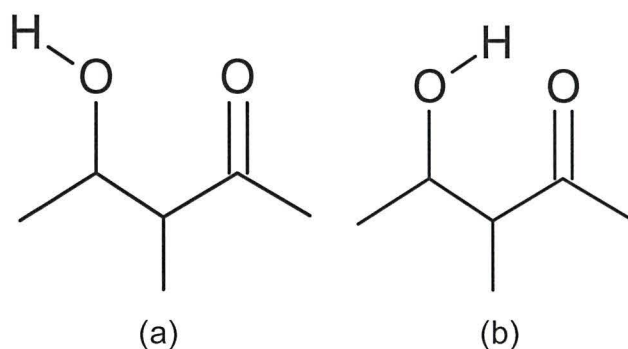


Figure 10. E orientation (a) Z orientation (b)
(always relative to the nearest hydroxyl group)

Etter^[21] described a method of designating different intermolecular hydrogen bonding according to the nature of the donors and acceptors. The designations being:

- C for a chain
- R for a ring
- D for a dimer or other finite set
- S for intramolecular hydrogen bonding

The number of donors and acceptors used within each motif were assigned as subscripts and superscripts respectively. The number of atoms within the repeat unit was indicated in parenthesis. As Etter's method did not subcategorize intramolecular hydrogen bonds^[21], a series of custom designations were generated, taking into account both ring size and the nature of the interaction as not alternative method was available.

A 6-membered ring hydrogen bond to the carbonyl group was redefined as a "R6" interaction, whilst the corresponding 5-membered ring was similarly redefined as "R5". The remaining hydrogen bonds were designated "OH5" as this formed a 5-membered hydrogen bond to an adjacent hydroxyl group. Images of the 3 types of interactions that were used at this point can be seen in Figure 11.

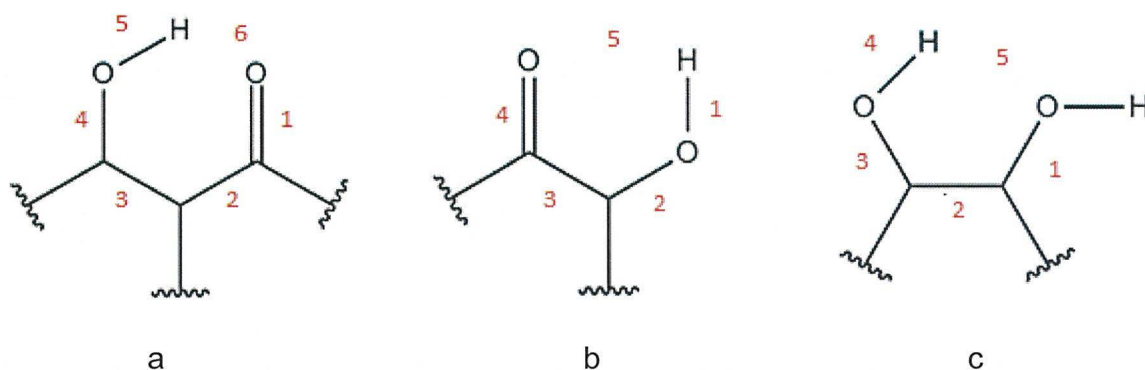


Figure 11. Custom designations for specific hydrogen bonds. (a) R6, (b) R5 and (c) OH5. Ring size counting indicated in red.

The aforementioned bond counting rule was extended using:

- E_{R6} / N_{R6} - the energy and number of "R6" type interactions (a figure 8)
- E_{R5} / N_{R5} - the energy and number of "R5" type interactions (b figure 8)
- E_{OH5} / N_{OH5} - the energy and number of "OH5" type interactions (c figure 8)

Giving the equation:

$$E = E_0 + N_b E_b + N_{R6} E_{R6} + N_{R5} E_{R5} + N_{OH5} E_{OH5}$$

Rule 2. Extended BCR with R6, R5 and OH5 terms added

As the number of degrees of freedom generates a graph with greater than three dimensions, statistics were obtained using multiple linear regression.

Table 8. ANOVA table of multiple linear regression results for rule 2 (378 observables). Standard errors and coefficients quoted to 0 d.p.

Regression Statistics	
Multiple R	0.999999997
R Square	0.999999994
Adjusted R Square	0.999999994
Standard Error (kJ mol ⁻¹)	18

Energy component	Coefficients (kJ mol⁻¹)	Standard Error (kJ mol⁻¹)
Intercept	-44	3
Hydroxyl	-196574	1
R6	-44	1
R5	-35	1
OH5	-23	1

From the above ANOVA table (Table 8), the rule is statistically significant, although there appears to be some discrepancy in specific terms. The intercept is incorrect as it should pass through the origin (given as the parent 1,4-naphthoquinone). The R6 interaction has slightly weakened, whilst the R5 term appears to be stronger. Both effects may be possibly due to the cooperative effect of neighbouring interactions.

Examining neighbouring hydroxyl groups, e.g. 2,3-, 5,6- and 6,7- in more detail, a series of interactions were conceived (Table 9). The interaction was identified in which the both hydroxyl groups pointing towards each other. To determine the energy of this new interaction was to specifically examine the 6,7-dihydroxy-1,4-naphthoquinone molecules, as this has an easily identifiable baseline structure, where neither of the hydroxyl groups are interacting with other parts of the molecule.

Table 9. Table of interactions occurring within neighbouring dihydroxy structures. 6,7 substitution is the only one to have a baseline as it has a none interacting pair.

Molecule name	Interaction of first OH	Interaction of second OH	HF energy (kJ mol ⁻¹)	HF energy (kJ mol ⁻¹) relative to baseline
23_EE	C6	C6	64	-
23_EZ	OH5	R5	8	-
23_ZZ	R5	R5	0	-
56_EE	OH5	-	46	-
56_EZ	C6	C6	81	-
56_ZE	R6	-	23	-
56_ZZ	R6	OH5	0	-
67_EE	C6	C6	35	+19
67_ZE	OH5	-	0	-16
67_ZZ	-	-	16	0

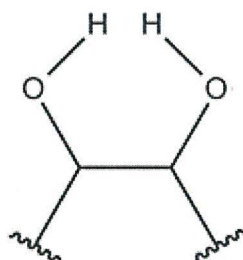


Figure 12. Designation for C6 interaction

A “C6” term (Figure 12) was chosen for the additional term as it could be classed as a “close contact” or “steric interference”. From table 9, a destabilisation energy of ca. 19 kJ mol⁻¹ was identified between the 67_ZZ (non-interacting) and 67_EE (C6) conformers. This new term was added to the bond counting rule and a new multiple linear regression was undertaken.

Table 10. ANOVA table of multiple linear regression results for rule 3 (378 observables).
Standard errors and coefficients quoted to 0 d.p.

Regression Statistics	
Multiple R	0.999999998
R Square	0.999999996
Adjusted R Square	0.999999995
Standard Error (kJ mol ⁻¹)	16

Energy Component	Coefficients (kJ mol ⁻¹)	Standard Error (kJ mol ⁻¹)
Intercept	-24	3
Hydroxyl	-196587	1
R6	-34	1
R5	-25	1
C6	26	2
OH5	-13	1

Regression confirms that the average C6 interaction is destabilizing, verifying the previous results for a single unique configuration. The destabilizing nature leads to a decrease in energy and should be avoided by limiting the number of these within the bond counting rule. The OH5 term does not change its definition, although its value changes within the regression equation due to its separation from the C6 term.

The new bond counting rule is now shown in rule 3 with the number of C6 interactions (N_{C6}) and the energy of the C6 added (E_{C6}).

$$E = E_0 + N_b E_b + N_{R6} E_{R6} + N_{R5} E_{R5} + N_{OH5} E_{OH5} + N_{C6} E_{C6}$$

Rule 3. BCR with the new "C6" term added

Table 11. The energies for the base and mono substituted 1,4-naphthoquinone including hydrogen bond count

Position	Rel Energy (kJ mol ⁻¹) (0 d.p.)	Hydrogen Bond
0	0	-
2 E	-196606	-
2 Z	-196630	R6
5 E	-1965780	-
5 Z	-196623	R5
6 E	-196608	-
6 Z	-196611	-

Table 11 revealed that grouping all hydroxyl positions as a single term may not have been the best approach. The data indicates that position may be more statistically significant than first thought. To accommodate for this, the single hydroxyl term was replaced by three new hydroxyl terms. Each successive position around the ring was given its own term. The 2- (3-) positions were defined as alpha (α), with 5- (8-) and 6- (7-) positions as beta (β) and gamma (γ) respectively, producing:

$$E = E_0 + N_\alpha E_\alpha + N_\beta E_\beta + N_\gamma E_\gamma + N_{R6} E_{R6} \\ + N_{R5} E_{R5} + N_{OH5} E_{OH5} + N_{C6} E_{C6}$$

Rule 4. BCR with the new positional terms added

Although the bond counting rule statistics improved (Table 12), there was still a large standard error within the model. To possibly alleviate this, baseline interactions within the molecule were considered.

Table 12. ANOVA table of multiple linear regression results for rule 4 (378 observables).

Standard errors and coefficients quoted to 0 d.p.

Regression Statistics	
Multiple R	0.999999999
R Square	0.999999999
Adjusted R Square	0.999999999
Standard Error (kJ mol ⁻¹)	8

Energy Component	Coefficients (kJ mol ⁻¹)	Standard Error (kJ mol ⁻¹)
Intercept	-19	2
Alpha Position	-196597	1
Beta Position	-196572	1
Gamma Position	-196600	1
R6	-42	1
R5	-20	1
C6	30	1
OH5	-10	1

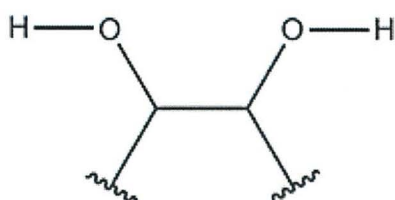


Figure 13. Designation for M4 interaction

Inclusion of the M4 (Figure 13) term has correctly shifted the intercept towards the origin (unsubstituted parent) (Table 13). A “M4” (4-membered non-interacting) baseline interaction which occurs for 67_ZZ, was included within the bond counting rule. The baseline interactions for the R5 and R6 terms, did not, however, need to be included, as the baselines (incorporated as positional terms) are mutually exclusive to the R5 and R6 terms.

Table 13. ANOVA table of multiple linear regression results for rule 5 (378 observables).
Standard errors and coefficients quoted to 0 d.p.

Regression Statistics	
Multiple R	1.00
R Square	1.00
Adjusted R Square	1.00
Standard Error (kJ mol ⁻¹)	4

Energy Component	Coefficients (kJ mol ⁻¹)	Standard Error (kJ mol ⁻¹)
Intercept	1	1
Alpha Position	-196602	1
Beta Position	-196576	1
Gamma Position	-196614	1
R6	-47	1
R5	-26	1
C6	35	1
M4	20	1
OH5	0	1

$$E = E_0 + N_\alpha E_\alpha + N_\beta E_\beta + N_\gamma E_\gamma + N_{R6} E_{R6} \\ + N_{R5} E_{R5} + N_{OH5} E_{OH5} + N_{C6} E_{C6} + N_{M4} E_{M4}$$

Rule 5. BCR with the new “M4” terms added

The M4, C6 and OH5 terms appear to be destabilizing in Table 13. However the OH5 (stabilizing -20 kJ mol⁻¹ agreeing with R5) and C6 terms (destabilising 15 kJ mol⁻¹) should, however, be reported relative to the M4 baseline. Care must be taken to avoid confusion between the positive OH5 term and its overall stability.

The C6, M4 and OH5 terms were split into benzenoid(aromatic) and quinoid (none aromatic) components to try to lower the standard error, giving:

$$E = E_0 + N_\alpha E_\alpha + N_\beta E_\beta + N_\gamma E_\gamma + N_{R6} E_{R6} + N_{R5} E_{R5} + N_{OH5B} E_{OH5B} + N_{OH5Q} E_{OH5Q} + N_{C6B} E_{C6B} + N_{C6Q} E_{C6Q} + N_{M4B} E_{M4B} + N_{M4Q} E_{M4Q}$$

Rule 6. BCR with the new B/Q (benzenoid and quinoid) terms added

Table 14. ANOVA table of multiple linear regression results for rule 6 (378 observables).
Standard errors and coefficients quoted to 0 d.p.

Regression Statistics	
Multiple R	1.00
R Square	1.00
Adjusted R Square	1.00
Standard Error (kJ mol ⁻¹)	4

Energy Component	Coefficients (kJ mol⁻¹)	Standard Error (kJ mol⁻¹)
Intercept	1	1
Alpha Position	-196605	1
Beta Position	-196575	1
Gamma Position	-196612	1
R6	-47	<1
R5	-25	1
C6 Benzenoid	34	1
C6 Quinoid	39	1
M4 Benzenoid	19	1
M4 Quinoid	23	1
OH5 Benzenoid	-2	1
OH5 Quinoid	7	1

2.4 Comparison of bond counting rules

As shown in section 2.3, qualitative methods for bond counting rule generation have been constructed, that can successfully predict the total energies for any polyhydroxy-1,4-naphthoquinone conformer. It has been shown that a detailed understanding of all interactions present with the molecule is essential for success (Table 15). Inclusion of additional terms into the bond counting rule decreased the standard error. As rule 6 lowered the standard error only by 0.32 kJ mol⁻¹, at the significant expense of three additional terms, it was deduced that rule 5 offered a compromise between accuracy and usability.

Table 15. Error in different methods for the adapted BCR.

Initial and Rule 1 were not analysed using linear regression.

	Bond counting rule terms	Standard Error (kJ/mol)
Initial (H-bonds)	2	N/A
Rule 1 (OHs and H-bonds)	3	N/A
Rule 2 (H-bonds split into R6, R5 & OH5)	5	18.161
Rule 3 (C6 added)	6	15.569
Rule 4 (OHs split into α , β and γ positions)	8	8.233
Rule 5 (M4 term added)	9	4.496
Rule 6 (benzenoid / quinoid splitting)	12	4.170

The conformation and energetics of a molecule can be predicted (either by simple calculations or on “the back of an envelope”) without the need for hundreds of calculations to be performed. Multiple linear regression for the entire training set of 378 unique conformers generates an **average** set of interaction energies for each component, which may differ due to hydrogen bond cooperativity. **Minimal** Bond counting rules (Table 16) agreeing with the average bond counting rule, may be also derived from 17 unique conformers which describe key interactions.

Table 16. Comparison of coefficient energies between the extensive and basic bond counting rules.

Energy Component	Coefficients of extensive BCR (kJ/mol)	Coefficients of basic BCR (kJ/mol)
Intercept	1	N/A
Alpha Position	-196602	-196606
Beta Position	-196576	-196580
Gamma Position	-196614	-196608
R6	-47	-44
R5	-26	-24
C6	35	35
M4	20	19
OH5	0	1

2.5 Sieving

The bond counting rule can be employed:

- as an overall predictive tool for relative total energies
- for sieving of low energy conformers

The second method uses the bond counting rule as a sieve to rule out high energy containing destabilizing interactions whilst preferentially keeping those that have strong stabilising intramolecular interactions. The procedure on the next page describes the reduction of thirty six hexahydroxy-1,4-naphthoquinone conformers to two low-energy conformers. The procedure can be modified to locate high-energy structures or conformers with interesting properties for further analysis.

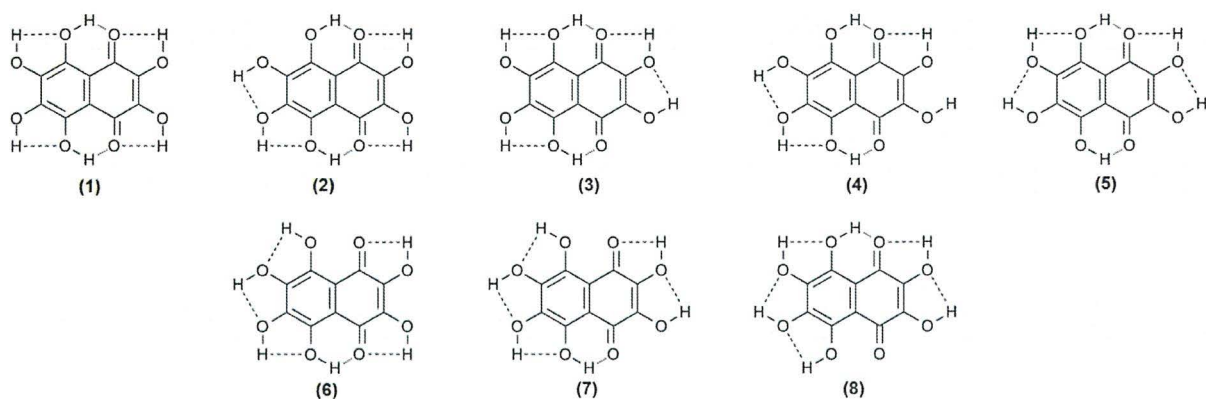


Figure 14. Low energy conformers for hexahydroxy-1,4-naphthoquinone obtained by removal of all C6 interactions. Energies are quoted to the nearest kJ mol^{-1} relative to the global minimum: (1) 0, (2) 2, (3) 8, (4) 10, (5) 12, (6) 23, (7) 30, (8) 36.

Rotamer (6) has C_{2v} symmetry; the remainder have C_s symmetry

A test case for this was performed on 36 unique hexahydroxy-1,4-naphthoquinone conformers. The steps for the sieving method are detailed below:

1. Remove all molecules that have destabilizing C6 interactions ($+15 \text{ kJ mol}^{-1}$).
 - This removes sixteen molecules leaving only eight (entire Figure 14).
2. Maximize the number of R6 interactions (in this case, two) (-47 kJ mol^{-1}).
 - This removes three molecules leaving five (top row of Figure 14).
3. Maximize the number of R5 interactions (in this case, two) (-26 kJ mol^{-1}).
 - Two molecules remain (first two in Figure 14)
4. Maximize the number of OH5 interactions (-20 kJ mol^{-1}).
 - As the bond counts are identical (albeit with different positions), further reduction is not possible. The relative energies of both conformers (global **(1)** and local **(2)** minima) lie within 2 kJ mol^{-1} of each other.

2.6 Summary and future work

The successful development of both quantitative (multiple linear regression) and qualitative (sieving) of a bond counting rule for intramolecular hydrogen bonding in (poly)hydroxy-1,4-naphthoquinones has been described. The techniques described in this chapter, may be used (albeit with modification) to describe intramolecular hydrogen bonding in other systems.

In order to fundamentally understand and characterise the interactions within the bond counting rule, vibrational frequency (Chapter 3) and Quantum Theory of Atoms In Molecules (QTAIM) (Chapter 4) analyses will be undertaken.

2.6.1 Consideration for an unknown molecule

This work has furthered understanding of different hydrogen-bonding types. The common notion that hydrogen bonds possess set of amounts of energy is not valid. This seminal work has provided an excellent framework for future studies, including a prototype study of 1,2-, 1,5-, 1,7-, 2,3- and 2,6-polyhydroxynaphthoquinones.^[131]

The correct parent structure must be identified. Although this is straightforward for naphthoquinones, it is, however, ambiguous whether benzene or phenol should be the correct parent for polyhydroxybenzenes / polyphenols. Different substitution positions must be accounted for. Application of molecular symmetry to reduce the number of positions aids in this matter. Interactions between single substituents and the parent must be included, accounting for any mutually exclusive baseline interactions. Single, double or aromatic bonding can affect the terms due to different interatomic distances. Interactions between neighbouring substituents must be defined (*e.g.* novel 7-membered interactions), including donor / acceptor atoms, *e.g.* different 5-membered hydrogen bonds between neighbouring hydroxyls and thiols:

- Donor oxygen and acceptor sulphur, O-H \cdots S-H
- Donor sulphur and acceptor oxygen, S-H \cdots O-H



Chapter

III

Chapter 3 - Polyhydroxy-1,4-naphthoquinone

Vibrational Frequencies

3.1 Introduction

Prior to the advent of computational techniques, hydrogen bonding was investigated using spectroscopic methods such as IR (infrared) and Raman vibrational spectroscopy, in which red-shifted O-H stretching harmonic vibrational frequencies (ν OH) were used to prove the existence of a hydrogen bond. Even the dawn of X-ray diffraction techniques could not make IR spectroscopy redundant.

There are three main types of IR that look are used to look at different vibrational analysis. These are near-, mid- and far- IR, the names stem from their proximity to the visible spectrum. The near-IR is in the region of 14000-4000 cm^{-1} , these high energy IR wavelengths can be used to excite overtone or harmonic vibrations. The mid-IR 4000-400 cm^{-1} , can be used to look at the fundamental vibrations as well as rotational/vibrational structural analysis. The final far-IR is mainly only used for rotational spectroscopy as it is very close to the microwave region been only 400-10 cm^{-1} .

The main feature of IR analysis is based on the fact that molecules absorb frequencies that are specific to the structures contained within the molecule. These resonant frequencies that match the transition energies, are determined by the overall shape of the potential energy surface as well as the atoms and their bonding/vibrational coupling.

3.2 Methodology

Harmonic frequency calculations were run using Gaussian^[169] using HF/6-311++G(*d,p*) optimised geometries obtained through the use of the WebMo drawing package. Ultrafine geometry optimisation convergence criteria were used to ensure the geometry was as close to its minimum as possible to give as accurate vibrational data as possible. As computationally derived vibrational data is always over estimating the vibrational frequencies a scaling factor is always needed to convert the figures into a more realistic value.

Suitable scaling factors have been published which depend not only upon method but also basis set.^[170] As no specific value could be obtained for HF/6-311++G(*d,p*), unadjusted frequencies are quoted in the following sections. Approximate scaled frequencies appear to agree with traditional ranges for hydroxyl harmonic vibrational frequencies.

3.3 Results and discussion

3.3.1 Monosubstitution

Selected monohydroxy-1,4-naphthoquinone conformers have been analysed (Table 17). “Baseline” vibrational frequencies (ca. 4180 cm⁻¹) with nigh identical bond lengths of 0.941 Å are exhibited by 6E and 6Z. This confirms that the γ position does not significantly interact with the carbonyl.

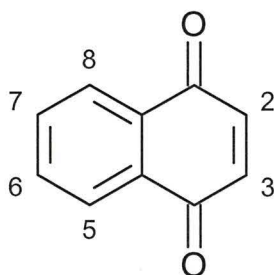


Figure 15. Substitution Positions for 1,4-naphthoquinone.

Table 17. Doppler shift effects calculated for mono-substituted hydroxynaphthoquinones. ν_{OH} (cm^{-1}), r_{OH} (\AA). ^a Non indicating non-interacting.

Position	ν_{OH}	r_{OH}	Type ^a
2 E	4160	0.943	Baseline
2 Z	4078	0.947	R5
5 E	4181	0.941	Baseline
5 Z	4001	0.949	R6
6 E	4180	0.941	Non
6 Z	4177	0.941	Non

A clear red-shift can be seen of ca. 180 cm^{-1} (Table 17) for the (5Z) strong R6 6-membered hydrogen bond at the β -position, with hydroxyl bond length elongation of ca. 0.008 \AA relative to the 6E/6Z baselines. The mutually exclusive 5E conformer shows no shift in either frequency or bond length, showing “baseline” characteristics, confirming the choice to not generate an extra term for this interaction within the bond counting rule as it is the β positional term (Chapter 2.3).

A weaker red-shift ca. 80 cm^{-1} (Table 17) occurs for the (2Z) moderately strong R5 5-membered hydrogen bond at the α -position, with hydroxyl bond length elongation of 0.006 \AA relative to the 6E/6Z baselines, confirming the relative stabilisations observed within the bond counting rule. Although the mutually exclusive 2E quinoid conformer is also assumed to be “baseline”, it shows slight red shifting compared to the aromatic 6-values. The reason for this red-shift is unknown, as similar 6-membered rings possess blue shifts.^[171] Nevertheless, vibrational analysis confirms that 2E is the correct α positional term (Chapter 2.3).

3.3.2 Dihydroxy (non-interacting)

Non-interacting dihydroxy-1,4-naphthoquinones (2,5-, 2,6-, 2,7-, 2,8-, 5,7- and 5,8-) followed the same trends as the corresponding monohydroxy species. All R6 and R5 interactions showed large and weaker red-shifts respectively. As the interactions do not interact with each other and no additional interactions could be studied, the results have been omitted for clarity.

3.3.3 Dihydroxy (interacting)

Table 18. Doppler shift effects calculated for di-substituted hydroxynaphthoquinones.

ν_{OH} (cm^{-1}), r_{OH} (\AA). ^a Non indicating that this OH is non-interacting.

Position	ν_{OH} (1)	r_{OH} (1)	Type (1) ^a	ν_{OH} (2)	r_{OH} (2)	Type (2) ^a
6 7 E E	4243	0.938	C6	4218	0.938	C6
6 7 Z E	4148	0.943	OH5	4183	0.941	Non
6 7 Z Z	4179	0.941	M4	4180	0.941	M4

The study of interacting dihydroxy-1,4-naphthoquinones focused on the 6,7-substitution, omitting any additional interactions that could cloud the results (Table 18). The 5,6- or 2,3- interactions have been examined. Analysis (not presented) is not straightforward due to hydrogen bonding cooperativity, but paints a similar picture to that obtained for the 6,7- species.

The M4 interaction shows a “baseline” vibrational frequency of *ca.* 4180 cm^{-1} . The bond length also matches with the mono-substituted results of 0.941 \AA (Table 18). This confirms the assumption made within the bond counting rule of setting the M4 interaction to be a baseline interaction (Chapter 2.3).

The OH5 interaction shows a weak red-shift *ca.* 30 cm^{-1} and slight bond length elongation of 0.002 \AA (Table 18), indicating weak hydrogen bonding is taking place compared to both the R5 and R6 interactions.

The C6 interaction, however, shows a Doppler blue-shift with the frequency increasing by *ca.* 80 cm^{-1} and the bond length shortening by 0.003 \AA (Table 18). This indicates that the interaction, previously referred to as an “anti-hydrogen” bond,^[161] is destabilising.

The C6 interaction creates a pair of real symmetric and anti-symmetric normal modes, in which the protons remain planar. Another pair of symmetric and anti-symmetric non-planar bending imaginary modes is generated simultaneously per C6 interaction. A molecule with one, two or three C6 interactions will respectively be at best a 2nd, 4th and 6th order transition state. This confirms the choice of minimizing the number of C6 interactions as the first stage of the qualitative sieving bond counting rule approach (Chapter 2.5).

3.4 Summary

Vibrational frequency analysis was used to characterise the interactions within the bond counting rule, confirming the initial assumption for certain interactions as being “baseline”, stabilising or destabilising in character :-

- The R6 was shown to have a large Doppler red-shift in its vibrational frequency as well as the hydrogen bond shortening, this shows that the bond is stabilizing in nature.
- The R5 was also shown to be stabilizing, but less than the R6, having a Doppler red-shift and bond shortening.
- The OH5 interaction is also slightly stabilizing in nature have low Doppler red-shift.
- The M4 Interaction has no noticeable change in vibrational frequency or bond length.
- The destabilizing C6 has been shown to have Doppler blue-shift with its vibrational frequency increasing as well as a bond shortening.

Further characterisation based upon Quantum Theory of Atoms in Molecules (QTAIM) will be described in the next chapter.



Chapter

IV

Chapter 4 - Hydrogen bonding QTAIM analyses

4.1 Introduction

Analysing the electron density probability distribution within a molecule can give further insight into bonding and how changes in electron density may affect certain properties. AIM2000^[172] is based of the work by Bader^[173] and co-workers on the Quantum Theory of Atoms in Molecules (QTAIM).^[173] By using QTAIM within this work some chemical bonding and structure properties can be determined by analysing topological features of the electron density, such as stationary points and gradient paths.^[174] Greater information can be garnered concerning the interaction bond strengths and order through the use of this analysis which will be looked at in more detail later in this chapter. The characterization of interactions as open (shared) or closed shell and bond ellipticity^[175-178], will also be looked at to help characterize the interactions further.

4.2 Methodology

Different intramolecular interactions present in polyhydroxy-1,4-naphthoquinone are analysed using QTAIM. These interactions include those introduced in Chapter 2, in addition to other new interactions, form adapted bond counting rules. HF/6-311++G(*d,p*) and B3LYP/6-311++G(*d,p*) calculations are reported. Hybridised functions were used as they have correctional terms contained within them that make weaker interactions more closely approximate the real life values. The basis sets are suitable for hydrogen bonding and other long-range polarized interactions, whilst density functional theory (DFT) in the form of B3LYP functional provides a better description of electron exchange and correlation than HF can by nature. Molecules were geometry optimized using Gaussian^[169]. Ultrafine geometry optimisation convergence criteria ensured accuracy of both vibrational frequencies

and molecular conformation. Ultrafine SCF convergence criteria in conjunction with $6d$ and $10f$ Cartesian (rather than pure $5d$ and $7f$) d - and f -function basis sets are necessary for QTAIM analysis. Wavefunctions were exported as .wfn files. Formatted checkpoint files (.fchk) were generated from unformatted checkpoint files (.chk), and translated using cubegen into .cube files for graphical plotting within GaussView 5.

4.3 Terminology

4.3.1 Critical points

A critical point (CP) is a point at which the gradient (first derivatives) of the electron density vanishes, *i.e.*

$$\nabla\rho = \mathbf{i}\frac{\partial\rho}{\partial x} + \mathbf{j}\frac{\partial\rho}{\partial y} + \mathbf{k}\frac{\partial\rho}{\partial z} = \mathbf{0}$$

In the above equation \mathbf{i} , \mathbf{j} and \mathbf{k} are unit vectors in the x , y and z direction respectively. Critical points can be identified using a Hessian matrix of second derivatives. The eigenvalues λ_1 , λ_2 and λ_3 of the Hessian represent curvatures of the electron density with respect to each eigenvector. Critical points (ω , σ) are classified according to their rank (ω) and signature (σ). The former represents the number of non-zero curvatures of the electron density at the critical point, whilst the latter is the algebraic sum (positive contributing +1, and negative contributing -1) of the curvatures.

There are four types of stable critical points:

- Nuclear Critical Point (NCP) – (+3, -3): small pink/purple ball
- Bond Critical Point (BCP) – (+3, -1): small red ball
- Ring Critical Point (RCP) – (+3, +1): small yellow ball
- Cage Critical Point (CCP) – (+3, +1): small green ball

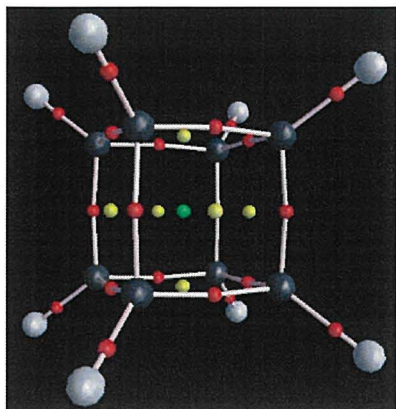


Figure 16. Cubene AIM analysis depicting Bond/Ring/Cage Critical Points (Red/Yellow/Green), the Nuclear critical points are hidden by the atom spheres.

The number and type of critical points that can be located in an isolated molecule follow the Poincaré-Hopf relationship:^[25,179]

$$n_{\text{NCP}} - n_{\text{BCP}} + n_{\text{RCP}} - n_{\text{CCP}} = 1$$

Where n denotes the number of the subscripted type of critical point. A similar equation exists for infinite periodic lattices.^[180]

Violation of the Poincaré-Hopf relationship implies an inconsistent characteristic set, *i.e.* a CP has been missed, requiring further searches for the missing CP. On the other hand, satisfaction of the relationship does not prove its completeness, as if a BCP and RCP are both missing, the relationship is still valid.^[172] The chances of missing both a BCP and a RCP are small. Satisfaction of the Poincaré-Hopf relationship is usually taken as proof of consistency and completeness.

A RCP will always be found in the interior of a ring of chemically bonded atoms. A CCP is formed when several rings are connected so that they enclose an interstitial space. As this thesis focusses upon planar molecules, CCPs are never observed. Occasionally, local maxima in the electron density, known as non-nuclear attractors (NNA) occur at positions other than those of atomic nuclei, and are of substantial theoretical interest. Davies^[171] confirmed the presence of NNA in S-H bonds for related poly(thio)quinones.

4.3.2 Bond paths

Bond paths are single lines of maximum electron density linking the nuclei of two chemically-bonded atoms. The bond path is a universal indicator of different types of chemical bonding interactions:^[175]

- Weak
- Strong
- Closed-shell
- Open-shell

For equilibrium geometries, the molecular graph is defined as collections of bond paths linking bonding nuclei together with any associated CPs. Similar virial paths and graphs chart potential energy instead of electron density. Bond and virial path analyses have been used to examine closed-shell hydrogen-hydrogen bonding (which differs from dihydrogen bonding)^[181,182] in phenanthrene. This interaction is similar in nature to the C6 interaction introduced in Chapter 2.

If a bond path is coincident with the internuclear axis, the sum of the associated bond radii, the bond path length, equals the bond length. If the bond path is curved, as seen in hydrogen-bonded systems,^[179] or chemically strained, the bond path length exceeds the bond length.

4.3.3 Laplacian

The Laplacian, $\nabla^2 \rho(\mathbf{r})$, indicates regions of local electronic charge concentration ($\nabla^2 \rho(\mathbf{r}) > 0$, Lewis base / electron donor) or depletion ($\nabla^2 \rho(\mathbf{r}) < 0$, Lewis acid / electron acceptor). The Laplacian at the BCP is the sum of the three curvatures of the electron density at the critical point; the two perpendicular to the bond path, λ_1 and λ_2 , being negative ($|\lambda_1| > |\lambda_2|$ by convention), whilst the third, λ_3 , which lies along the bond path, is positive. For open-shell covalent bonding ($\nabla^2 \rho_b < 0$), the two negative curvatures dominate (e.g. $\nabla^2 \rho_b = -1.1$ a.u. for C-H bonds^[179]). For closed-shell bonding ($\nabla^2 \rho_b > 0$), such as ionic, hydrogen-bonding or van der Waals

interactions, depletion of electron density within the contact region between the two atoms occurs. Examples of N-H...O=C hydrogen bonds have $\nabla^2 \rho_b = +0.03$ a.u.^[179] For strongly polar bonding such as C-X where X = O, N, F, there is significant accumulation of electron density between the nuclei, but the Laplacian can be of either sign.

4.3.4 Electron density at the BCP

The strength of a chemical bond and its associated bond order, BO, is reflected in the electron density at the BCP (ρ_b).^[173,183] For shared (covalent) bonding, ρ_b is typically 0.20 atomic units. For closed-shell interactions such as ionic, van der Waals, hydrogen, hydrogen-hydrogen and dihydrogen bonding, ρ_b is typically 0.10 a.u or less. ρ_b is strongly correlated with the binding energy for several types of bonding interaction^[183-189] and with S-S bond lengths.^[190]

4.3.5 Bond ellipticity

Ellipticity, defined as:

$$\varepsilon = \frac{\lambda_1}{\lambda_2} - 1$$

Where $|\lambda_1| > |\lambda_2|$, measures the extent to which density is preferentially accumulated in a given plane containing the bond path. Cylindrically symmetric bonds such as the C-C bond in ethane or the C≡C triple bond in ethyne have $\varepsilon = 0$. The ellipticity reaches a maximum for a double bond. Ellipticities of 0.23 and 0.45 have been obtained for aromatic bonds in benzene and formal double bonds in ethene respectively.^[179]

4.3.6 Other QTAIM features

Potential, kinetic and total energy densities may be used to summarise bonding interactions. Potential energy density at BCP is highly correlated with hydrogen bond energies.^[185] Full interaction potentials for hydrogen bonds have been recovered

from potential energy densities.^[191] Hydrogen bond donor capacity,^[192] basicity^[193] and pK_a of weak acids^[194] may be predicted from atomic properties derived from computationally intensive grid-based integration. To obtain accurate integrated properties, such as electron delocalisation indices which link to bond order, the wavefunction must be converged using self-consistent field (SCF) theory to at least fine or ultrafine convergence criteria. Within the previous chapters, both SCF and geometry optimisation convergence criteria were set to ultra-fine.

4.3.7 Calculation set-up

For these calculations the molecules were sketched out using and WebMo and the structures obtained. These structures were then run through Gaussian using both the HF and B3LYP parameters to give two output files. The QTAIM package has a few steps that are needed to be performed before the data is in the form seen in the later sections of this chapter. First the Nuclear Critical Points (NCP) must be identified. From these another series of calculations is then performed to determine the Bond Critical Points (BCP) by looping over the previously discovered NCPs. The next step is to then locate the Ring Critical Points which is done by trying to locate the point at which the electron density ceases to stop dropping within the plane of BCPs. Finally the bonding paths are drawn in on the now built up diagram and can now be inspected to give their respective bonding values.

4.4 Interactions

In addition to interactions introduced within Chapter 2:

- R5 - 5-membered O-H \cdots O=C interaction
- R6 - 6-membered O-H \cdots O=C interaction
- C6 - 6-membered O-H \cdots H-O interaction
- M4 - 4-membered H-O \cdots O-H interaction
- OH5 - 5-membered O-H \cdots O-H interaction

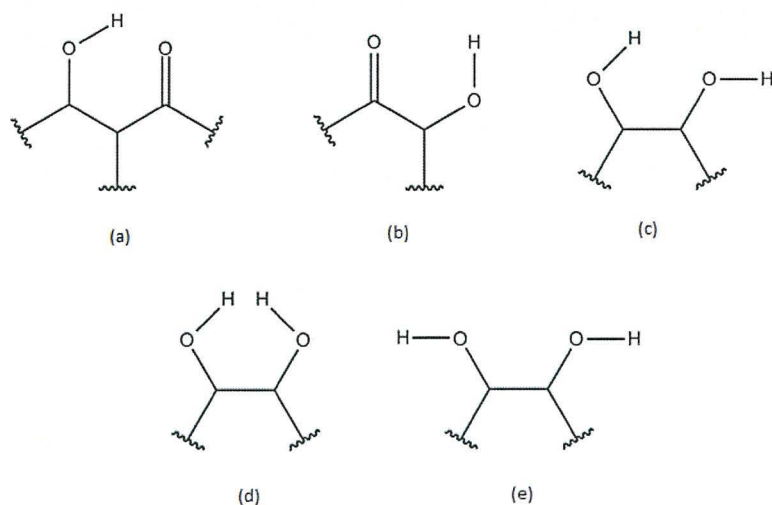


Figure 17. (a) R6, (b) R5, (c) OH5, (d) C6 and (e) M4
Interactions as seen in Section 2

Two baseline interactions not included within the bond counting rule will also be characterized. The terms were not explicitly included within the bond counting rule as they are mutually exclusive to R5 and R6 respectively:

- OO4 - 4-membered H-O...O=C interaction, mutually exclusive to R5
- OO5 - 5-membered H-O...O=C interaction, mutually exclusive to R6

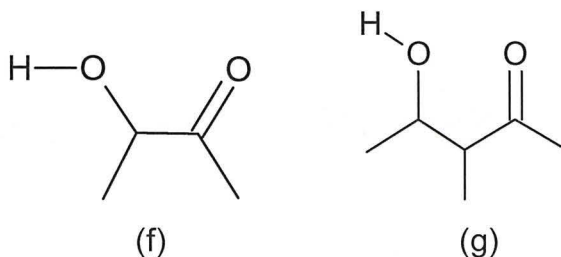


Figure 18. (f) OO4 and (g) OO5 - New interactions in this section

The two types of critical point that will be investigated during this study are the bond and ring critical points. Firstly the bond critical point will indicate if there is any hydrogen bonding present, if one is present further information about the bonding structure can be obtained by further analysis of the critical point. The second critical point is the ring critical point and this will only be used as a rough indicator of bond strength by looking at the distance from the bond critical point with no further analysis been carried out upon it.

4.5 R6 Interaction

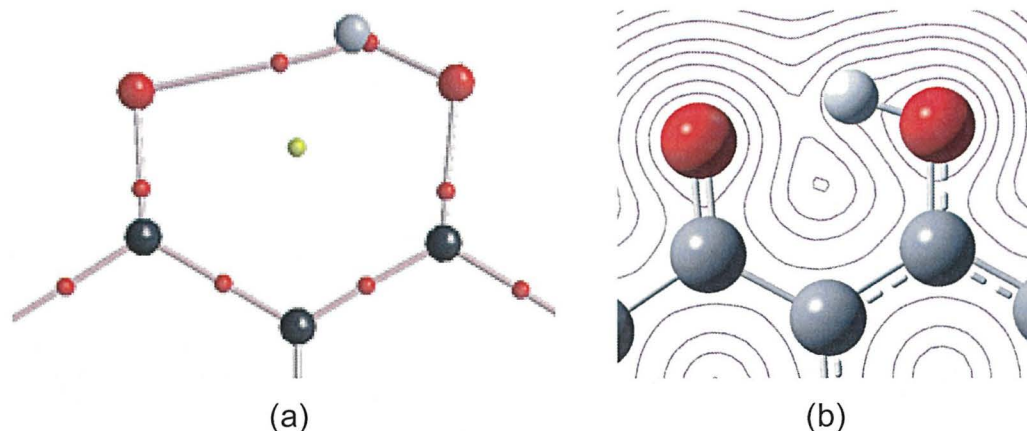


Figure 19. R6 interaction for both HF and B3LYP methods using a 6-311++G(*d,p*) basis set: (a) bond graph, (b) electron density contour plot

The previously observed but unclassified^[178] R6 interaction describes not only the bonding present within the 6-membered intramolecular hydrogen bond, but other surrounding bonds. Figure 19 shows a clear BCP with straight bond paths indicating an interaction between the donor proton of the hydroxyl and the acceptor oxygen atom of the neighbouring carbonyl. The RCP is almost in the centre of the 6-membered ring, the large BCP-RCP distance reflects the strength of the interaction.

Table 19. R6 QTAIM data (quoted to 3 d.p.): distance, r (Å); BCP electron density, ρ_{BCP} (a.u.); Hessian eigenvalue, λ (a.u.); Laplacian, $\nabla^2\rho_{\text{BCP}}$ (a.u.); ellipticity, ϵ .

	BCP of Hydrogen Bond	BCP of Hydrogen Bond	BCP of O-H bond on hydroxyl	BCP of O-H bond on hydroxyl
	HF	B3LYP	HF	B3LYP
r (Å)	1.853	1.725	0.949	0.986
ρ_{BCP} (a.u.)	0.031	0.046	0.373	0.337
λ_1 (a.u.)	-0.046	-0.075	-2.196	-1.716
λ_2 (a.u.)	-0.045	-0.074	-2.158	-1.688
λ_3 (a.u.)	0.218	0.285	1.451	1.036
$\nabla^2\rho_{\text{BCP}}$ (a.u.)	0.127	0.136	-2.903	-2.368
ϵ (a.u.)	0.022	0.014	0.018	0.017

The small positive $\nabla^2\rho_{\text{BCP}}$ indicates that the hydrogen bond is closed-shell in nature, whilst the large negative $\nabla^2\rho_{\text{BCP}}$ for the O-H bond reflects both its polar and covalent nature (Table 19). The ρ_{BCP} for the hydrogen bond is approximately a tenth of that of the hydroxyl group, reflecting the relative differences in bond energy between the two interactions. The low ellipticities reflect almost zero π -bond order for both bonds.

4.6 R5 Interaction

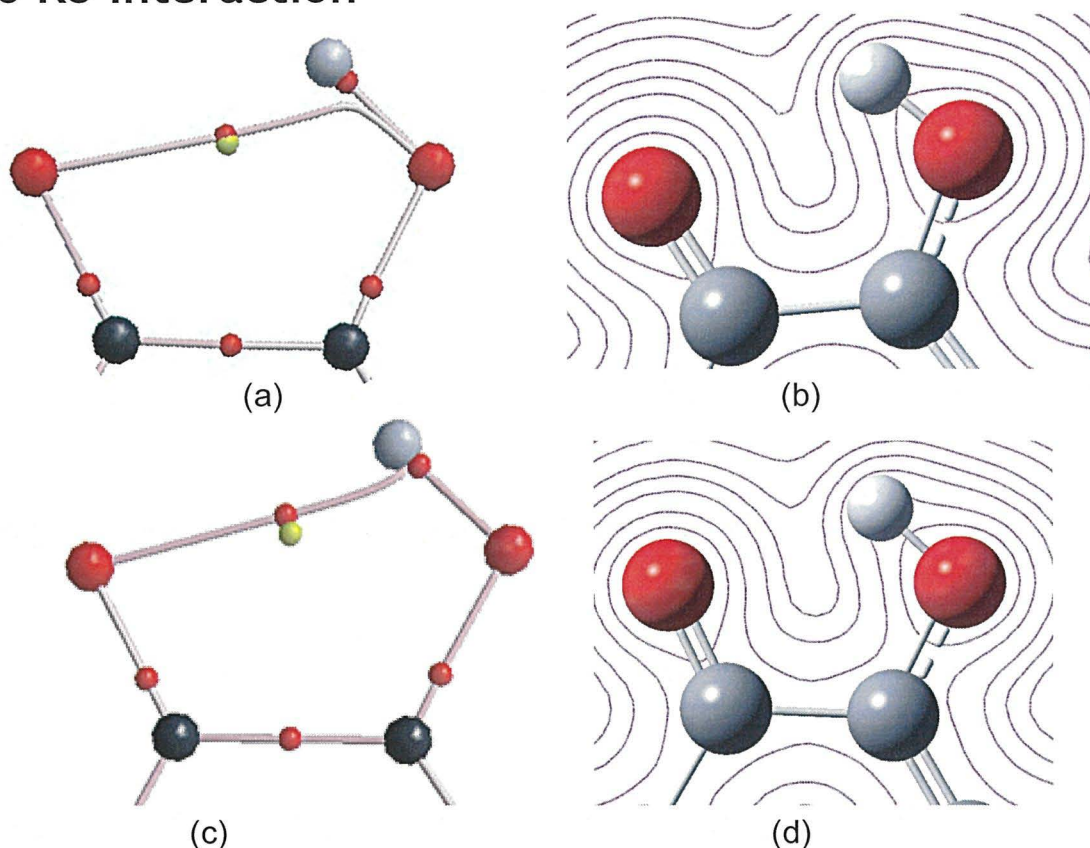


Figure 20. R5 interaction using a 6-311++G(*d,p*) basis set: (a) HF bond graph, (b) HF electron density contour plot, (c) B3LYP bond graph, (d) B3LYP contour plot

Both B3LYP and HF produce differing pictorial representations (Figure 20) of the R5 interaction. B3LYP (with improved descriptions of electron repulsion, exchange and correlation) correctly describes a bond path in which the proton of the hydroxyl acts as the donor, whilst the oxygen of the neighbouring carbonyl acts as the acceptor. On the other hand, HF describes an interaction between the two oxygen atoms, which travels almost parallel to the O-H bond before deviating away prior to the O-H BCP. Both cases depict near BCP/RCP coalescence (possibly responsible for the differing models) reflecting the weak nature of the R5 interaction.

Table 20. R5 QTAIM data (quoted to 3 d.p.): distance, r (Å); BCP electron density, ρ_{BCP} (a.u.); Hessian eigenvalue, λ (a.u.); Laplacian, $\nabla^2\rho_{\text{BCP}}$ (a.u.); ellipticity, ε .

	BCP of Hydrogen Bond	BCP of Hydrogen Bond	BCP of O-H bond on hydroxyl	BCP of O-H bond on hydroxyl
	HF	B3LYP	HF	B3LYP
r (Å)	2.069	1.998	0.947	0.977
ρ_{BCP} (a.u.)	0.023	0.028	0.379	0.349
λ_1 (a.u.)	-0.027	-0.035	-2.150	-1.747
λ_2 (a.u.)	-0.004	-0.023	-2.108	-1.714
λ_3 (a.u.)	0.151	0.165	1.362	1.013
$\nabla^2\rho_{\text{BCP}}$ (a.u.)	0.120	0.107	-2.896	-2.448
ε (a.u.)	5.750	0.522	0.020	0.019

Although a study with different basis sets (*e.g.* Dunning/Huzinaga vs Pople) and methods was initially planned, it was postponed as the hydrogen bond distance is extremely sensitive to method, basis set and hydrogen bond cooperativity from neighbouring groups. The hydrogen bond BCP is only visible if the hydrogen bond length is less than 2.1 Å. Nevertheless, all other data appears to be consistent with Table 19, albeit reflecting a weaker R5 compared to the R6 interaction.

High ellipticities for both HF and B3LYP within Table 20 seem to indicate high π -bond order for the hydrogen bond. The ellipticities appear to be significantly greater than observed for formal double (0.45 a.u.) and aromatic (0.23 a.u.) C=C bonds.^[179] The larger ellipticities may reflect the change in atom type. The high π -bond character for the hydrogen bond at first appears to be extremely confusing as hydrogen atoms do not usually possess p -electrons (although empty p -orbitals are available). Since the basis set employs polarising $2p$ and $3d$ electrons for hydrogen and oxygen respectively, the π -bond order may artificially result from the basis set. As mentioned the R5 is weaker than R6 and does not always show if the distance is above 2.1 Å, which could lead to the figures deviating more from the standard bonding types, seen in the distorted bonding paths in Figure 13 (a).

4.7 C6 Interaction

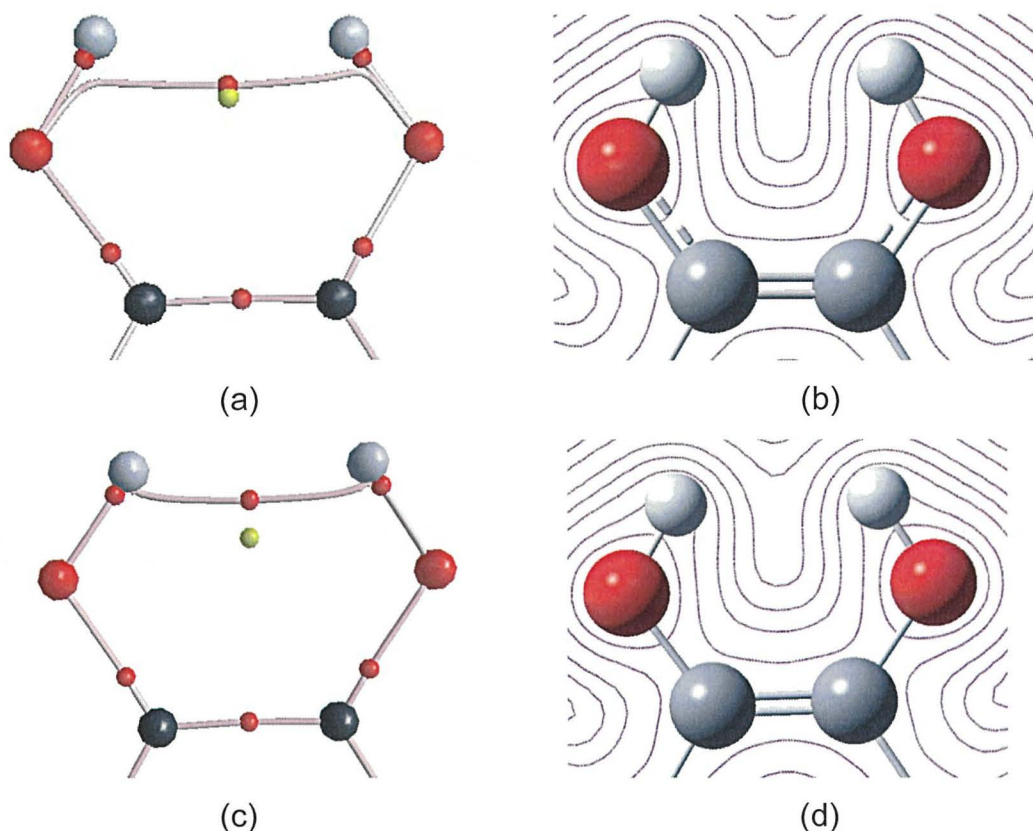


Figure 20. C6 interaction using a 6-311++G(d,p) basis set: (a) HF bond graph, (b) HF electron density contour plot, (c) B3LYP bond graph, (d) B3LYP contour plot

Both B3LYP and HF generate vastly differing pictorial representations (Figure 20) for the C6 interaction. B3LYP again correctly describes a concave bond path (with moderate BCP-RCP distance) in which the proton of the hydroxyl and the proton of the neighbouring hydroxyl. On the other hand, HF describes a convex interaction (with near BCP/RCP coalescence) between the two oxygen atoms, in which the bond paths travel almost parallel to both O-H bonds before deviating away prior to each O-H BCP. This mirrors the two different R5 models (Section 4.6).

High ellipticities (in general agreement with Section 4.6) for both HF and B3LYP are seen within Table 21 indicating possible high π -bond order for the “*anti*-”hydrogen bond.

The nature of close non-bonded hydrogen-hydrogen contacts is ca. 0.3 Å shorter than the sum of the Van der Waals radii.^[195] During a conformational study of cyclohexane, Rzepa^[196] with an on-line blog, questioned whether the hydrogen-hydrogen interaction^[197] within D_{2d} cyclooctane was attractive or repulsive in nature. The symmetric A_1 and antisymmetric B_2 combinations respectively decreased and increased the hydrogen-hydrogen distance. The symmetric vibration was red-shifted relative to the antisymmetric vibration.

In an addendum, Rzepa reported that anharmonic frequencies may cast light on this issue. The argument was as follows:^[196]

“The A_1 vibrational mode decreases both H...H distances simultaneously. If the H...H interaction was attractive, then the potential might be distorted and the mode would be expected to become more anharmonic. The B_2 vibration, for which one H...H distance increases and the other decreases, might self-compensate and the anharmonic correction would be smaller. If the H...H region is in fact repulsive, the reverse would be true, i.e. the A_1 mode would exhibit a smaller anharmonic effect than the B_2 .”

The reported harmonic frequencies for the A_1 and B_2 modes were 3096 cm^{-1} and 3103 cm^{-1} respectively; whilst the reported anharmonic values were 3001 cm^{-1} and 2983 cm^{-1} . Rzepa concluded that the hydrogen-hydrogen interaction is indeed repulsive in nature,^[196] despite the large electron density at the bond critical point normally indicating attraction. The anharmonic correction produced frequencies compatible with experiment.

This agrees with the interpretation that the destabilising C6 interaction is primarily due to Coulombic repulsion, although the covalent nature of hydrogen-hydrogen bond partially (but not fully) stabilises the interaction. Anharmonic frequency calculations were begun but were terminated due to the extremely computational cost.^[171]

Although the electron density at the BCP is low, direct comparison against R6, R5 and OH5 interactions cannot be made due to the different terminal atoms.

Table 21. C6 QTAIM data (quoted to 3 d.p.): distance, r (Å); BCP electron density, ρ_{BCP} (a.u.); Hessian eigenvalue, λ (a.u.); Laplacian, $\nabla^2\rho_{\text{BCP}}$ (a.u.); ellipticity, ε .

Multiple values reported for different hydroxyl groups.

	BCP of C6 interaction	BCP of C6 interaction	BCP of O-H bond on hydroxyl	BCP of O-H bond on hydroxyl
	HF	B3LYP	HF	B3LYP
r (Å)	1.890	1.811	0.937, 0.937	0.961, 0.961
ρ_{BCP} (a.u.)	0.014	0.016	0.393, 0.394	0.368, 0.367
λ_1 (a.u.)	-0.016	-0.019	-2.130, -2.135	-1.785, -1.792
λ_2 (a.u.)	-0.004	-0.012	-2.084, -2.091	-1.748, -1.753
λ_3 (a.u.)	0.082	0.085	1.283, 1.285	1.028, 1.031
$\nabla^2\rho_{\text{BCP}}$ (a.u.)	0.062	0.054	-2.931, -2.941	-2.505, -2.514
ε (a.u.)	3.000	0.583	0.022, 0.021	0.021, 0.022

4.8 OH5 Interaction

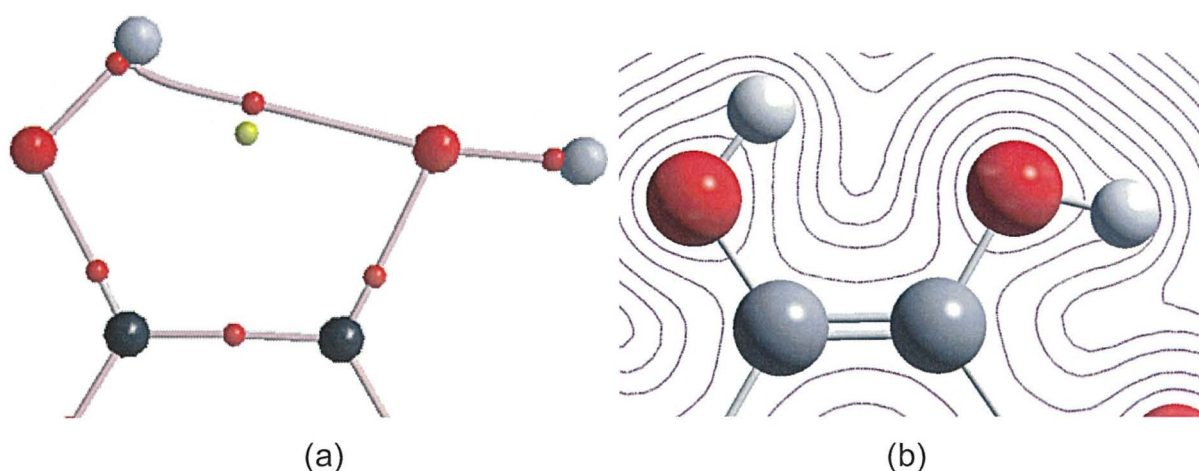


Figure 22. B3LYP/6-311++G(d,p) OH5 interaction: (a) bond graph; (b) contour plot.

The BCP and RCP for the OH5 interaction do not appear for HF/6-311++G(d,p).

The OH5 interaction (Figure 22) is not observed for HF/6-311++G(*d,p*) dihydroxy-1,4-naphthoquinone isomers due to the hydrogen bond distance being larger than the perceived AIM2000 cut-off of 2.1 Å. This does not imply that the OH5 interaction will never be observed using HF theory for larger substitutions, as hydrogen bond cooperativity between neighbouring groups can promote or thwart hydrogen bonding. OH5 interactions observed for higher polyhydroxy-1,4-naphthoquinones appear to possess similar properties to the R5 interaction (Section 4.6), albeit with weaker hydrogen bonds.

The bond path between the donor proton and the BCP appears to be slightly concave in nature, whilst the corresponding bond path between BCP and acceptor oxygen appears to be linear. The relatively small BCP-RCP distance again reflects the weak nature of the OH5 interaction, which appears to possess significant π -bond character (Table 22) in accord with previous R5 (Section 4.6) and C6 (Section 4.7) B3LYP results.

Table 22. OH5 QTAIM data (quoted to 3 d.p.): distance, r (Å); BCP electron density, ρ_{BCP} (a.u.); Hessian eigenvalue, λ (a.u.); Laplacian, $\nabla^2\rho_{\text{BCP}}$ (a.u.); ellipticity, ε .
Multiple values reported for different hydroxyl groups.

	BCP of Hydrogen Bond	BCP of O-H bond on hydroxyl
r (Å)	2.061	0.968, 0.963
ρ_{BCP} (a.u.)	0.021	0.261, 0.364
λ_1 (a.u.)	-0.024	-1.808, -1.815
λ_2 (a.u.)	-0.013	-1.773, -1.776
λ_3 (a.u.)	0.135	1.037, 1.046
$\nabla^2\rho_{\text{BCP}}$ (a.u.)	0.098	-2.544, -2.545
ε (a.u.)	0.846	0.020, 0.022

4.9 M4 and OO4 Interactions

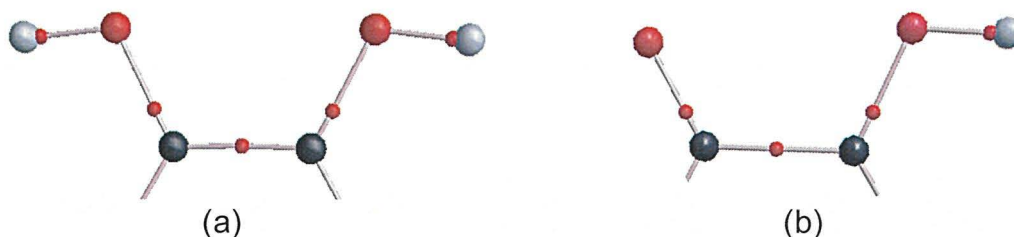


Figure 23. HF and B3LYP/6-311++G(*d,p*) bond graphs: (a) M4; (b) OO4.

The 4-membered M4 and OO4 interactions (Figure 23) appear to be non-bonding due to the lack of any BCP / RCP between the two oxygen atoms, due to mismatch with known distance and angle criteria for hydrogen bonds.^[198,199]

Mills and Dean's^[198] work covers the use of derived spaces that hydrogen bonds can form within and the bonding propensity (natural tendency) for the atoms in question. This gives rise to a set of data that contains the determined angles and distances that work for hydrogen bonding with their respective atom types. The work further goes on to use this data as a method of testing bond in molecular similarity studies.

The reasoning detailed in Mills and Dean's^[198] work supports the original assumption that M4 and OO4 are baseline interactions as the bonding for these interactions is highly unlikely to take place given the angles and distances involved. Therefore within the bond counting rule the use of these as baseline interactions still holds true (Section 2.3). Since OO4 and R5 are mutually exclusive, the OO4 term was replaced by a single positional term within the bond counting rule.

4.10 OO5 Interaction

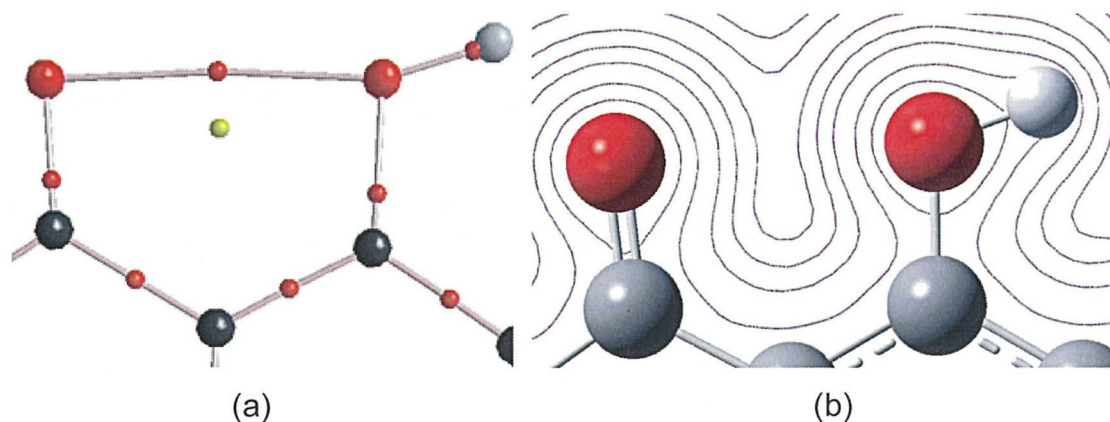


Figure 24. OO5 interaction for both HF and B3LYP methods using a 6-311++G(*d,p*) basis set: (a) bond graph, (b) electron density contour plot

In a similar vein to R5 and OO4, the previously observed but unclassified^[30] OO5 partial oxygen-oxygen interaction (Figure 24) is a baseline for the R6 term within the bond counting rule. The BCP-RCP distance lies between that of the R6 and R5 (or OH5) interactions, indicating that the closed-shell interaction is moderate in strength.

Table 23. OO5 QTAIM data (quoted to 3 d.p.): distance, r (Å); BCP electron density, ρ_{BCP} (a.u.); Hessian eigenvalue, λ (a.u.); Laplacian, $\nabla^2\rho_{\text{BCP}}$ (a.u.); ellipticity, ε . Multiple values reported for different hydroxyl groups.

	BCP of OO5 interaction		BCP of O-H bond on hydroxyl	
	HF	B3LYP	HF	B3LYP
r (Å)	2.672	2.673	0.941	0.964
ρ_{BCP} (a.u.)	0.014	0.014	0.390	0.366
λ_1 (a.u.)	-0.012	-0.012	-2.136	-1.797
λ_2 (a.u.)	-0.012	-0.012	-2.093	-1.761
λ_3 (a.u.)	0.090	0.086	1.294	1.028
$\nabla^2\rho_{\text{BCP}}$ (a.u.)	0.066	0.062	-2.935	-2.53
ε (a.u.)	0.000	0.000	0.021	0.020

The zero ellipticity (Table 23) indicates zero double bond character between the two oxygen atoms. It is unknown whether the interaction is truly attractive or repulsive in nature. A study of the harmonic and anharmonic vibrational modes (Section 4.7) may illuminate this.

4.11 Summary

Each interaction present within the bond counting rule has been characterised using QTAIM. Additionally, the OO5 and OO4 baseline interactions were also investigated during this investigation. The relative stability's and bonding paths were probed to give further information into the nature of the bonding present with each interaction.

Although all interactions appeared to be closed-shell in nature, the attractive or repulsive character of the C6 and OO5 interactions are still unclear. The 4 and OO4 interactions gave no results for any type of bonding taking place, therefore providing support to the fact that these interactions are to be used as baselines within the bond counting rule. Nevertheless, the QTAIM analyses agree with relative bond counting rule energies (Chapter 2) and vibrational frequencies (Chapter 3), which can aid the definition of baselines.

The ellipticity of the interaction however gave mixed results depending on the strength and atoms involved. There seems to be a discrepancy with how weaker forces are to be characterised using this method, if they can be at all. As seen with all but the R6 and OO5 the visible interactions have a large π -bond character, this might be due to the ring and bond critical points coalescing as mentioned previously in Section 1.6 .

Although relative conformer energies provide a clue as to the shape of the potential energy surface and any associated rotational barriers are still left unknown. A comprehensive survey follows in Chapter 5 in which state-of-the-art graphic and haptic scientific visualization techniques are used in conjunction with rotational energy calculations.



Chapter

V

Chapter 5 - Methodology for the use of PES

5.1 Introduction

Stationary points have been investigated in Chapters 2 and 4, in Chapter 2 energies of specific planar stationary points were examined. Although relative energies of conformers may provide a clue towards rotational barriers^[200] and the topology of a potential energy surface (PES) in general, this chapter seeks to probe polyhydroxy-1,4-naphthoquinones further.

The output took the form of 1-D and 2-D relative potential energy scans depending upon the number of hydroxyl groups to be rotated. The scans were performed using Gaussian.^[169] 1-D scans produced a 2-D graph which plotted the relative energy against a given dihedral angle, an example is shown in Figure 25. This output is easy to visualize using a simple graphing tool, such as *Excel* or *GnuPlot*. The more problematic scans to visualize came from the 2-D scans as these needed to be visualized as 3-D hyper-surfaces. The 1-D scans were performed with either HF or DFT at a basis set of 6-311++G(d,p), whilst the 2-D scans were performed with HF/6-31G(d) basis set to save computational cost.

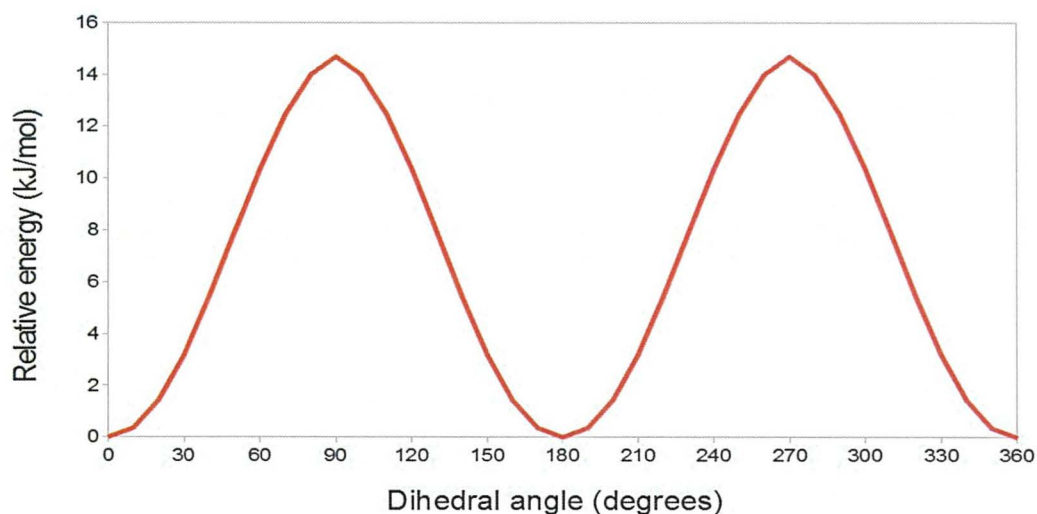


Figure 25. Example of a plotted 1D scan. B3LYP/6-311++G(d,p) PES scan for rotation of C-O bond in phenol.

One analogy for a 3D potential energy hyper-surface is to think of a geographical landscape consisting of hills and valleys^[201,202]. The height of the landscape represents the relative energy that is present at a given location, the directions north to south and east to west therefore represent the two independently scanned variables or geometrical parameters. In this case the geometrical parameters that were scanned were the dihedral angles for the hydroxyl groups in question within the molecule.

However this method is not just limited to the dihedral angles other internal and external coordinates that can be used^[203,204] are:

- bond length
- bond angle
- dihedral angle
- out-of-plane distance

A resulting PES can have many points of interest found within them, these points of interest can give a greater level of understanding to the topic that is being investigated within the hyper-surface. The most important of these points of interest is the global minimum, which corresponds to the most stable molecular configuration from within the scanned perimeters. Other interesting features that can be studied on a PES surface are the low energy reaction or rearrangement pathways that are seen as reaction coordinates on the surface. Local minima can also be seen that can be interpreted as reactive intermediates, the last main features that can be located are the saddle points or maxima that correspond to transition state structures high in energy.

5.2 Design of parser

5.2.1 Data manipulation

For this approach to work for the 2D scans a few different methods were investigated to try and determine the best method that could be employed for different situations. To aid in this process a Python based parsing tool had to be created that can be found in Appendix 1. The main point of the Python parser was to take the Gaussian output file and then convert this data into these different formats:

- A CSV file format that could be read by GNUPlot
- A VRML file format for 3D visualization
- A X3D file format for better 3D visualization but less accessibility
- A H3D file format that would allow for 3D Haptic rendering for tactile feedback

While haptically probable potential energy surfaces have been created before it presented a haptic quantum chemical approach for the study of chemical reactivity,^[205,206] through the use of novel computational methods in C++.

The first problem for the parser was to find the energy outputted by the Gaussian program as this can be found in two locations both with the output file. each location has its own set of advantages and disadvantages.

Firstly the data is outputted in grid format along with the z-matrix conformation. The advantage of looking here is that the data is numerically order and that the parameters that were been probed can also be checked. The disadvantage of this location is that if the energy of the system is greater than -9999.99 the output will not be printed and will be replaced with *****, meaning that the data can no longer be read from this point.

The second location is within the data file can be found at the end in a dump format along with all the other different types of output that are created within the scan. The

advantage of looking here is that no matter how large the energy gets it will always be printed out. The disadvantage is that the energies cross line breaks and is harder to extract, as well as an error within Gaussian that sometimes causes this data dump not to be outputted. In response to these facts it was chosen then the parser would first try for the data from the dump section of the file by amalgamating every line together and then removing white spaces, after this was done the section can be then split by a delimiter of “//” that breaks every section apart. This data now in list format had each value checked to see if there was the unique character set of “HF=” when this was found the values for all the points could then be extracted from this section and stored.

If this section did not exist, the parser would then try to read the data from the grid section, while this has the advantage for having data that was easy to extract by only having to check for a specific number lines after a break, and then store the data. However if the parser found that this section had the ***** format for its energies it would then inform the user that there was no way to extract the data and then close without performing any further operations.

The next task for the parser is to determine the maximum and minimum energy values for the scanned coordinates. This allows the resulting 3D plot to be scaled to fit with a certain area by making all the energies relative to the global minimum, this is done by subtracting the minimum energy located from every energy that was found. To allow any 3D plot to be view this way a maximum height was chosen to keep the plot with a viewable area for the screen when outputted, this is done by generating a scaling factor for every plot that the parser runs on.

The minimum is taken away from the maximum to give the range of values that are present this is then used as a variable in the working out of the scaling factor. By having the maximum range allowed to be divided by the known range for the data the resulting value is then used as the scaling factor by which all data values are then multiplied by.

5.2.2 Colour scaling

Using this now calibrated data height a colouring factor can now be generated that will colour the VRML, X3D and H3D plots, by using a rainbow colour mapping system the lowest points will look dark purple and the highest will be red. The different colour gradients generated within this allow the user to see more detail on the slopes and ridges of the plot, as if the colour change is very gradual then a gentle gradient is present, if however the colours change is very rapid then it can be determined that the gradient is very steep.

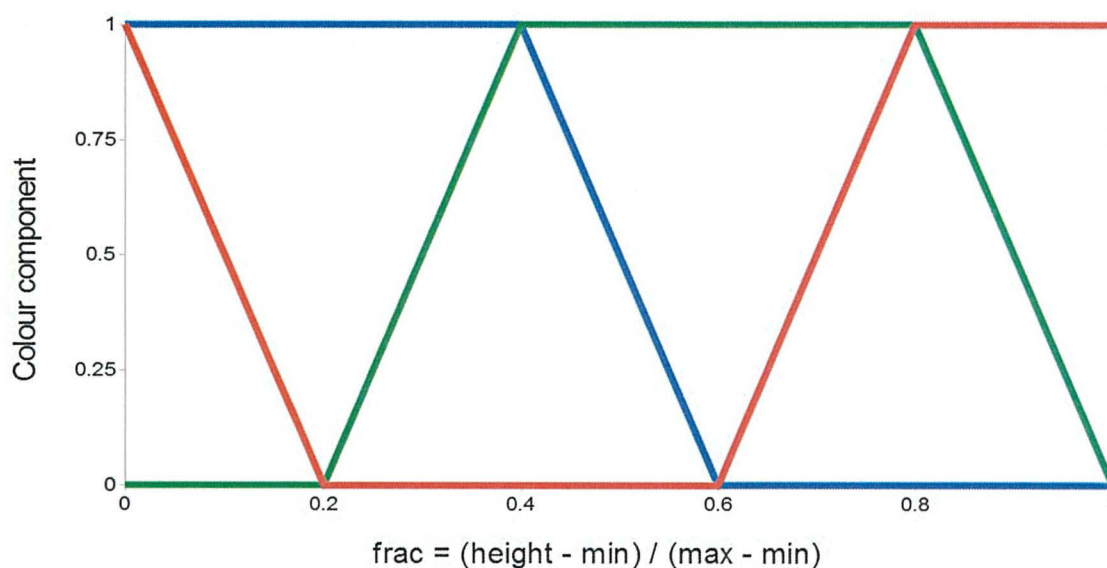


Figure 26. Rainbow colour mapping chart

5.2.3 Output types

The first type of output that can be generated is the GNUPlot .csv file formats, this has a range of further options available to the user:

- Output the energies in Hartrees without any formatting
- Output the energies in relative energies in Hartrees
- Output the energies in relative kCal per mole
- Output the energies in relative kJ per mole

5.2.3.1 CSV format

For each of the different outputs the data is given as a three column .csv file format with the first and second columns been the scanned coordinates and the final column been the energy with the appropriated scaling applied.

There is however one extra piece of formatting that needs to be done to the data to make it compatible with the GNUPlot program. This is the fact that after every full scan of the second coordinate the data must then be reversed, giving a snaking pattern to the data instead of the general line by line approach.

To accommodate for this a double looping system was employed and if the outer loop was an even number then the data would be done in the standard forward method, however if the outer loop was odd then the data would go in the reverse fashion. The method chosen to achieve this was to shift the data to the final value of that row and then minus the inner loop value instead of the normal addition for the even rows.

To test this approach two methods of viewing the resulting output data were generated, the first was a simple contour plot for the data, this method allows the user to view the data as if looking at an ordnance survey map, shown in Figure 27.

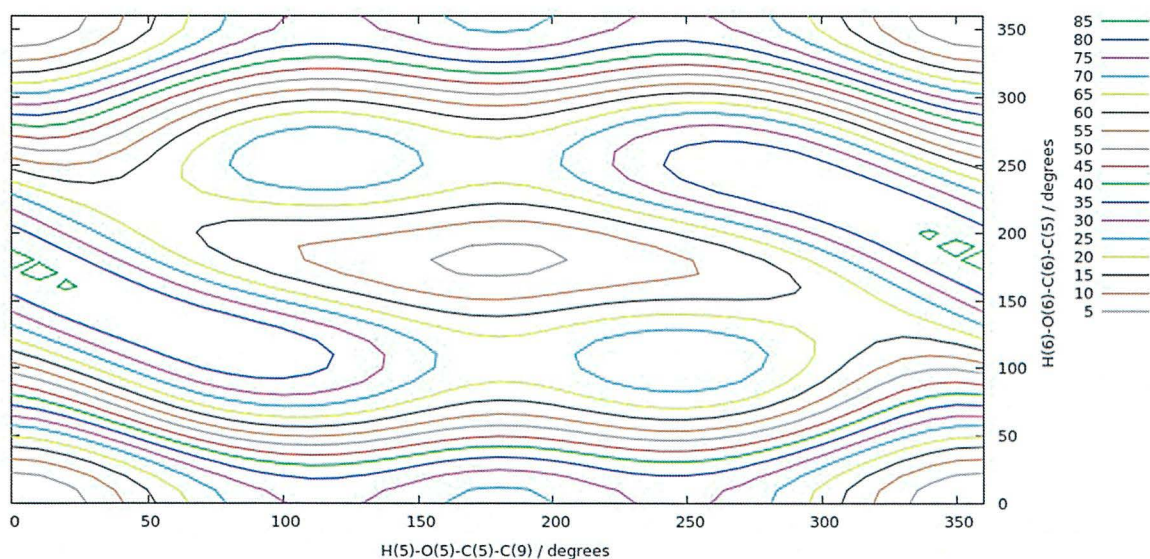


Figure 27. Contour plot of 5,6-dihydroxy-1,4-naphthoquinone

The second method allows the user to view the data as a wireframe 3D graph plot, this plot does not however employ the colour gradient scheme previously mentioned. While both of these methods allow for quick and easy data viewing, without the need for unconventional software, the other methods shown later in this chapter give a better visualization of the data for presentations or additional features not available within GNUPlot.

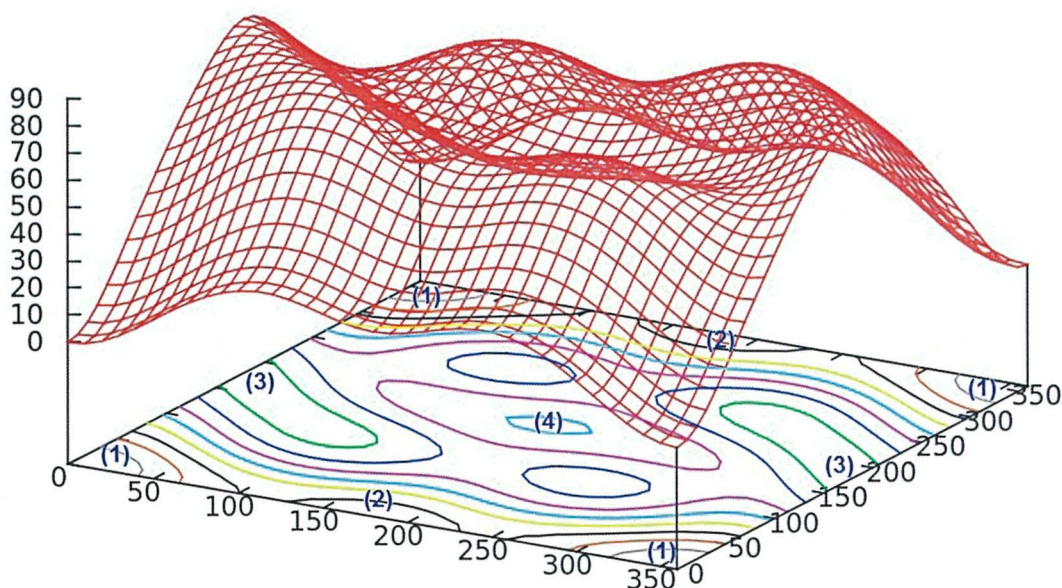


Figure 28. Wireframe GNUPlot of 5,6-dihydroxy-1,4-naphthoquinone

5.2.3.2 VRML format

The second type of output that can be generated by the python parser is the VRML .wrl file format; this has a range of further options available to the user:

- Output the surface as a set of points
- Output the surface as a wireframe
- Output the surface as a normal solid surface

For this section new information has to be constructed depending on the option selected. For the point surface output only the x , y and z coordinates need to be given along with the colours for every point. Through the use of the nested looping system a method was devised that not only added the correct data for the point but also worked out the x and y coordinates from the step counter for the loop.

This data was then added to a string variable so that it could be inserted later into the file that is being generated. The colours that had been previously calculated would now be used and added into the generation of the output file to give each point an emissive colour.

For the second option an extra data set is needed to be generated as well as the two previously mentioned data sets (points and colours). This new data set is the data that allows the VRML program to generate the wireframe surface by specifying the points the lines need to be drawn between. First the horizontal lines need to be generated by giving each point along the row by recording each x coordinate and then when the row is done moving on to the next one by adding a number of values in a row.

```
for i in range(0,37):
    val = i*37
    lines1 = lines1 + "\t\t\t"
    for j in range(0,37):
        lines1 = lines1 + str(val + j)+", "

    lines1 = lines1 + "-1,\n"
```

Code Extract 1. Generation of Horizontal lines

As seen in Code Extract 1 this was done through the use of loops, i is the current row number, val stores the amount that needs to be added on to retrieve the data from the set of points and j steps through the number with the line. The final line adds on a "-1" value which is used within VRML to indicate that that is the end of the current line. The same procedure is then carried out on the vertical lines and is then stored as a single text string with all the line data contained within.

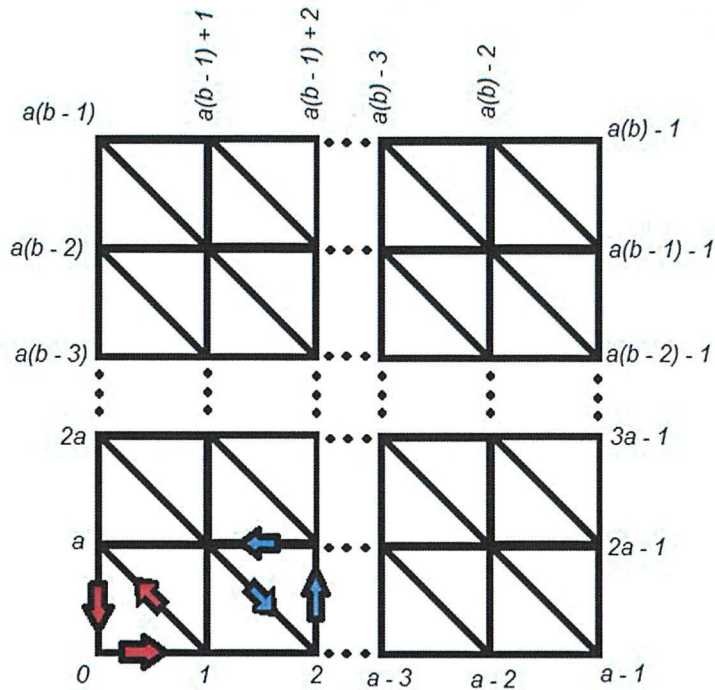


Figure 29. Rectangular $a \times b$ grid construction including 'up' (red) & 'down' (blue) triangles.

5.2.3.3 X3D/H3D format

The final option is a data set that allows the generation of the surface plot with VRML, to do this sets of triangles need to be created that then build up across the grid of points. One thing to note when the triangles are generated is that two sets of triangles are made for each pair of rows and both must be made with the same rotational pattern as shown in Figure 29. This is done using similar methods to the generation of the lines, for full coding see Appendix 1.

After the correct types of data sets are generated these are then written into a new text file with all the information that is needed to generate the correct data type with the VRML program. This was done to automate the process of generating multiple output types for users that had little or no programming skills while still allowing them the benefit of using this type of file format. The image shown in Figure 30 shows a surface plot from the VRML output file.

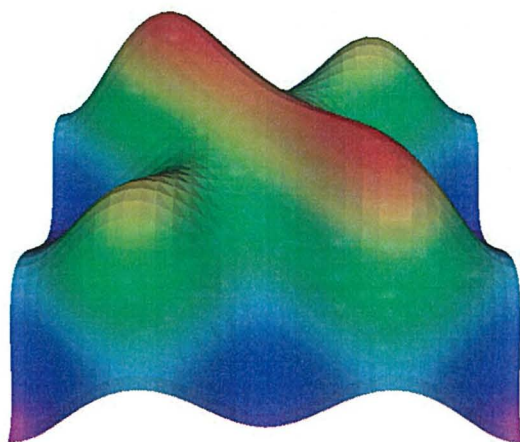


Figure 30. VRML output of 2,3-dihydroxy-1,4-naphthoquinone.

The final two data types, X3D and H3D, use the same coding style. The same data sets were needed as described for the VRML data. The only differences are when the text file is been written as the coding is slightly different from the VRML output. Another difference is when the H3D output is selected an extra line stating that the surface is to become a simple smooth surface, this allows the use of a haptics device to “feel” the virtual surface.

The surface output is also tiled to allow the user to correctly file the points of interest that would have been at the edge, where the haptics stylus could disengage from the surface, not allowing the user to fully feel and identify these points. The 2 x 2 tiling removed this problem but putting one corner of the plot in the middle and place the other 3 plots around it, shown in Figure 31. Without this tiling effect, the valley running down the centre of the model in Figure 31 would not be “Feelable”, as there would only be one side of the valley. The use of haptics for teaching and demonstrations has been done previously.^[207-211]

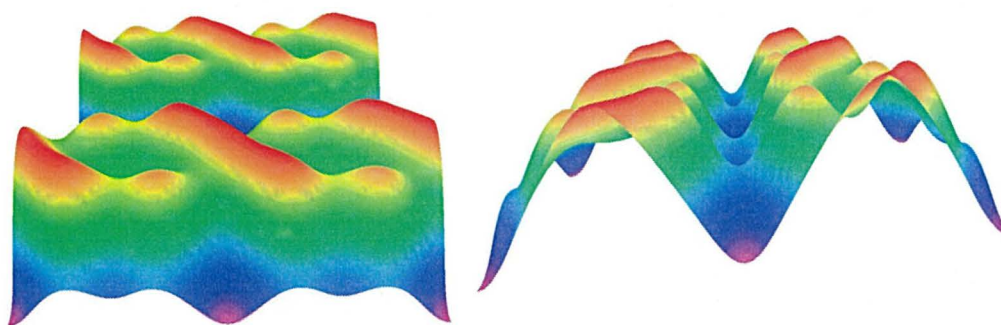


Figure 31. X3D output of 5,6-dihydroxy-1,4-naphthoquinone.

5.3 Results and Discussion

5.3.1 1-D scans

A simple 2-D plot comprising a series of 1-D scans depicting rotation of C-O bonds (C-C-O-H dihedral angle) for each hydroxyl group within hydroxy-1,4-naphthoquinone is shown in Figure 32.

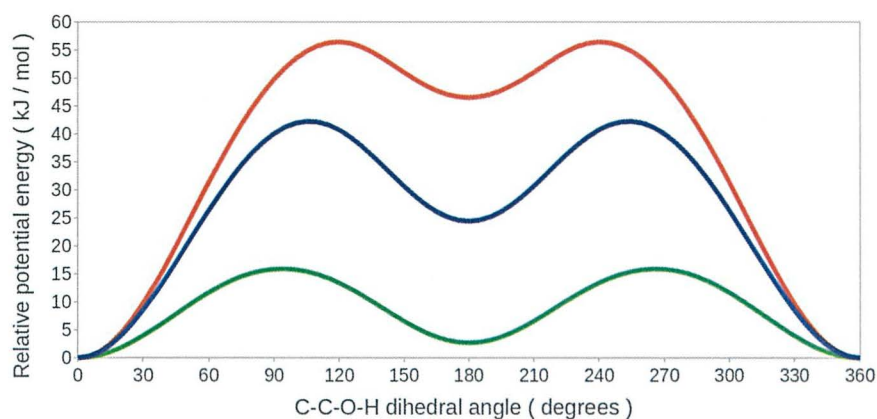


Figure 32. Variation of HF/6-31G(d) potential energy (kJ mol^{-1}) vs C-C-O-H dihedral, for hydroxy-1,4-naphthoquinones: 2(α)-position (blue), 5(β)-position (red), 6(γ)-position (green). Potential energy is quoted relative to the global minimum for each positional isomer

The barrier to rotation for the 2-Hydroxy-1,4-naphthoquinone is *ca.* 42 kJ mol^{-1} , with a late (105°) transition structure. The barrier to free rotation reflects the strength of the 5-membered intramolecular hydrogen bond between O-H and C=O which must be broken for free rotation to occur. The 5-Hydroxy-1,4-naphthoquinone rotational barrier is *ca.* 56 kJ mol^{-1} , with a later (120°) transition structure. The high rotational barrier reflects the increased strength of the 6-membered intramolecular hydrogen bond which must be broken for free rotation to occur. Due to the lack of hydrogen bonding within 6-hydroxy-1,4-naphthoquinone, a small rotational barrier of *ca.* 16 kJ mol^{-1} , with a slightly late (95°) transition structure, giving rise to free rotation.

5.3.2 2-D non-interacting results

5.3.2.1 2,5- and 2,8-dihydroxy-1,4-naphthoquinone

2-D contour and 3-D surface plots depicting extremely similar C-C-O-H torsional scans for each hydroxyl group in both 2,5- and 2,8-dihydroxy-1,4-naphthoquinone are shown in Figures 33 and 34 respectively.

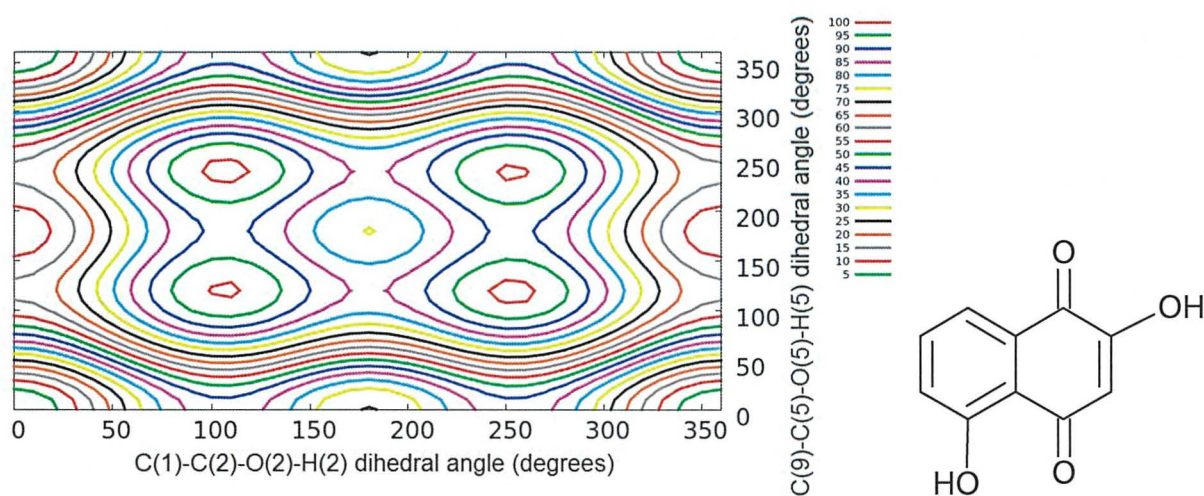


Figure 33. Variation of HF/6-31G(d) potential energy (kJ mol⁻¹) vs C-C-O-H dihedral for 2,5-dihydroxy-1,4-naphthoquinone as a contour plot.

Potential energy is quoted relative to the global minimum.

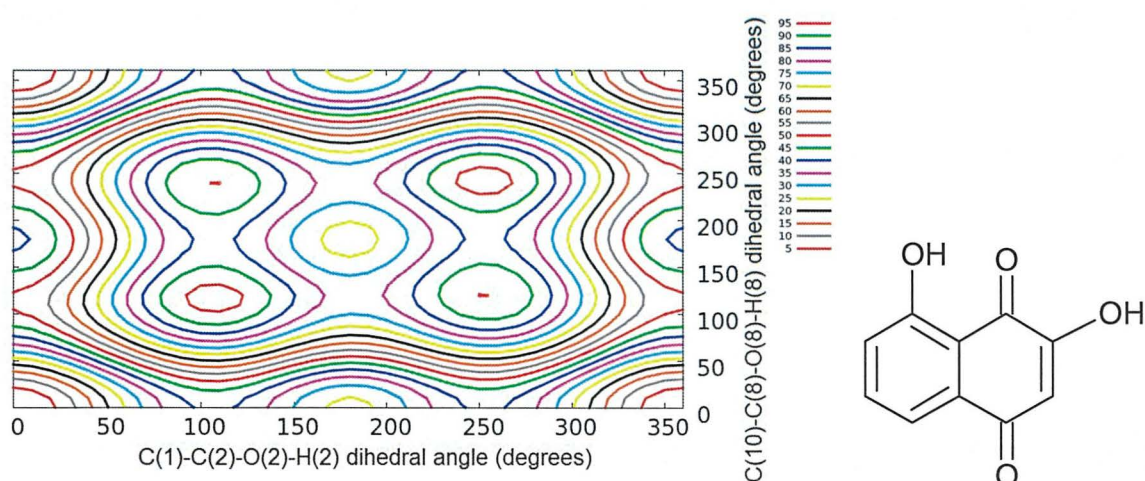


Figure 34. Variation of HF/6-31G(d) potential energy (kJ mol⁻¹) vs C-C-O-H dihedral for 2,8-dihydroxy-1,4-naphthoquinone as a contour plot.

Potential energy is quoted relative to the global minimum.

A classic “egg box” shape can be observed for the PES (Figure 35) that is indicative of non-interacting hydroxyl groups. The steep gradients indicate large rotational barriers for the 5- or 8- (β) position with moderate gradients / rotational barriers for the 2- (α) position. Both barriers reflect the activation energy required to break the intramolecular hydrogen bonds prior to free rotation. Four planar minima can be identified for both 2,5- and 2,8- dihydroxy-1,4-naphthoquinone corresponding to:

- a) Strongly & moderately stabilising 6- & 5-membered $\text{OH}\cdots\text{O}=\text{C}$ hydrogen bond (R6 & R5 respectively)
- b) One strongly stabilising 6-membered $\text{O}-\text{H}\cdots\text{O}=\text{C}$ hydrogen bond (R6) and one base-line 4-membered $\text{H}-\text{O}\cdots\text{O}=\text{C}$ (OO4)
- c) Moderately stabilising 5-membered $\text{O}-\text{H}\cdots\text{O}=\text{C}$ hydrogen bond (R5) & base-line 5-membered $\text{H}-\text{O}\cdots\text{O}=\text{C}$ (OO5)
- d) Base-line 4-membered $\text{H}-\text{O}\cdots\text{O}=\text{C}$ (OO4) & base-line 5- membered $\text{H}-\text{O}\cdots\text{O}=\text{C}$ (OO5)

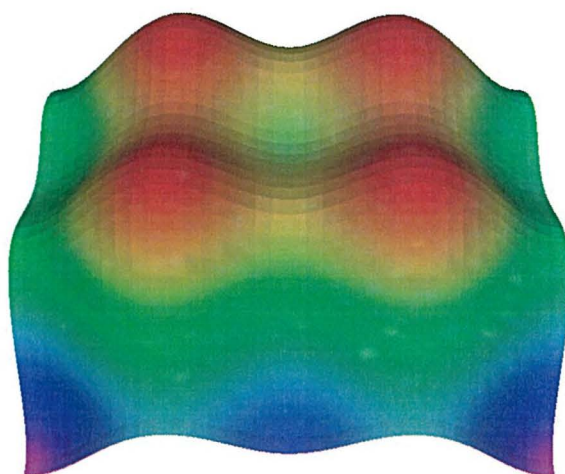


Figure 35. Variation of HF/6-31G(d) potential energy (kJ mol^{-1}) vs C-C-O-H dihedral for 2,8-dihydroxy-1,4-naphthoquinone as a VRML surface. Image identical to 2,5- dihydroxy-1,4-naphthoquinone so omitted for clarity.

Potential energy is quoted relative to the global minimum.

5.3.2.2 2,6- & 2,7-Dihydroxy-1,4-naphthoquinone

The 2-D contour and 3-D “egg box” surface plots depicting nigh identical C-C-O-H torsional scans for each hydroxyl group in both 2,6- (Figure 36) and 2,7-dihydroxy-1,4-naphthoquinone (Figure 37).

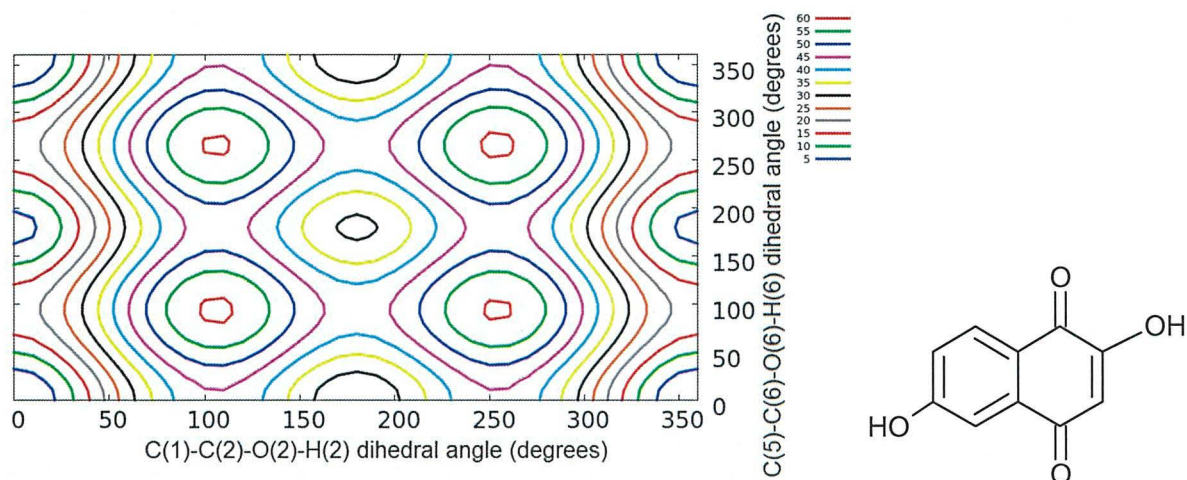


Figure 36. Variation of HF/6-31G(d) potential energy (kJ mol⁻¹) vs C-C-O-H dihedral for 2,6-dihydroxy-1,4-naphthoquinone as a contour plot. Potential energy is quoted relative to the global minimum.

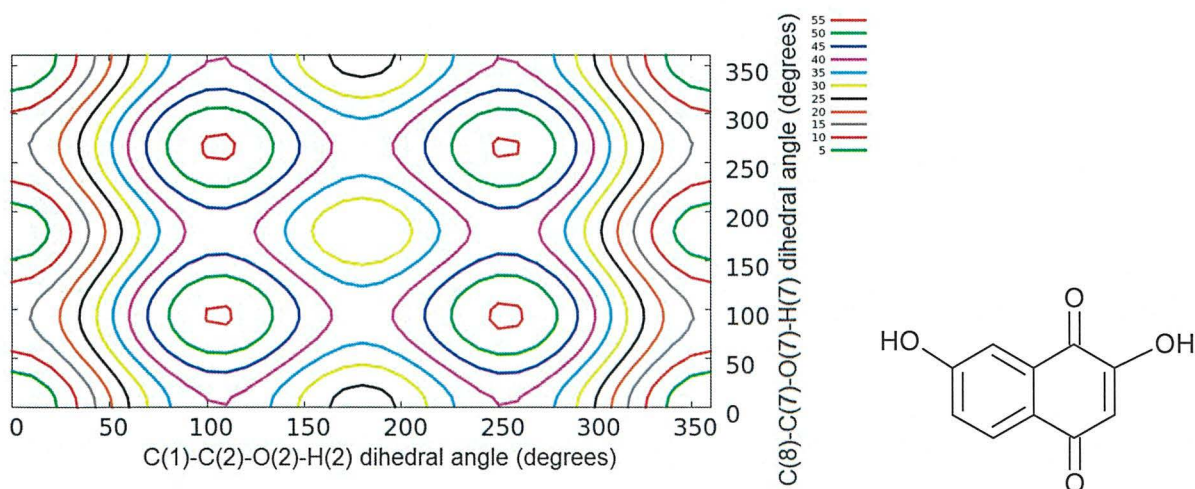


Figure 37. Variation of HF/6-31G(d) potential energy (kJ mol⁻¹) vs C-C-O-H dihedral for 2,7-dihydroxy-1,4-naphthoquinone as a contour plot. Potential energy is quoted relative to the global minimum.

The high identical energies for each maxima indicate that the hydroxyl groups are non-interacting. A shallow gradient is observed for the 6- or 7- (γ) position indicating negligible rotational barriers (*i.e.* free rotation). A moderate gradient / barrier for the 2- (α) position, reflects the activation energy required to break the intramolecular hydrogen bond prior to free rotation. Four planar minima can again be identified for both 2,6- and 2,7-dihydroxy-1,4-naphthoquinone (Figure 38), due to the fact that the 6- or 7- (γ) position has no way to hydrogen bond in this configuration only one interaction is observed for each minima:

- a) Moderately stabilising 5-membered O-H \cdots O=C hydrogen bond (R5)
- b) Moderate stabilising 5-membered O-H \cdots O=C hydrogen bond (R5)
- c) Base-line 4-membered H-O \cdots O=C (OO4)
- d) Base-line 4-membered H-O \cdots O=C(OO4)

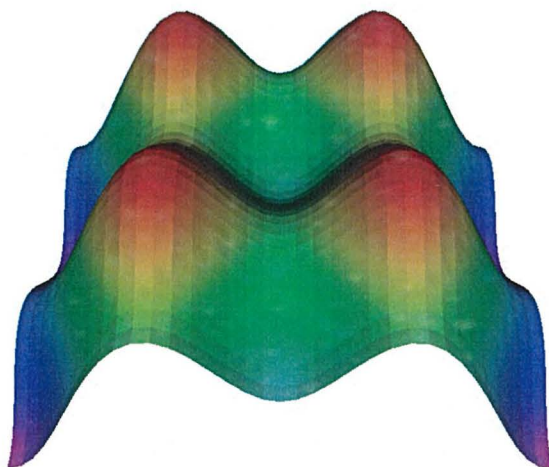


Figure 38. Variation of HF/6-31G(d) potential energy (kJ mol^{-1}) vs C-C-O-H dihedral for 2,6-dihydroxy-1,4-naphthoquinone as a VRML surface. Image identical to 2,7- dihydroxy-1,4-naphthoquinone so omitted for clarity.

Potential energy is quoted relative to the global minimum

5.3.2.3 5,7-Dihydroxy-1,4-naphthoquinone

2-D contour and 3-D surface plots depicting C-C-OH torsional scans for non-interacting hydroxyl groups in 5,7-dihydroxy-1,4-naphthoquinone (Figure 39).

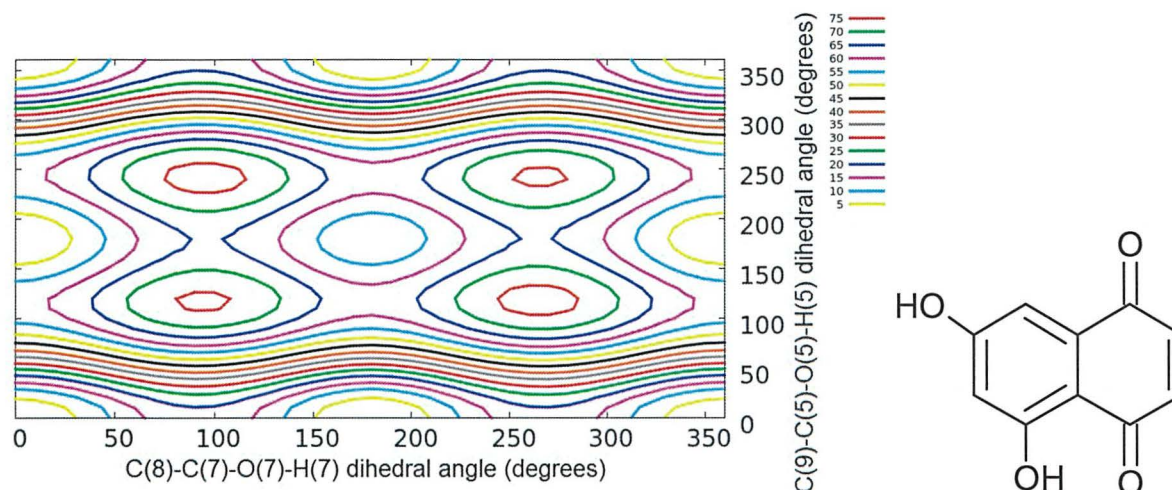


Figure 39. Variation of HF/6-31G(d) potential energy (kJ mol^{-1}) vs C-C-O-H dihedral for 5,7-dihydroxy-1,4-naphthoquinone as a contour plot. Potential energy is quoted relative to the global minimum

The “egg box” surface is once again present within both the contour and PES plots. The slight gradients one again indicating negligible barriers (free rotation) is observed for the 7- (γ) position. While steep gradients (large barriers to free rotation) are seen for the 5- (β) position reflecting the large activation energy required to break the R6 intramolecular hydrogen bond prior to free rotation. Four planar minima can be identified (Figure 40), with the 7- (γ) position been once again unable to hydrogen bond only one interaction is seen per minima:

- Strongly stabilising 6-membered $\text{O-H}\cdots\text{O}=\text{C}$ hydrogen bond (R6)
- Strongly stabilising 6-membered $\text{O-H}\cdots\text{O}=\text{C}$ hydrogen bond (R6)
- Base-line 5-membered $\text{H-O}\cdots\text{O}=\text{C}$ (OO5)
- Base-line 5-membered $\text{H-O}\cdots\text{O}=\text{C}$ (OO5)

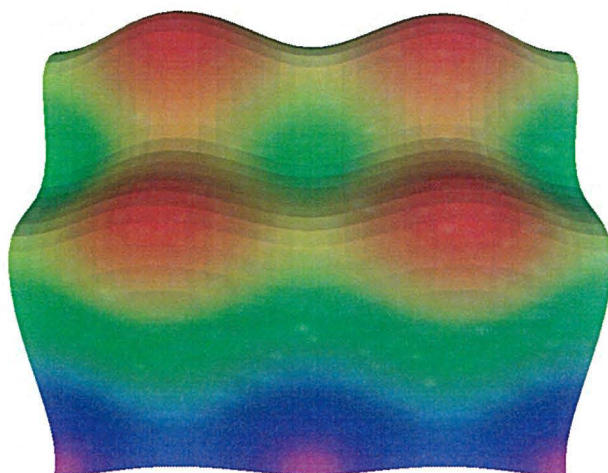


Figure 40. Variation of HF/6-31G(d) potential energy (kJ mol^{-1}) vs C-C-O-H dihedral for 5,7-dihydroxy-1,4-naphthoquinone as a VRML surface. Potential energy is quoted relative to the global minimum

5.3.2.4 5,8-Dihydroxy-1,4-naphthoquinone

The final non-interacting 2-D contour and 3-D surface plots depicts C-C-O-H torsional scans for naphthazarin, 5,8-dihydroxy-1,4-naphthoquinone (Figure 41).

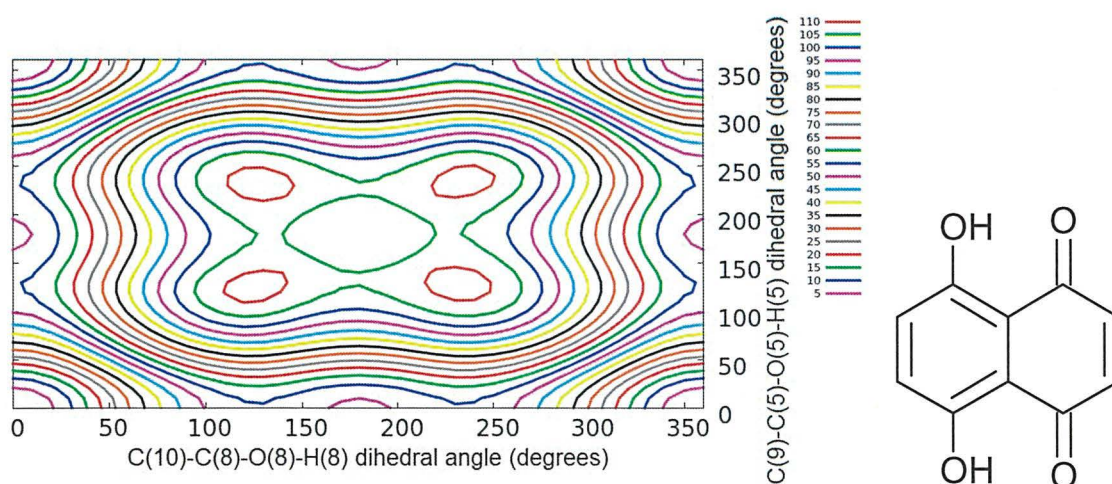


Figure 41. Variation of HF/6-31G(d) potential energy (kJ mol^{-1}) vs C-C-O-H dihedral for 5,8-dihydroxy-1,4-naphthoquinone as a contour plot. Potential energy is quoted relative to the global minimum

The presence of degenerate structures generates a symmetric PES for this scan. Large rotational barriers (steep gradients) show the activation energy required to break the R6 intramolecular hydrogen bond prior to free rotation, observed for both the 5- and 8- (β) positions which are equivalent. Three unique planar minima can be identified (Figure 42):

- a) Two strongly stabilising 6-membered $\text{O-H}\cdots\text{O}=\text{C}$ hydrogen bonds (R6)
- b) One strongly stabilising 6-membered $\text{O-H}\cdots\text{O}=\text{C}$ hydrogen bond (R6) and one base-line 5-membered $\text{H-O}\cdots\text{O}=\text{C}$ (OO5)
- c) Two base-line 5-membered $\text{H-O}\cdots\text{O}=\text{C}$ (OO5)

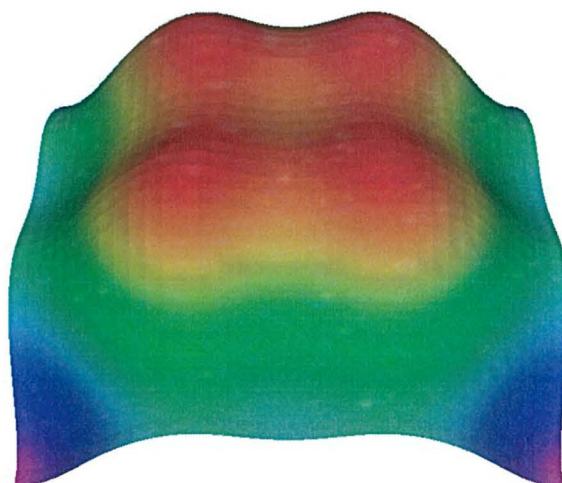


Figure 42. Variation of HF/6-31G(d) potential energy (kJ mol^{-1}) vs C-C-O-H dihedral for 5,8-dihydroxy-1,4-naphthoquinone as a VRML surface. Potential energy is quoted relative to the global minimum

5.3.3 2-D interacting results

5.3.3.1 2,3-Dihydroxy-1,4-naphthoquinone

2-D contour and 3-D surface plots depicting C-C-O-H torsional scans for each hydroxyl group in 2,3-dihydroxy-1,4-naphthoquinone, Figure 43.

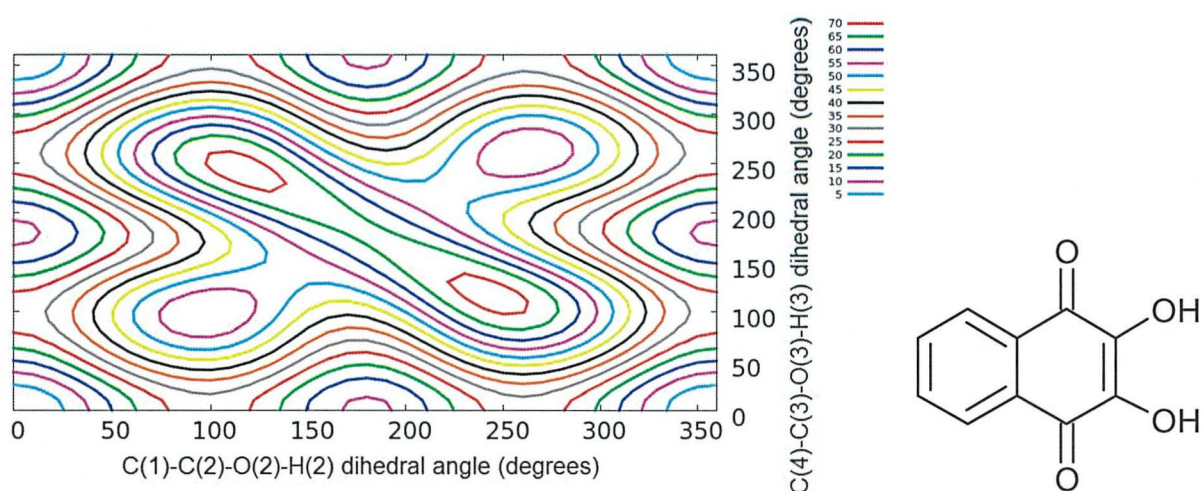


Figure 43. Variation of HF/6-31G(d) potential energy (kJ mol^{-1}) vs C-C-O-H dihedral for 2,3-dihydroxy-1,4-naphthoquinone as a contour plot.

Potential energy is quoted relative to the global minimum

The complex shape of the PES is indicative of interacting, neighbouring hydroxyl groups, whilst a degenerative structure still allows the generation of a symmetric PES (Figure 44). Moderate gradients and rotational barriers are observed for the equivalent 2- and 3- (α) positions. The 5-membered O-H \cdots O-H hydrogen bond (OH5) is ca. 9 kJ mol^{-1} less stable than the 5-membered O-H \cdots O=C hydrogen bond (R5). The non-planar global (co-parallel) and local (anti-parallel) maxima have energies of 72 kJ mol^{-1} and 59 kJ mol^{-1} respectively, which are lower than predicted (ca. 84 kJ mol^{-1} using the barriers from Section 5.3.1), indicating stabilising interactions are taking place. A destabilising interaction is evident for C6 which is the “anti-“ hydrogen bond, ca. 18 kJ mol^{-1} less stable than expected.

Three unique planar species can be identified (Figure 44):

- a) Two moderately stabilising 5-membered $\text{O-H}\cdots\text{O}=\text{C}$ hydrogen bonds (R5) and one base-line 4-membered $\text{H-O}\cdots\text{O-H}$ (M4)
- b) One moderately stabilising 5-membered $\text{O-H}\cdots\text{O}=\text{C}$ hydrogen bond (R5), one weakly stabilising 5-membered $\text{O-H}\cdots\text{O-H}$ hydrogen bond (OH5) and one base-line 4-membered $\text{H-O}\cdots\text{O}=\text{C}$ (OO4)
- c) Two base-line 4-membered $\text{H-O}\cdots\text{O}=\text{C}$ (OO4) and one moderately destabilising 6-membered "anti"- hydrogen bond (C6). Vibrational frequency analysis indicates that this is a 1st order transition structure, with a quasi-disrotatory imaginary mode.

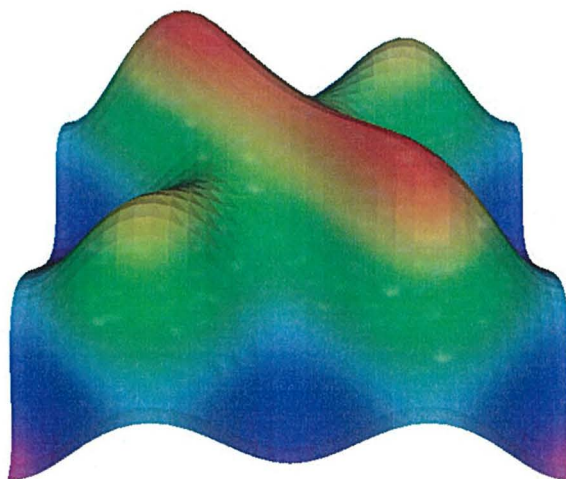


Figure 44. Variation of HF/6-31G(d) potential energy (kJ mol^{-1}) vs C-C-O-H dihedral for 2,3-dihydroxy-1,4-naphthoquinone as a contour plot. Potential energy is quoted relative to the global minimum

5.3.3.2 5,6-Dihydroxy-1,4-naphthoquinone

2-D contour and 3-D asymmetric surface plots depicting 2-D C-C-O-H torsional scans for each hydroxyl group in 5,6-dihydroxy-1,4-naphthoquinone (Figure 45).

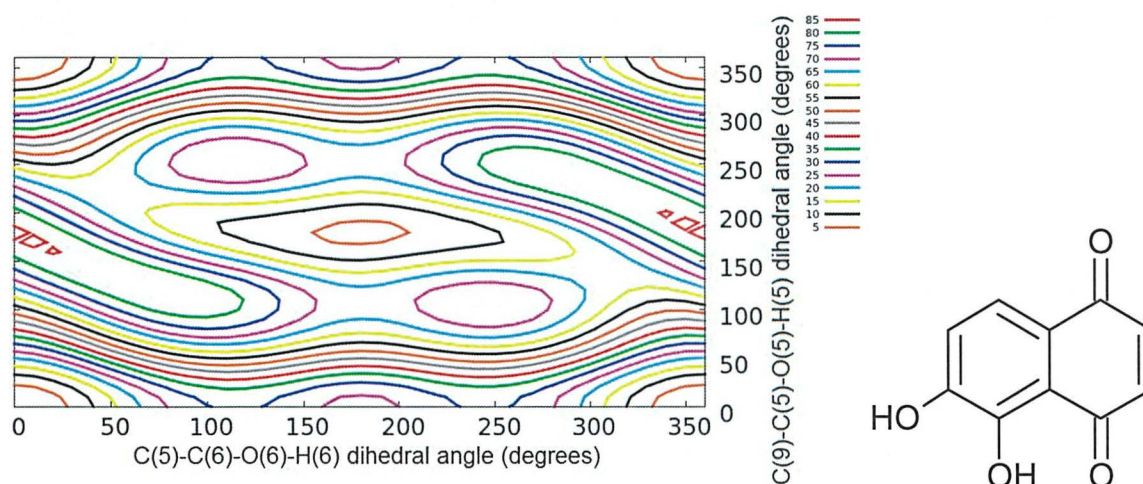


Figure 45. Variation of HF/6-31G(d) potential energy (kJ mol^{-1}) vs C-C-O-H dihedral for 5,6-dihydroxy-1,4-naphthoquinone as a contour plot.

Potential energy is quoted relative to the global minimum

The complex shape of the PES is again indicative of interacting, neighbouring hydroxyl groups, however due to no degenerative structures the plot is now non-symmetric. The severe gradients, indicating large barriers, are observed for the 5- (β) position with moderate gradients and rotation barriers for the neighbouring 6- (γ) position. The 5-membered O-H...OH hydrogen bond (OH5) stabilises the molecule by ca. 20 kJ mol^{-1} , meaning that the low barriers previously seen for the neighbouring 6- (γ) position have been lost.

The non-planar global (aligned parallel) and local (aligned antiparallel) maxima have energies of ca. 80 and 70 kJ mol^{-1} , which exceeds or comparable with predicted barriers of ca. 72 kJ mol^{-1} (Section 5.3.1). A destabilising interaction is also evident for the C6 in which the “anti-“ hydrogen bond is ca. 36 kJ mol^{-1} less stable than expected.

Four unique planar species can be identified (Figure 46):

- a) One strongly stabilising 6-membered O-H \cdots O=C hydrogen bond (R6) and one weakly stabilising 5-membered O-H \cdots O-H hydrogen bond (OH5)
- b) One strongly stabilising 6-membered O-H \cdots O=C hydrogen bond (R6) and one base-line 4-membered H-O \cdots O-H (M4)
- c) Weakly stabilising 5-membered O-H \cdots O-H hydrogen bond & base-line 5-membered H-O \cdots O=C
- d) Strongly destabilising 6-membered “*anti*”- hydrogen bond & baseline 5-membered H-O \cdots O=C. Vibrational frequency analysis indicates that this is a 2nd order transition structure, with both quasi-conrotatory & quasi-disrotatory imaginary modes

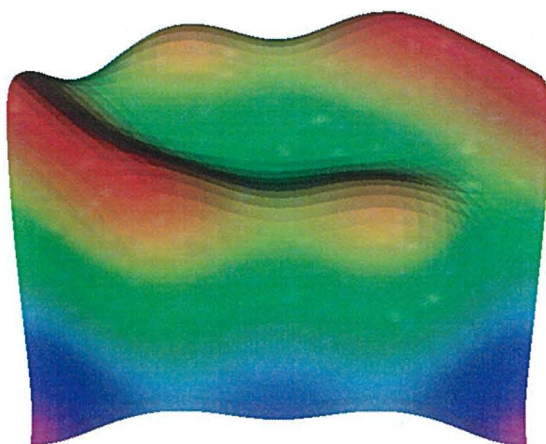


Figure 46. Variation of HF/6-31G(d) potential energy (kJ mol^{-1}) vs C-C-O-H dihedral for 5,6-dihydroxy-1,4-naphthoquinone as a contour plot.

Potential energy is quoted relative to the global minimum

5.3.3.3 6,7-Dihydroxy-1,4-naphthoquinone

2-D contour and 3-D surface plots depicting 2-D C-C-O-H torsional scans for each hydroxyl group in 6,7-dihydroxy-1,4-naphthoquinone (Figure 47).

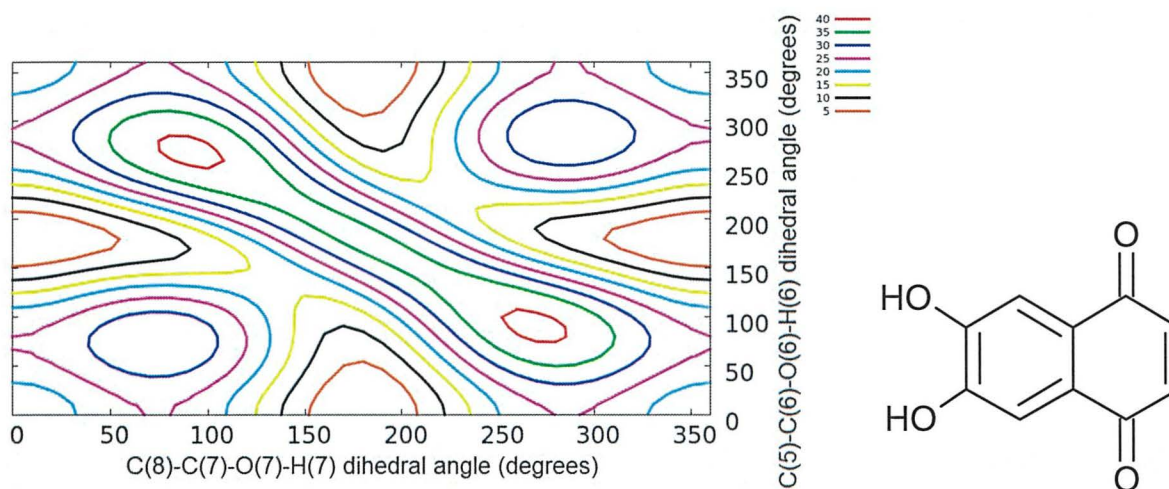


Figure 47. Variation of HF/6-31G(d) potential energy (kJ mol^{-1}) vs C-C-O-H dihedral for 6,7-dihydroxy-1,4-naphthoquinone as a contour plot.

Potential energy is quoted relative to the global minimum

The complex shape of the PES is one again indicative of interacting, neighbouring hydroxyl groups, whilst the presence of a degenerate structure generates a symmetric PES. Minimal gradients (low barriers) are generally observed for this PES as the equivalent 6- and 7- (γ) positions had low barriers to begin with (Section 5.3.1).

The non-planar global (aligned parallel) and local (aligned antiparallel) maxima have energies of *ca.* 40 and 30 kJ mol^{-1} , which exceeds or comparable with predicted barriers of *ca.* 32 kJ mol^{-1} (Section 5.3.1). A destabilising interaction is also evident for C6 in which the “anti-“ hydrogen bond is *ca.* 30 kJ mol^{-1} less stable than expected.

Three unique planar species can be identified (Figure 48):

- a) One base-line 4-membered H-O...O-H (M4)
- b) One weakly stabilising 5-membered O-H...O-H hydrogen bond (OH5)
- c) Strongly destabilising 6-membered "anti"- hydrogen bond. Vibrational frequency analysis indicates that this is a 2nd order transition structure, with both *quasi*-conrotatory and disrotatory imaginary modes.

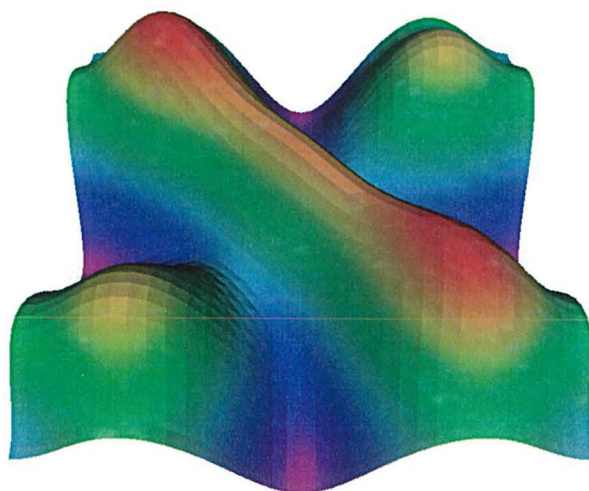


Figure 48. Variation of HF/6-31G(d) potential energy (kJ mol^{-1}) vs C-C-O-H dihedral for 6,7-dihydroxy-1,4-naphthoquinone as a contour plot. Potential energy is quoted relative to the global minimum

5.4 Summary and future developments

As shown the python parser allows multiple different outputs to be generated for the user, each type has its own set of pros and cons, however by including all the types in one package the user can chose the method that best for the problem at hand. If the user wants to generate contour plots the .csv file format output used in conjunction with GNUPlot is the best choice. If the user wants to generate images for use in publications then the VRML output allows the generation of colour graded images that depict the surface in question.

A future enhancement to the python parser would be to add the output type .stl, this would then allow the user to 3D print their surface, giving both a tactile and visual item for use within lectures and talks. While the python parser itself does not have this capability a preliminary test model has been printed. The 3D print has been used to look at interconversion paths via the use of a ball bearing that was allowed to roll down the hills towards the valleys that contain the stable structures. Figure 49 shows a 3D print of a calculation that was manually converted to the .stl format to look at the quality and usability of a 3D printed model.

The X3D and H3D outputs allow the use of a haptics device (such as the Novint Falcon depicted within Figure 50) that enables the user to tactically feel the points of interest that are present within a surface.

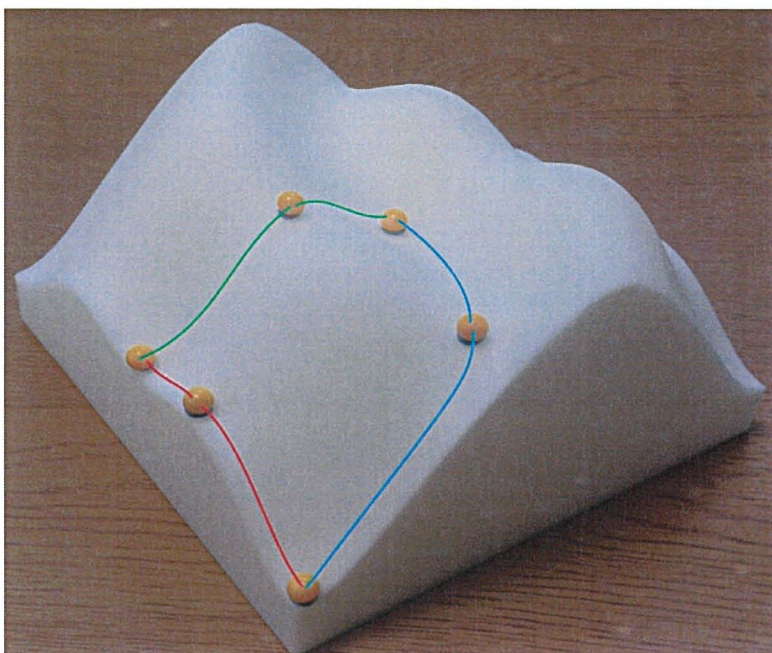


Figure 49. 3D print of 5,6-dihydroxy-1,4-naphthoquinone with ball bearings depicting key features and 3 different interconversion pathways. Red pathway is from M4 to OH5 with a continuous R6; Green pathway is from a OH5 with OO5 to an M4 with a R6; Blue pathway is from a OH5 with OO5 to a OH5 with R6 bypassing the C6 with OO5.

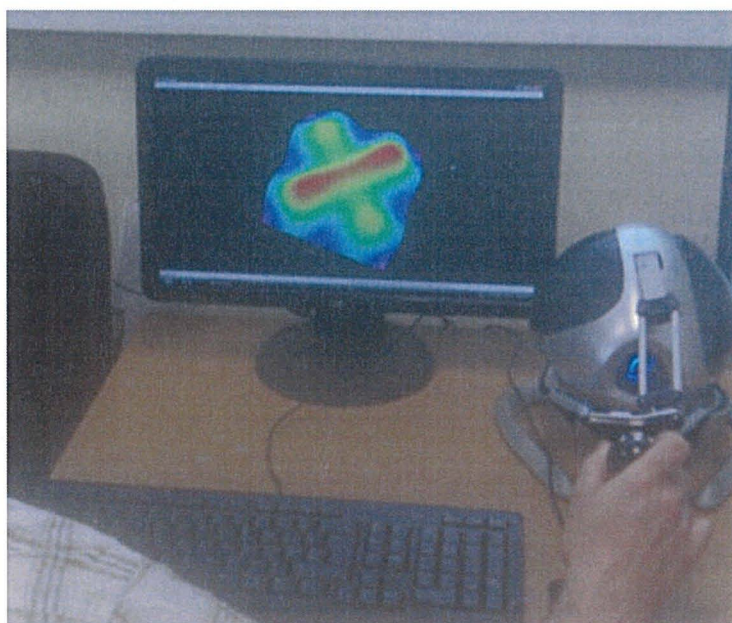


Figure 50. Use of a haptics device to tactile feel a PES



Chapter

VI

Chapter 6 - Effect of conformer upon electronic spectra

6.1 Introduction

A brief study of the UV spectra of selective hydroxy substituted 1,4-naphthoquinones has been undertaken in order to prove the need for identifying the correct global minimum structure, as some of these molecules are used as dyes.^[212] Structures possessing several low energy local minima and low rotational barriers must also be identified and investigated. To demonstrate the effect of structure upon chemical and physical properties, a simple study of electronic spectra was carried out. To do this Gaussian^[169] calculations were undertaken using the added flags of either CIS or TD, these flags tell Gaussian to run electronic (UV-VIS) spectra analysis and output the frequencies of the modes located. For HF-based methods, CIS (Configuration Interaction with Singles Excitation)^[213,214] is used for both open and closed shell systems, the systems under investigation are all closed shell systems. TD (Time Dependent) can be used with either HF (Hartree-Fock) or DFT (density functional theory) methods.^[215-221]

Previously this type of study was done by looking at the HOMO-LUMO gap,^[222-224](see Figure 51) the CIS and TD methods are an improvement on this. The HOMO-LUMO gap does not take into to account the excited state energies, if it does then in the best case scenario it is not very good at doing them. The CIS and TD-DFT take into count these excited states and are therefore a better indicator of the actual wavelengths that are obtained. This is done via an analysis of the vertical excitation energies which differs from adiabatic ones by not minimizing the electronic structure of the excited states. A TD-DFT C-PCM-TD-PBE0 study of a small selection of dyes was carried out by Jacquemin.^[225]

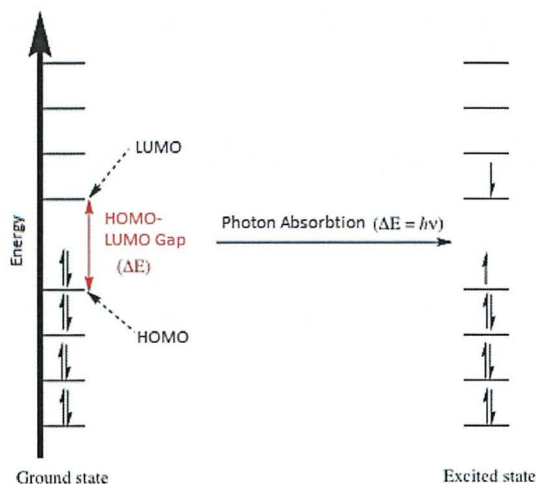


Figure 51. How the electronic configuration changes when absorbing light

6.2 Methodology

When trying to prove the colour of a molecule you must look at the absorption bands and then give it its complementary colour for the colour that would be seen after the absorption has taken place. One problem that could arise from this is that if a correct structure is not determined that the wavelength of light could be different. This can lead to problems as the yellow band of colour is only 20 nm wide (see Table 24). If the molecular structure is incorrect and the wavelengths differ by more than 20 nm then an incorrect colour could be given.

Table 24. Colour spectra and their relative wavelengths

Color	Wavelength
violet	380–450 nm
blue	450–495 nm
green	495–570 nm
yellow	570–590 nm
orange	590–620 nm
red	620–750 nm

6.3 Results and discussion

6.3.1 HF mono-substitution results

The excitation with the lowest excitation energy and highest lambda max is typically a triplet, the triplet excitations are symmetry forbidden leading to a zero f value (oscillator strength). Occasionally the lowest energy singlet excitation is given by A". The zero oscillator strength of this peak indicates symmetry forbiddance. Within Table 25 & Table 26, symmetry forbidden excitations have been omitted for clarity.

Table 25. Lowest Singlet-A' excitation energy for HF-CIS, E (eV) as a function of both ring position and rotamer orientation. The absorption wavelength, λ , (nm) and oscillator strength, f , are also included. Symmetry forbidden peaks have been omitted for clarity. ^a Interactions given as defined in Chapter 2.

Position	Interaction ^a	E (eV)	λ (nm)	f (a.u.)
2 Z	R5	4.9259	251.70	0.0078
2 E		5.1017	243.02	0.0003
5 Z	R6	4.8185	257.31	0.2218
5 E		5.0547	245.28	0.1888
6 Z		4.9635	249.79	0.0563
6 E		5.0279	246.59	0.0685

Table 26. Lowest Singlet-A' excitation energy for HF-TD, E (eV) as a function of both ring position and rotamer orientation. The absorption wavelength, λ , (nm) and oscillator strength, f , are also included. Symmetry forbidden peaks have been omitted for clarity. ^a Interactions given as defined in Chapter 2.

Position	Interaction ^a	E (eV)	λ (nm)	f (a.u.)
2 Z	R5	4.7279	262.24	0.0063
2 E		4.8933	253.37	0.0001
		5.2428	236.48	0.0846
5 Z	R6	4.5891	270.17	0.1796
5 E		4.8237	257.03	0.1582
6 Z		4.7536	260.82	0.0484
6 E		4.8169	257.39	0.0593

Care must be taken when comparing these results with experiment for 3 reasons (see section 6.3.3), first is the fact that these calculations underestimate the wavelengths. The second is that they are done in the gas phase so solvent effects are not taken into account. Finally, the quinoid ring 2- substitution should not be directly compared with (5- and 6-) positions on the benzenoid ring. Bathochromic shifts are observed with these results going from 6- to 5- indicating the effect of hydrogen bonding on the 5- compared to the non-interacting 6- position.

6.3.2 B3LYP hexa-substitution results

Table 27 and 28 demonstrate that just changing the rotational positions of the hydroxyl groups of the low energy hexahydroxy-1,4-naphthoquinone can lead to a great difference in wavelengths obtained. This is in part due to the different hydrogen bonding environments present within the molecules, leading to the changes in the wavelengths. It should also be noted that only the ZZZZZZ orientation has a C_{2V} symmetry all others have a C_s symmetry, the parent 1,4-naphthoquinone molecule has D_{2h} symmetry which is a symmetry forbidden vibration.

Table 27. Lowest singlet excitation energy for B3LYP-TD-DFT , E (eV) as a function of both ring position and rotamer orientation. The absorption wavelength, λ , (nm) and oscillator strength, f , are also included. Symmetry forbidden peaks have been omitted for clarity. ^a Interactions given as defined in Chapter 2.

Position	Interaction ^a	Type	E (eV)	λ , (nm)	f (a.u.)
ZZZZZZ	2R6 2R5 2OH5	B2	2.1822	568.17	0.0008
ZZZZEZ	2R6 2R5 2OH5	A'	2.2554	549.73	0.0036
ZEZZZZ	2R6 2R5 2OH5	A'	2.3154	535.49	0.0009
ZEZZEZ	2R6 1R5 3OH5	A'	2.3990	516.82	0.0002
ZEZEZZ	2R6 1R5 3OH5	A'	2.4158	513.21	0.0035
ZZZZEE	1R6 2R5 3OH5	A'	2.4060	515.31	0.0121
ZEZZEE	1R6 1R5 4OH5	A'	2.5665	483.09	0.0050
ZEEZZZ	1R6 1R5 4OH5	A'	2.6349	470.54	0.0099

Table 28. Lowest singlet excitation energy for B3LYP-CIS, E (eV) as a function of both ring position and rotamer orientation. The absorption wavelength, λ , (nm) and oscillator strength, f , are also included. Symmetry forbidden peaks have been omitted for clarity. ^a Interactions given as defined in Chapter 2.

Position	Interaction ^a	Type	E (eV)	λ , (nm)	f (a.u.)
ZZZZZZ	2R6 2R5 2OH5	B2	4.1067	301.90	0.0038
ZZZZEZ	2R6 2R5 2OH5	A'	4.1867	296.14	0.0120
ZEZZZZ	2R6 2R5 2OH5	A'	4.2674	290.54	0.0061
ZEZZEZ	2R6 1R5 3OH5	A'	4.3548	284.71	0.0032
ZEZEZZ	2R6 1R5 3OH5	A'	4.3511	284.95	0.0243
ZZZZEE	1R6 2R5 3OH5	A'	4.3783	283.18	0.0331
ZEZZEE	1R6 1R5 4OH5	A'	4.5681	271.42	0.0125
ZEEEEZ	1R6 1R5 4OH5	A'	4.5592	271.95	0.0424

6.3.3 Comparison with experimental results

The previous work of Davies^[222] showed that dyes could be split into three families :

- Polyenic
- Aromatic
- Polymethinic

The calculations were performed using various semi-empirical methods (PPP, EHT, CNDO, INDO, MINDO/3, MNDO, AM1, PM3 and ZINDO/S. Due to effects of electron correlation, the energy of the HOMO can be approximated as the negative of the first ionization energy. The calculated λ_{\max} of each dye did not match with experimental result, three separate linear regressions were obtained. Semi-empirical (and HF) overestimated the band gap therefore giving low lambda maxes. DFT on the other hand underestimated the band gap giving rise to large lambda maxes.

Without doing similar regression across large data series of varying dyes with different chromophores and functional groups it is not feasible to directly compare the calculated λ_{\max} against experimental values,^[226] with a peak at 475 nm (epsilon = 6060) containing two shoulders, one at 498 nm (epsilon = 4350), and the other at 459 nm (epsilon = 5350).

Taking this into account, lowest energy conformer from Table 27 has a λ_{\max} for a singlet of 568 nm. The first five structures within Table 27 (corresponding to λ_{\max} values of 568, 549, 535, 517 and 513 nm) contain maximum R6 bond counts.

As these results correspond to B3LYP energies they will be overestimated however the difference is still 55 nm and would have to be scaled down. An approximate value after scaling would be 40 nm this is still double the width of the yellow portion of the visible spectrum. If you take the variation across all eight structures that were probed then the variation is approximately 100 nm with is over the width of the visible violet region (second widest within the visible spectrum). This method however has been shown by Guillaumont^[227] to be effective in comparing these calculated wavelengths to experiment, however some care needs to be taken as the fit is not always accurate.

6.4 Conclusions

From these results the intramolecular interactions greatly affect the energetics and structure of a molecule that can be obtained via quantum mechanical calculations. The sieving method from the bond counting rule chapter stated that there were 8 low energy molecules that had further calculations performed on them. These results showed that the lambda maxes can vary greatly with only small changes to the structure. Even for molecules with the same basic bond count the different positioning of certain interactions leads to *c.a.* 20 nm worth of change.

These results are a small step into the UV analysis of these molecules, without large amounts of time been spent on this to get an accurate conversion rate these results should not be directly compared with any non-calculated data, however the overall trend that if an incorrect structure is chosen the results given by it will vary by a significant amount 30 nm or 100 nm across the set depending on the method chosen.



Chapter

VII

Chapter VII - Conclusions and future work

7.1 Overview

The hydrogen bond can be considered to be the bond of life. Without it, water would exist in as a gas (similar to methane and to a lesser extent ammonia and hydrogen fluoride). It is responsible for the double helix structure of DNA and for many biological processes. Despite the hydrogen bond being discovered a century ago, there is still considerable debate and redefining of its nature. A crystallographic survey of X-ray diffraction experiments for polyhydroxy-1,4-naphthoquinones seemed to indicate a preference for certain hydroxyl orientations due to both intra- and inter-molecular hydrogen bonding. As a significant amount of the surveyed molecules (1960s onwards) either could not locate the light proton, or had uncertainty in its position; a systematic re-investigation using state-of-the-art X-ray or neutron diffraction techniques is required.

As described in Chapter 2, the rarely known bond counting rule has been employed previously to examine alloy conformations in inorganic systems. The work in this thesis adapts the bond counting rule to organic polyhydroxy-1,4-naphthoquinones. The bond counting rule was developed using multiple linear regression for a training set of several hundred conformers. The quantitative bond counting rule showed that correctly identifying all interactions which may have an energetic effect was imperative to obtain accurate energies. Simple or elaborate extended bond counting rules could be developed, the latter at a cost of reduced usability and understanding.

A sieving approach was developed enabling low (or high) energy conformers to be identified, which significantly aids computational efficiency, particularly during conformational analysis. Symmetry can be used to initially reduce the number of unique conformers, *e.g.* from 64 to 36 for hexahydroxy-1,4-naphthoquinones. After sieving all conformers containing destabilising “anti-” hydrogen bonds (classified as C6), eight low energy conformers remained. Successive sieving beginning with the

most stabilising interaction produced two rotamers with high identical energies and hydrogen bond counts.

Unpublished studies on related polysubstituted benzo-, naphtho- and anthra-quinones and phenols including halogenated derivatives have demonstrated the effectiveness and transferability of the bond counting rule.^[160] Similarly, bond counting rules for polyborate anions are currently being developed. Future crystal packing studies, essential for pharmaceutical and materials chemistry could be based upon both intra- and inter-molecule hydrogen bonding to only minimise the number of conformers to be studied, but also to act as a predictive tool. The bond counting rule can also revolutionise carbohydrate or peptide conformational analysis, significantly reducing the number of conformers to be probed.

Vibrational frequency analysis (Chapter 3) was used to initially characterise the interactions which had been identified for use within the prototype bond counting rules. This helped to confirm some of the initial assumptions that certain interactions are “baseline”, stabilising or destabilising in nature. Quantum Theory of Atoms in Molecules (Chapter 4) analyses complimented the above assumptions and further characterised these interactions. The QTAIM analyses confirmed that carbonyl acceptors were better than hydroxyl groups, with 6-membered rings being generally more stabilising than 5-. The destabilising C6 interaction is believed to be mainly due to Coulombic repulsion with partial stabilisation from the partial H...H bond. Future studies of anharmonic vibrational frequencies could aid in this regard. Donor-acceptor interaction energies from natural bond order (NBO) analyses could be directly compared against bond counting rule interaction energies.

As only planar stationary points had been analysed within the previous chapters, Chapter 5 describes potential energy surfaces (PES) and associated rotational barriers for the polyhydroxy-1,4-naphthoquinones. The rotational barriers and potential energy surface topology provide further insight into the interconvertibility of polyhydroxy-1,4-naphthoquinone conformers.

Custom Python parsers were developed to convert Gaussian output into formats suitable for visualization e.g. using Gnuplot or Web3D technology. Graphic VRML (and X3D) and haptic H3D files can be outputted by the parser for use as interactive teaching aids, allowing the user to interact with, see and feel shaded solid surfaces in 3-D. VRML files can be converted to .stl files using third-party software and allowing 3-D rapid prototyped models to be printed, which provides the user with natural tangible perception and interaction.

An option to save PES as .stl files for 3-D printing could be included within the parser, although the use of free third-party conversion software could negate this need. The parser has already been adapted for use in creating graphic and haptic models of both SPM (e.g. STM / AFM) data^[228] and 2-D NMR (e.g. heteronuclear and homonuclear COSY) spectra.^[228] The large data sets required some code re-optimization.

In order to demonstrate the importance of obtaining the correct conformer, electronic spectra of specific polyhydroxy-1,4-naphthoquinone conformers were calculated using both CIS and TD approaches. Hartree-Fock wavelengths were underestimated due to an overestimation of the HOMO-LUMO gap, whilst DFT wavelengths gave opposite results.

Differences in hydrogen bonding caused large wavelength shifts. Although organic dye molecules could be characterised as polymethinic, aromatic or polyenic in character^[222] (each with a different linear regression), further work is needed to fully characterise the polyhydroxy-1,4-naphthoquinones.

7.2 Underling conclusions

The main advantages coming out of this work are the generation of a new novel way of working out the lowest energy structure from a set using one of two methods stemming from the bond counting rule. The first of these is the qualitative method to accurately work out the energy of each structure given enough data on the molecule. The second is the quantitative approach where the bond counting rules relative stabilities of the interactions is used as a sieve to reduce the number of possible conformational structures to a minimum, saving both time and computational cost.

Later in the work it was demonstrated that the use of haptics and 3D visualizations can be used to illustrate rotational paths in both a tactile and visual approach. As well as giving more insight into the rotational barriers that are present between the interactions discovered. The bond counting rule analysis has also lead to the discovery of new types of interactions that are available to a molecule. It has also ruled out some interactions that have been classically known as hydrogen bonding as the current definition for computationally derived structures means that they must possess a bonding path.

The concept of using bond counting rules in traditional rule-based cleaning tools within molecular modelling software could help solve the problem of the modelling software provide the wrong conformer even if the correct one is sketched into the document. Within WebMO, the outputted cleaned molecule appears to depend upon the Z-matrix connectivities rather than minimising non-bonded contacts. As the bond counting rule is mathematical / empirical in nature, it could be incorporated into commercial software. An example of this is depicted below in Figure 52.

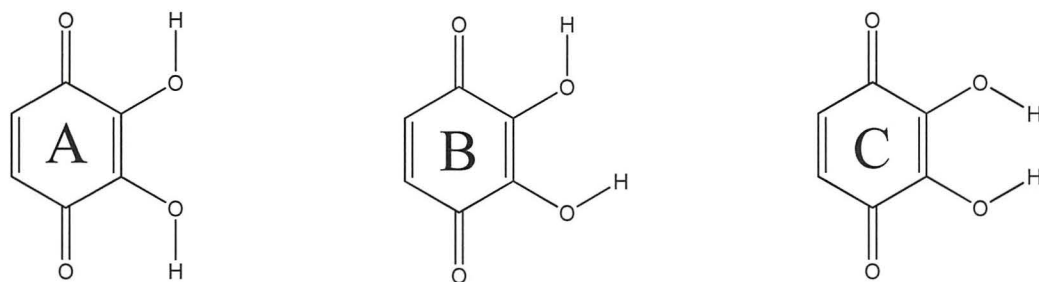


Figure 52. Three structures that are obtained from chemical modelling packages depending on how the user enters the data. A is the lowest energy structure, B is a local minimum, C is a very high energy local minimum.

Complete avoidance of structure C (due to “*anti*”- hydrogen bonds) would be essential. Although structure A is a local minimum, any calculated properties would differ from those of global minimum B. All three conformers were generated *via* cleaning during the course of this work.

7.3 Continuing development

The bond counting rule developed within this study is now been used to look at different aromatic environments with both benzoquinone and anthaquinone. Both of these studies initial results seem to suggest a similar trend in both the order of interactions as well as the interactions that are present as well. The work has also been transferred to different confirmations of the base naphthoquinone structure. This has lead to the discovery of new interactions that were not previously known about.

The 3D visualization work has been used to help undergraduate chemists come to understand reaction paths and rotational paths better through the use of the 3D printed model. It is also been looked at to produce a tiled version of the 3D printed model so that with the use of small ball bearings a student could place the ball at the maximum and they could then watch it roll down to its minimum along the rotational path.



References

References

1. R. A. J. Matthews, *European Journal of Physics*, 1995, **16**, 172-176
2. P. Dawson, I. Han, M. Cox, C. Black, L. Simmons, *Journal of Applied Microbiology*, 200, **102**, 945-953
3. G. Parkin, *Journal of Chemical Education*, 200, **83**, 791
4. I. Langmuir, *Journal of the American Chemical Society*, 1919, **41**, 868-934
5. G. N. Lewis, *Journal of the American Chemical Society*, 1916, **38**, 762-785
6. M. L. H. Green, *Journal of Organometallic Chemistry*, 1995, **500**, 127-148
7. I. Langmuir, *Science*, 1921, **54**, 59-67
8. W. B. Jensen, *Journal of Chemical Education*, 2005, **82**, 28
9. C. A. Tolman, *Chemistry Society Review*, 1972, **1**, 337-353
10. K. Wade, *Journal of the Chemical Society D*, 1971, 792-793
11. D. M. P. Mingos, *Nature Physical Science*, 1972, **236**, 99-102
12. A. J. Welch, *Chemical Communications*, 2013, **49**, 3615-3616
13. K. Wade, *Advances in Inorganic Chemistry and Radiochemistry*, 1976, **18**, 1-66
14. D. M. P. Mingos, *Accounts of Chemical Research*, 1984, **17**, 311-319
15. R. B. King, D. H. Rouvray, *Journal of the American Chemical Society*, 1977, **99**, 7834-7840
16. W. Markownikoff, *Annalen der Pharmacie*, 1870, **153**, 228-59
17. P. Hughes, *Journal of Chemical Education*, 2006, **83**, 1152
18. A. Saytzeff, *Justus Liebigs Annalen der Chemie*, 1875, **179**, 296-301
19. D. E. Lewis, *Bulletin for the History of Chemistry*, 2010, **35**, 115-124
20. B. Braida, V. Prana, P. C. Hibert, *Angewandte Chemie International Edition*, 2009, **48**, 5724-5728
21. R. B. Woodward, R. Hoffmann, *Journal of the American Chemical Society*, 1965, **87**, 395-397
22. H. E. Zimmerman, *Journal of the American Chemical Society*, 1966, **88**, 1564-1565
23. C. Morell, A. Grand, A. Toro-Labbè, *Journal of Physical Chemistry A*, 2005, **109**, 205-212
24. E. J. Corey, *Journal of Organic Chemistry*, 2004, **69**, 2917-2919
25. R. Hoffmann, *Angewandte Chemie International Edition*, 2004, **43**, 6586-6590
26. H. X. Yang, L. F. Xu, Z. Fan, C. Z. Gu, S. B. Zhang, *Physical Review Letters*, 2008, **100**, 026101.
27. D. J. Cram, F. Ahmed, A. A. Elhafez, *Journal of the American Chemical Society*, 1952, **74**, 5828-583

28. M. Chèrest, H. Felkin, N. Prudent, *Tetrahedron Letters*, 1968, **9**, 2199-2204
29. N. T. Anh, O. Eisenstein, *Nouveau Journal de Chimie*, 1977, **1**, 61
30. R. J. Gillespie, R. S. Nyholm, *Quarterly Review*, 1957, **11**, 339
31. R. J. Gillespie, *Journal of Chemical Education*, 1970, **47**, 18
32. E. McNelis, M. Blandina, *New Journal of Chemistry*, 2001, **25**, 772
33. E. Hückel, *Zeitschrift für Physik*, 1931, **70**, 204-85
34. E. Hückel, *Zeitschrift für Physik*, 1931, **70**, 628-648
35. J. D. Roberts, Jr. A. Streitweiser, C. M. Regan, *Journal of the American Chemical Society*, 1952, **74**, 4579-82
36. A. Hirsch, Z. Chen, H. Jiao, *Angewandte Chemie International Edition English*, 2000, **39**, 3915-17
37. R. B. Woodward, *Journal of the American Chemical Society*, 1941, **63**, 1123
38. L. F. Fieser, M. Fieser, S. Rajagopalan, *Journal of Organic Chemistry*, 1948, **13**, 800-806
39. S. H. Rhim, R. Saniz, J. Yu, L.-H. Ye, A. J. Freeman, *Physical Review B*, 2007, **76**, 184505.
40. S. H. Rhim, R. Saniz, A. J. Freeman, *Physical Review B*, 2009, **79**, 045313.
41. T. Wang, N. Moll, K. Cho, J. D. Joannopoulos, *Physical Review B*, 2000, **63**, 035306.
42. W. Wang, S. Chen, P.-X. Yang, C.-G. Duan, L.-W. Wang, *Journal of Material Chemistry A*, 2013, **1**, 1078–1085.
43. M. C. Righi, C. A. Pignedoli, R. D. Felice, C. M. Bertoni, A. Catellani, *Physical Review Letters*, 2003, **91**, 136101.
44. J. H. Lloyd-Williams, B. Monserrat, D. D. Vvedensky, A. Zangwill, *Physical Review B*, 2012, **85**, 161402.
45. J. Frantz, M. Rusanen, K. Nordlund, I. T. Koponen, *Journal of Physics: Condensed Matter*, 2004, **16**, 2995–3003.
46. A. Karima, M. Rusanen, I. T. Koponen, T. Ala-Nissila, T. S. Rahman, *Surface Science*, 2004, **554**, L113–L119.
47. M. Camarda, A. L. Magna, F. L. Via, *Journal of Computational Physics*, 2007, **227**, 1075–1093.
48. M. Masia, A. Fioruccia, M. Camarda, A. L. Magna, F. L. Via, *Thin Solid Films*, 2010, **518**, S6–S11.
49. D. Kulikov, L. Malerba, M. Hou, *Philosophical Magazine*, 2006, **86**, 141–172.
50. H. X. Yang, L. F. Xu, Z. Fan, C. Z. Gu, S. B. Zhang, *Physical Review Letters*, 2008, **100**, 026101.
51. S. F. Matar, E. Betranhandy, M. Nakhl, M. Zakhour-Nakhl, N. Ouaïnib, *Progress in Solid State Chemistry*, 2006, **34**, 21–66.

52. R. Mohammadi, R. B. Kaner, *Encyclopedia of Inorganic and Bioinorganic Chemistry*, John Wiley & Sons, Ltd, ch. Superhard Materials.
53. M. Mattesini, S. F. Mater, *International Journal of Inorganic Materials*, 2001, **3**, 943–957.
54. K. Yuge, *Journal of Physics: Condensed Matter*, 2009, **21**, 415403.
55. S. Chen, X. G. Gong, S.-H. Wei, *Phys. Status Solidi B - Basic Solid State Physics*, 2009, **246**, 589–593.
56. T. Kar, M. Cuma, S. Scheiner, *Journal of Physical Chemistry A*, 1998, **102**, 10134–10141.
57. Y. Li, W. Fan, H. Sun, X. Cheng, P. Li, X. Zhao, M. Jiang, *Journal of Physical Chemistry C*, 2010, **114**, 2783–2791.
58. X. F. Fan, Z. Zhu, Z. X. Shen, J.-L. Kuo, *Journal of Physical Chemistry C*, 2008, **112**, 15691–15696.
59. J.-H. Yang, Y. Zhai, H. Liu, H. Xiang, X. Gong, S.-H. Wei, *Journal of the American Chemistry Society*, 2012, **134**, 12653–12657.
60. K. Wade, *Electron Deficient Compounds*, T. Nelson & Sons Ltd., London, 1971, chapter **4**, p. 62.
61. *Book of Data*, ed. H. Ellis, Pearson Education Limited, 1984, p. 51.
62. F. Hibbert, K. J. Spiers, *Journal of the Chemical Society-Perkin Transactions 2*, 1987, 1617–1620.
63. R. H Thomson, *Naturally Occurring Quinones*, Second Edition, Academic Press, London and New York, 1971
64. R. G. Cooke, J. B. Robinson, J. R. Cannon, R. W. Retallac, *Australian Journal of Chemistry*, 1970, **23**, 1029.
65. N. P. D. Preez, D. P. Venter, Vanvuure.Pj, G. J. Kruger, J. Dekker, *Journal of Organic Chemistry*, 1971, **36**, 485.
66. Courseil.C, J. Gaultier, C. Hauw, M. Schvoere, *Comptes Rendus Hebdomadaires Des Seances De L Academie Des Sciences Serie C*, 1970, **270**, 687.
67. J. H. Gough M. D. Sutherland, *Australian Journal of Chemistry*, 1970, **23**, 1839.
68. L. L. Marking, *Transactions of the American Fisheries Society*, 1970, **99**, 510.
69. S. S. Sawhney, *Journal of the Indian Chemical Society*, 1977, **54**, 641–642.
70. H. Chang, S. E. Suzuka, *Biochemical and Biophysical Research Communications*, 1982, **107**, 602–608.
71. R. Lantz, *Bulletin De La Societe Chimique De France*, 1971, 253.
72. B. M. Badri and S. M. Burkinshaw, *Dyes and Pigments*, 1993, **22**, 15–25.
73. P. D. Cradwick, D. Hall, *Acta Crystallographica Section B-Structural Crystallography and Crystal Chemistry*, 1971, **B 27**, 1468.

74. C. J. Soderquist, *Journal of Chemical Education*, 1973, **50**, 782-783.
75. K. C. Joshi, P. Singh, G. Singh, *Zeitschrift Fur Naturforschung Section B - a Journal of Chemical Sciences*, 1977, **32**, 890-892.
76. C. Kuroda, M. Okajima, *Proceedings of the Japan Academy*, 1958, **34**, 616--618.
77. C. Kuroda, M. Okajima, *Proceedings of the Japan Academy*, 1967, **43**, 41—44
78. T. W. Goodwin, E. Lederer, L. Musajo, *Cellular and Molecular Life Sciences*, 1951, **7**, 375-376.
79. M. Fehlmann, A. Niggli, *Helvetica Chimica Acta*, 1965, **48**, 305
80. S. -M. Peng, Y. Wang, H. -R. Chang, C. -P. Tang, C. -J. Wang, *Proceedings of the National Science Council, Republic of China*, 1981, **5**, 139
81. J. Gaultier, C. Hauw, *Acta Crystallographica*, 1965, **19**, 580
82. N. R. Sperandeo, A. Karlsson, S. Cuffini, S. Pagola, P. W. Stephens, *AAPS PharmSciTech*, 2005, **6**, 82
83. C. Pascard-Billy, *Acta Crystallographica*, 1962, **15**, 519
84. C. Pascard-Billy, *Bulletin de la Societe Chimique de France*, 1962, 2293
85. P. Srivastava, *Indian Journal of Physics and Proceedings of the Indian Association for the Cultivation of Science*, 1961, **35**, 640
86. W. I. Shiau, E. N. Duesler, I. C. Paul, D. Y. Curtin, W. G. Blann, C. A. Fyfe, *Journal of the American Chemical Society*, 1980, **102**, 4546
87. M. S. Lehmann, F. H. Herbstein, M. Kapon, G. M. Reisner, *European Crystallographic Meetings*, 1982, **7**, 170
88. F. H. Herbstein, M. Kapon, G. M. Reisner, M. S. Lehman, R. B. Kress, R. B. Wilson, W. -I. Shiau, E. N. Duesler, I. C. Paul, D. Y. Curtin, *Proceedings of the Royal Society of London Series B*, 1985, **399**, 295
89. S. S. Sawhney, *Thermochimica Acta*, 1984 **74**, 361
90. S. Salunke-Gawali, S. Y. Rane, V. G. Puranik, C. Guyard-Duhayon, F. Varret, *Polyhedron*, 2004, **23**, 2541
91. J. Gaultier, C. Hauw, *Acta Crystallographica*, 1965, **19**, 919
92. P. D. Cradwick, D. Hall, *Acta Crystallographica, Section B*, 1971, **27**, 146
93. P. D. Cradwick, D. Hall, M. K. Wood, *Acta Crystallographica, Section B*, 1977, **33**, 2380
94. A. Hussain, M. R. Hussain, S. Mehdi, *Journal of Applied Crystallography*, 1981, **14**, 145
95. K. M. Ghose, B. R. Rao, *Zeitschrift fuer Kristallographie, Kristallgeometrie, Kristallphysik, Kristallchemie*, 1974, **139**, 335
96. N. H. Gokhale, K. Shirisha, S. B. Padhye, S. L. Croft, H. D. Kendrick, V. Mckee, *Bioorganic and Medicinal Chemistry Letters*, 2006, **16**, 430

97. Borgen , *Acta Chemica Scandinavica*, 1966, **20**, 2885
98. A. P. Neves, G. B. da Silva, M. D. Vargas, C. B. Pinheiro, L. do C. Visentin, J. D. B. M. Filho, J. raujo, L. V. Costa-Lotufu, C. Pessoa, M. O. de Moraes , *Dalton Transactions*, 2010, **39**, 10203
99. S. B. Zaware, S. Dagade-Waghmode, R. G. Gonnade, D. Srinivas, S. Y. Rane, *Journal of Molecular Structure*, 2009, **938**, 328
100. H. Nasiri, M. Bolte , *Private Communication*, 2009
101. J. Dekkers, H. Kooijman, J. Kroon, E. Grech , *Acta Crystallographica Section C*, 1996, **52**, 2896
102. V. Bertolasi, P. Gilli, V. Ferretti, G. Gilli , *Chemistry - European Journal*, 1996, **2**, 925
103. A. V. Todkary, R. Dalvi, S. Salunke-Gawali, J. Linares, F. Varret, J. Marrot, J. V. Yakhmi, M. Bhadbhade, D. Srinivas, S. P. Gejji, S. Y. Rane , *Spectrochimica Acta Part*, 2006, **63**, 130
104. N. H. Gokhale, S. B. Padhye, S. L. Croft, H. D. Kendrick, W. Davies, C. E. nson, K. Powell , *Journal of Inorganic Biochemistry*, 2003, **95**, 249
105. L. Malpezzi, C. Fuganti, E. Maccaroni, N. Masciocchi, J. Nardi, *Thermal Analysis and Calorimetry*, 2010, **102**, 203
106. Wen-Ming Zhou, Han Liu, Da-Ming Du, *Organic Letters.*, 2008, **10**, 2817
107. J. R. Cannon, V. Lojanapiwatna, C. L. Raston, W. Sinchai, H. White, *Australian Journal of Chemistry*, 1980, **33**, 1073
108. A. V. Gerasimenko, S. Fedoreev, N. P. Mishchenko, *Kristallografiya*, 2006, **51**, 48
109. K. Peters, E. M. Peters, H. G. von Schnering, G. Bringmann, C. Kehr, R. D. Haller, S. Bar, M. Isahakia, S. Robertson , *Zeitschrift fuer Kristallographie*, 1995, **210**, 290
110. A. D. Bukhtoyarova, T. V. Rybalova, L. V. Ektova , *Zhurnal Organicheskoi Khimii*, 2010, **46**, 860
111. J. G. Rodriguez, P. Smith-Verdier, F. Florencio, S. Garcia-Blanco, *Journal of Molecular Structure*, 1984, **112**, 101
112. K. Peters, E. -M. Peters, I. Klein, D. Spitzner , *Zeitschrift fuer Kristallographie - New Crystal Structures*, 2004, **219**, 241
113. P. Rubio, F. Florencio, S. Garcia-Blanco, J. G. Rodriguez , *Acta Crystallographica Section C*, 1985, **41**, 1797
114. O. Veshkurova, Z. Golubenko, E. Pshenichnov, I. rzanova, V. Uzbekov, E. Sultanova, S. Salikhov, H. J. Williams, J. H. Reibenspies, L. S. Puckhaber, R. D. Stipanovic , *Phytochemistry*, 2006, **67**, 2376
115. P. D. Cradwick, D. Hall , *Acta Crystallographica, Section B*, 1971, **27**, 1990
116. F. H. Herbstein, M. Kapon, G. M. Reisner, M. S. Lehman, R. B. Kress, R. B. Wilson, W. -I. Shiau, E. N. Duesler, I. C. Paul, D. Y. Curtin , *Proceedings of the Royal Society*

- of London, Series - Mathematical, Physical and Engineering Sciences, 1985, **399**, 295
117. G. Weber, T. Hubner, Gieren, J. Sonnenbichler, T. Kowalski, O. Holdenrieder, *Zeitschrift fuer Naturforschung. Teil C, Biochemie, Biophysik, Biologie, Virologie*, 1987, **42**, 1
 118. P. J. Cox, R. Howie, *Acta Crystallographica Section C*, 1990, **46**, 1349
 119. K. Ohta, F. Kasahara, T. Ishimaru, Y. Wada, T. Kanamaru, H. Okazaki, *Journal of antibiotics*, 1987, **40**, 1239
 120. S. Neufeind, N. Hulsken, J. -M. Neudorfl, N. Schlorer, H. -G. Schmalz, *Chemistry - European Journal*, 2011, **17**, 2633
 121. D. R. da Rocha, C. G. de Souza, J. L. C. Resende, W. C. Santos, E. dos Santos, C. Pessoa, M. O. de Moraes, L. V. Costa-Lotufu, R. C. Montenegro, V. F. Ferreira, *Organic and Biomolecular Chemistry*, 2011, **9**, 4315
 122. K. Krohn, K. Khanbabaee, U. Florke, P. G. Jones, A. Chrapkowski, *Justus Liebigs Annalen der Chemie*, 1994, 471
 123. D. T. -C. Tan, H. Osman, H. Kamaruddin, S. R. Jebas, H. -K. Fun, *Acta Crystallographica Section E*, 2009, **65**, 871
 124. J. Zhou, L. Duan, H. Chen, X. Ren, Z. Zhang, F. Zhou, J. Liu, D. Pei, K. Ding, *Bioorganic and Medicinal Chemistry Letters*, 2009, **19**, 5091
 125. J. Vijayalakshmi, S. S. Rajan, R. Srinivasan, *Acta Crystallographica Section C*, 1987, **43**, 2375
 126. M. Ozawa, T. Taguchi, T. Itoh, Y. Ebizuka, K. I. Booker-Milburn, G. R. Stephenson, K. Ichinose, *Tetrahedron*, 2003, **59**, 8793
 127. J. Padwal, W. Lewis, C. J. Moody, *Organic and Biomolecular Chemistry*, 2011, **9**, 3484
 128. D. T. -C. Tan, H. Osman, H. Kamaruddin, R. Kia, H. -K. Fun, *Acta Crystallographica Section E*, 2008, **64**, 1523
 129. J. G. Rodriguez, A. de Pablo, P. Smith-Verdier, F. Florencio, S. Garcia-Blanco, *Bulletin of the Chemical Society of Japan*, 1986, **59**, 3957
 130. G. A. Jeffrey, W. Saenger, *Hydrogen Bonding in Biological Structures*, Springer, Berlin, 1991.
 131. E. Arunan, G. R. Desiraju, R. A. Klein, J. Sadlej, S. Scheiner, I. Alkorta, D. C. Clary, R. H. Crabtree, J. J. Dannenberg, P. Hobza, H. G. Kjaergaard, A. C. Legon, B. Mennucci, David J. Nesbitt, *Pure Applied Chemistry*, 2011, **83**, 1637–1641
 132. T. Steiner, *Angewandte Chemie International Edition*, 2002, **41**, 48–76.
 133. B. Schiøtt, B. B. Iversen, G. K. H. Madsen, F. K. Larsen, T. C. Bruice, *Proceedings of the National Academy of the United States of America*, 1998, **95**, 12799–12802.

134. W. W. Cleland, M. M. Kreevoy, *Science*, 1994, **264**, 1887–1890.
135. R. Custelcean, J. E. Jackson, *Chemical Reviews*, 2001, **101**, 1963–1980.
136. M. P. Brown, R. W. Heseltine, *Chemical Communications (London)*, 1968, 1551–1552.
137. R. H. Crabtree, P. E. M. Siegbahn, O. Eisenstein, A. L. Rheingold, T. F. Koetzle, *Accounts of Chemical Research*, 1996, **29**, 348–354.
138. N. V. Belkova, E. S. Shubina, L. M. Epstein, *Accounts of Chemical Research*, 2005, **38**, 624–631.
139. M. Brookhart, M. L. H. Green, *Journal of Organometallic Chemistry*, 1983, **250**, 395–
140. M. Brookhart, M. L. H. Green, G. Parkin, *Proceedings of the National Academy of the United States of America*, 2007, 104, 6908–6914.
141. C. F. Matta, J. Hernández-Trujillo, T. Tang, R. F. W. Bader, *Chemistry - A European Journal*, 2003, **9**, 1940–1951
142. J. D. Dunitz, A. Gavezzotti, *Angewandte Chemie International Edition*, 2005, **44**, 1766–1787.
143. J. Poater, R. Visser, M. Sola, F. M. Bickelhaupt, *Journal of Organic Chemistry*, 2007, **72**, 1134–1142.
144. P. Sanz, O. Mó, M. Yáñez, J. Elguero, *J. Phys. Chem. A*, 2007, **111**, 3585–3591.
145. S. M. LaPointe, S. Farrag, H. J. Bohórquez, R. J. Boyd, *Journal of Physical Chemistry B*, 2009, **113**, 10957–10964
146. U. Koch, P. L. A. Popelier, *Journal of Physical Chemistry*, 1995, **99**, 9747–9754
147. M. Mandado, A. M. Graña, R. A. Mosquera, *Physical Chemistry Chemical Physics*, 2004, **6**, 4391–4396
148. J. M. Hermida-Ramón, R. A. Mosquera, *Chemical Physics*, 2006, **323**, 211–217
149. M. Mandado, R. A. Mosquera, C. Van Alsenoy, *Tetrahedron*, 2006, 62, 4243–4252
150. F. Fuster, S. J. Grabowski, *Journal of Physical Chemistry A*, 2011, **115**, 10078–10086
151. S. J. Grabowski, M. Małecka, *Journal of Physical Chemistry A*, 2006, **110**, 11847–11854
152. S. J. Grabowski, J. M. Ugalde, *Journal of Physical Chemistry A*, 2010, **114**, 7223–7229
153. J. Hernández-Trujillo, C. F. Matta, *Structural Chemistry*, 2007, **18**, 849–857
154. J. Cioslowski, S. T. Mixon, *Canadian Journal of Chemistry* 1992, **70**, 443
155. S. J. Grabowski, J. Leszczynski, *Chemical Physics*, 2009, **355**, 169–176
156. Z. Huang, L. Yu, Y. Dai, *Structural Chemistry*, 2010, **21**, 565–572
157. M. F. de Carvalho, R. A. Mosquera, R. Rivelino, *Chemical Physics Letters*, 2007, **445**, 117–124

158. S. J. Grabowski, *Journal of Physical Chemistry A*, 2012, **116**, 1838–1845
159. J. M. Hermida-Romón, A. M. Graña, *Journal of Computational Chemistry*, 2007, **28**, 540–546
160. P. Lenain, M. Mandado, R. A. Mosquera, P. Bultinck, *Journal of Physical Chemistry A*, 2008, **112**, 7898–7904
161. B. G. Oliveira, M. C. A. Lima, I. R. Pitta, S. L. Galdino, M. Z. Hernandez, *Journal of Molecular Modelling*, 2010, **16**, 119–127
162. M. V. Vener, A. V. Manaev, A. N. Egorova, V. G. Tsirelson, *Journal of Physical Chemistry A*, 2007, **111**, 1155-1162
163. R. F. W. Bader, T. T. Nguyen-Dang, Y. Tal, *Journal of Chemical Physics*, 1979, **70**, 4316-4329
164. D. K. Taylor, I. Bytheway, D. H. R. Barton, M. B. Hall, *Journal of Organic Chemistry* 1995, **60**, 435-444.
165. P. L. A. Popelier, R. F. W. Bader, *Chemical Physics Letters*, 1992, **189**, 542-548.
166. R. J. Boyd, S. C. Choi, *Chemical Physics Letters*, 1985, **120**, 80-85.
167. J. W. Larson, T. B. McMahon, *Inorganic Chemistry*, 1984, **14**, 2029- 2033
168. J. Emsley, *Chemical Society Reviews*, 1980, **9**,91-124
169. Gaussian 09, Revision A.1, M. J. Frisch, G. W. Trucks, H. B. Schlegel, G. E. Scuseria, M. A. Robb, J. R. Cheeseman, G. Scalmani, V. Barone, B. Mennucci, G. A. Petersson, H. Nakatsuji, M. Caricato, X. Li, H. P. Hratchian, A. F. Izmaylov, J. Bloino, G. Zheng, J. L. Sonnenberg, M. Hada, M. Ehara, K. Toyota, R. Fukuda, J. Hasegawa, M. Ishida, T. Nakajima, Y. Honda, O. Kitao, H. Nakai, T. Vreven, J. A. Montgomery, Jr., J. E. Peralta, F. Ogliaro, M. Bearpark, J. J. Heyd, E. Brothers, K. N. Kudin, V. N. Staroverov, R. Kobayashi, J. Normand, K. Raghavachari, A. Rendell, J. C. Burant, S. S. Iyengar, J. Tomasi, M. Cossi, N. Rega, J. M. Millam, M. Klene, J. E. Knox, J. B. Cross, V. Bakken, C. Adamo, J. Jaramillo, R. Gomperts, R. E. Stratmann, O. Yazyev, A. J. Austin, R. Cammi, C. Pomelli, J. W. Ochterski, R. L. Martin, K. Morokuma, V. G. Zakrzewski, G. A. Voth, P. Salvador, J. J. Dannenberg, S. Dapprich, A. D. Daniels, Ö. Farkas, J. B. Foresman, J. V. Ortiz, J. Cioslowski, and D. J. Fox, Gaussian, Inc., Wallingford CT, (2009).
170. I. M. Alecu, J. Zheng, Y. Zhao, D. G. Truhlar, *Journal of Chemical Theory and Computation*, 2010, **6**, 2872-2887
171. R. A. Davies, *unpublished results*
172. P. L. A. Popelier, *Atoms in Molecules: An Introduction*, Longman, Singapore , 2000
173. R.F.W. Bader, *Atoms in Molecules: A Quantum Theory*, Oxford University Press, New York, 1990
174. R. F. W. Bader, *Journal of Physical Chemistry A*, 1998, **102**, 7314-7323.

175. M. D. Esrafil, *Structural Chemistry*, 2013, **24**, 39-47.
176. M. D. Esrafil, *Journal of Molecular Modeling*, 2013, **19**, 1417-1427.
177. M. Jablonski and M. Palusiak, *Chemical Physics*, 2013, **415**, 207-213.
178. B. K. Paul and N. Guchhait, *Computational and Theoretical Chemistry*, 2013, **1012**, 20-26.
179. C. F. Matta, R. J. Boyd, *An Introduction to the Quantum Theory of Atoms in Molecules in: The Quantum Theory of Atoms in Molecules*, C. F. Matta, R. J. Boyd (editors), chapter 1, Wiley, 2007
180. P. Coppens, *X-ray Charge Densities and Chemical Bonding*, Oxford University Press Inc., New York, 1997
181. C. F. Matta, J. Herna´ndez-Trujillo, T. H. Tang, R. F. W. Bader, *Chemistry European Journal*, 2003, **9**, 1940–1951.
182. C. F. Matta, Chapter 9 in: *Hydrogen Bonding – New Insight*, S. J. Grabowski (editors), Springer, 2006
183. R. J. Boyd, S. C. Choi, *Chemical Physics Letters*, 1986, **129**, 62–65.
184. M. T. Carroll, R. F. W. Bader, *Molecular Physics*, 1988, **65**, 695–722.
185. E. Espinosa, E. Molins, C. Lecomte, *Chemical Physics Letters*, 1998, **285**, 170–173.
186. S. J. Grabowski, *Journal of Physical Chemistry A*, 2001, **105**, 10739–10746.
187. M. Domagala, S. Grabowski, K. Urbaniak, G. Mloston, *Journal of Physical Chemistry A*, 2003, **107**, 2730–2736.
188. S. Grabowski, W. A. Sokalski, J. Leszczynski, *Journal of Physical Chemistry A*, 2005, **109**, 4331–4341.
189. M. Domagala, S. Grabowski, *Journal of Physical Chemistry A*, 2005, **109**, 5683–5688.
190. O. Knop, R. J. Boyd, S. C. Choi, *Journal of the American Chemical Society*, 1988, **110**, 7299–7301.
191. E. Espinosa, E. Molins, *Journal of Chemical Physics*, 2000, **113**, 5686–5694.
192. J. A. Platts, *Physical Chemistry Chemical Physics*, 2000, **2**, 973–980.
193. J. A. Platts, *Physical Chemistry Chemical Physics*, 2000, **2**, 3115–3120.
194. K. R. Adam, *Journal of Physical Chemistry A*, 2002, **106**, 11963–11972.
195. M. Mantina , A. C. Chamberlin , R. Valero , C. J. Cramer, D. G. Truhlar, *Journal of Physical Chemistry A*, 2009, **113**, 5806–5812.
196. H.S. Rzepa, “The conformational analysis of cyclo-octane”, <http://www.ch.imperial.ac.uk/rzepa/blog/?p=1603> accessed on 6th August 2013.
197. S. Grimme, C. Mück-Lichtenfeld, G. Erker, G. Kehr, H. Wang, H. Beckers, H. Willner, *Angewandte Chemie International Edition*, 2009, **48**, 2592-2595.

198. J. E. Mills, P. M. Dean, *Journal of Computer Aided Molecular Design*, 1996 **10**, 607-622.
199. I. K. McDonald, J. M. Thornton, *Journal of Molecular Biology*, 1994, **238**, 777–793.
200. M. A. Basharov, *European Biophysics Journal with Biophysics Letters*, 2012, **41**, 53-61.
201. R. A. Davies, N. W. John, J. N. Macdonald and K. H. Hughes, Proc. 10th Int. Conf. Web 3D Tech. '05, 2005, pp. 143–150.
202. R. A. Davies, Proc. EG UK TPCG07, 2007, pp. 243–250.
203. G. Czako, B. C. Shepler, B. J. Braams and J. M. Bowman, *Journal of Chemical Physics*, 2009, **130**, 19.
204. S. Gomez, D. Guerra, J. David and A. Restrepo, *Journal of Molecular Modeling*, 2013, **19**, 2173-2181.
205. K. H. Marti, M. Reiher, *Journal of Computational Chemistry*, 2009, **30**, 2010
206. K. H. Marti, M. Reiher, *Journal of Chemical Physics and Physical Chemistry*, 2011, **12**, 3204
207. S. Comai and D. Mazza, *Technology Enhanced Learning: Quality of Teaching and Educational Reform*, 2010, **73**, 338-344.
208. E. Harvey and C. Gingold, IEEE International Conference on Information Visualisation, London, England, 2000.
209. P. B. Persson, M. D. Coopert, L. A. E. Tibell, S. Ainsworth, A. Ynnerman and B. H. Jonsson, *IEEE Virtual Reality 2007, Proceedings*, 2007, 171-178.
210. G. Sankaranarayanan, S. Weghorst, M. Sanner, A. Gillet and A. Olson, *11th Symposium on Haptic Interfaces for Virtual Environment and Teleoperator Systems - Haptics 2003, Proceedings*, 2003, 363-366.
211. K. J. Schonborn, P. Bivall and L. A. E. Tibell, *Computers & Education*, 2011, **57**, 2095-2105.
212. J. Griffiths, *Colour and Constitution of Organic Molecules*, Academic Press, London, 1976
213. J. B. Foresman and Æ. Frisch, *Exploring Chemistry with Electronic Structure Methods*, 2nd ed. Gaussian, Inc., Pittsburgh, PA, 1996.
214. J. B. Foresman, M. Head-Gordon, J. A. Pople, and M. J. Frisch, *Journal of Physical Chemistry*, 1992, **96**, 135-149.
215. R. Bauernschmitt and R. Ahlrichs, *Chemical Physical Letters*, 1996, **256**, 454-464
216. M. E. Casida, C. Jamorski, K. C. Casida, and D. R. Salahub, *Journal of Chemical Physics*, 1998, **108**, 4439-49.
217. R. E. Stratmann, G. E. Scuseria, and M. J. Frisch, *Journal of Chemical Physics*, 1998, **109** 8218-24.

218. C. Van Caillie and R. D. Amos, *Chemical Physical Letters*, 1992, **308**, 249-55.
219. C. Van Caillie and R. D. Amos, *Chemical Physical Letters*, 2000, **317**, 159-64.
220. F. Furche and R. Ahlrichs, *Journal of Chemical Physics*, 2002 **117**, 7433-47.
221. G. Scalmani, M. J. Frisch, B. Mennucci, J. Tomasi, R. Cammi, and V. Barone, *Journal of Chemical Physics*, 2006, **124**,1-15.
222. R. A. Davies, PhD Thesis, University of Wales, Bangor, 1999
223. Y. Kubo , K. Yoshida , M. Adachi ,S. Nakamura , S. Maeda, *Journal of the American Chemical Society*, 1991, **113**, 2868–2873
224. M. D. Rozeboom, I-M. Tegmo-Larsson, and K. N. Houk, *Journal of Organic Chemistry*, 1981,**46**, 2338-2345
225. D. Jacquemin, J. Preat, V. Wathélet, E. A. Perpète, *Chemical Physics*, 2006, **328**, 324–332
226. I. Singh, R. T. Ogata, R. E. Moore, C. W. J. Chang and P. J. Scheuer, *Tetrahedron*, 1968, **18**, 6053-6073
227. D. Guillaumont, S. Nakamura, *Dyes and Pigments*, 2000, **46**, 85–92
228. S. E. Hughes, R. A. Davies, *unpublished results*

Appendix

I


```

#!/usr/bin/python

#uses system args in next step
import sys
all = ""
data = []
info = []
second_one = False
obtain = False
all_info = ""

#assigning of input arguments
#file name
input = sys.argv[1]
#dihedral angles
D1 = sys.argv[2]
D2 = sys.argv[3]
#output methods
Type = int(sys.argv[4])
Code = int(sys.argv[5])

#initial variables for max, min, difference and multiplication of gradient
mini = 0.0
maxi = 0.0
diffi = 0.0
multi = 1.0

colours = []

#conversion factors
KJ = 2625.5
HA = 1.0
KC = 627.509

points = ""
lines1 = ""
lines2 = ""
triangles = ""
archive = True

#open input file
text_file1 = open(input, 'r').readlines()
print "\nObtaining 'HF=' Values\n"

for line in text_file1:

    if obtain:
        info.append(line.replace("\n",""))
        #dumped into array minus carriage return

    if "Population analysis using the SCF density" in line and second_one :
        obtain = True
        #second time of appearance

    elif "Population analysis using the SCF density" in line:
        second_one = True
        #first time it appears

    if "This type of calculation cannot be archived." in line :
        archive = False
        print "ERROR : The job was not archived, attempting retrieval.\n"
        #error in file

if archive :

```

```

for i in range(0,len(info)):

    all_info =all_info + str(info[i])
    #creates single sting of all information

info = []
#info is cleared

info = all_info.split("\\")
#splitting string at each backslash

all_info =""

for i in range(0,len(info)):

    if "HF=" in info[i]:          #see if HF= in box
        all_info = info[i]

all_info = all_info[3:]
#removes HF=

data = all_info.split(",")
#bit we acutally want in array form

for k in range(0,len(data)):
    if " " in data[k]:
        data[k] = data[k].replace(" ","")
        #remove all white space

else :
    #is no archive

    info = []
    obtain = False

    for line in text_file1:

        if "Summary of Optimized Potential Surface Scan" in line :
            obtain = True
            #finds the table of data

        if "Largest change from initial coordinates is atom" in line :
            obtain = False
            #end of table

        if obtain == True and "Eigenvalues" in line :
            info.append(line.replace("\n",""))
            #takes only hf values

        if obtain == True and "*****" in line :
            print "Retrieval not possible, values in exess of 1000. Exiting procedure."
            exit() #kills program
            #checks for miss print

    for i in range(0,len(info)):

        if "Eigenvalues" in info[i]:

            info[i] = info[i].replace(" Eigenvalues","")
            #removes text

```

```

for i in range(0,len(info)):

    if " " in info[i]:

        info[i] = info[i].replace(" ","")
        #removes whitespace

for i in range(0,len(info)):

    if "--" in info[i]:

        info[i] = info[i].replace("--","")
        #removes divider

for k in range(0,len(info)):
    if "-" in info[k]:
        info[k] = info[k].replace("-","#-")
        #adds splitable item

for i in range(0,len(info)):

    all_info =all_info + str(info[i])
#create single string

info = all_info[1:]
#removal of first #

data = info.split("#")
#split via added charcater

#all if staments ended

print "'HF=' Values are now been sorted\n"

for k in range(0,len(data)):
    if k == 0:
        #first point sets all
        mini = float(data[k])
        maxi = float(data[k])
    else:
        mini = min(mini ,float(data[k]))
        maxi = max(maxi ,float(data[k]))

print maxi

print mini
#prints to terminal

diffi = (maxi - mini) * KJ
#difference in KJ mol-1

multi = 180.0 / diffi
#colour set via height with arbitrary height value

#setting the colours array
for i in range(0,37): #y-coord
    for j in range(0,37): #x-coord
        val = i*37
        if i%2 == 0:
            #even row so forward direction
            var = (float(data[val+j])-mini)/(maxi-mini)
            # pecentage hight from min

```

```

if var <= 0.2:
    colours.append(str(1-(5*var))+ ' 0 1')

elif var > 0.2 and var <= 0.4:
    colours.append('0 '+str(0+(5*(var-0.2)))+ ' 1')

elif var > 0.4 and var <= 0.6:
    colours.append('0 1 '+ str(1-(5*(var-0.4))))

elif var > 0.6 and var <= 0.8:
    colours.append(str(0+(5*(var-0.6)))+ ' 1 0')

elif var > 0.8:
    colours.append('1 '+str(1-(5*(var-0.8)))+ ' 0')

else:
    #reverse direction for odd
    var = (float(data[val+36-j])-mini)/(maxi-mini)
    #move up 36 then minus position

    if var <= 0.2:
        colours.append(str(1-(5*var))+ ' 0 1')

    elif var > 0.2 and var <= 0.4:
        colours.append('0 '+str(0+(5*(var-0.2)))+ ' 1')

    elif var > 0.4 and var <= 0.6:
        colours.append('0 1 '+ str(1-(5*(var-0.4))))

    elif var > 0.6 and var <= 0.8:
        colours.append(str(0+(5*(var-0.6)))+ ' 1 0')

    elif var > 0.8:
        colours.append('1 '+str(1-(5*(var-0.8)))+ ' 0')

#error handling if no input codes given

if Code ==None:
    Code = 0

if Type ==None:
    Type = 0

print "Starting file creation \n"

if Type == 0: #csv output
    if Code == 0:
        print "Creating file output Hartrees\n"
        text_file3 = open(input[0:-4]+"_output_None.csv","w")
        #calls new file imputed file name removing the extention in write mode
        for i in range(0,37): #y-coord
            for j in range(0,37): #x-coord
                val = i*37
                if i%2 == 0:
                    text_file3.write(str(j*10)+" "+str(i*10)+" "+str(data[val+j])+"\n")
                else:
                    text_file3.write(str(j*10)+" "+str(i*10)+" "+str(data[val+36-j])+"\n")
            text_file3.write("\n")
        text_file3.close()

    elif Code == 1:

        for k in range(0,len(data)):
            data[k] = str(( float(data[k])-mini)*HA)

```

```

print "Creating file output relative Hartrees\n"
text_file3 = open(input[0:-4]+"_output_HA_Rel.csv","w")
for i in range(0,37):
    for j in range(0,37):
        val = i*37
        if i%2 == 0:
            text_file3.write(str(j*10)+" "+str(i*10)+" "+str(data[val+j])+"\n")
        else:
            text_file3.write(str(j*10)+" "+str(i*10)+" "+str(data[val+36-j])+"\n")
    text_file3.write("\n")
text_file3.close()

elif Code == 2:

for k in range(0,len(data)):
    data[k] = str(( float(data[k])-mini)*KC)
print "Creating file output relative KCal\n"
text_file3 = open(input[0:-4]+"_output_KCal_Rel.csv","w")
for i in range(0,37):
    for j in range(0,37):
        val = i*37
        if i%2 == 0:
            text_file3.write(str(j*10)+" "+str(i*10)+" "+str(data[val+j])+"\n")
        else:
            text_file3.write(str(j*10)+" "+str(i*10)+" "+str(data[val+36-j])+"\n")
    text_file3.write("\n")
text_file3.close()

elif Code == 3:
for k in range(0,len(data)):
    data[k] = str( (float(data[k])-mini)*KJ)
print "Creating file output relative KJmol\n"
text_file3 = open(input[0:-4]+"_output_KJ_Rel.csv","w")
for i in range(0,37):
    for j in range(0,37):
        val = i*37
        if i%2 == 0:
            text_file3.write(str(j*10)+" "+str(i*10)+" "+str(data[val+j])+"\n")
        else:
            text_file3.write(str(j*10)+" "+str(i*10)+" "+str(data[val+36-j])+"\n")
    text_file3.write("\n")
text_file3.close()

else:
    print "Code Option Selected is not valid\n"
    exit()

elif Type == 1: #.wrl

if Code == 0:#rel kJ
    for k in range(0,len(data)):
        data[k] = str( (float(data[k])-mini)*KJ)

    points = ""
    #write the indented points section of the wrl file
    for i in range(0,37):
        for j in range(0,37):
            val = i*37
            if i%2 == 0:
                points = points + "\t\t\t\t" + str((j*10)-180)+" "+str((i*10)-180)+"
"+str(float(data[val+j])*multi)+"\n"
            else:
                points = points + "\t\t\t\t" + str((j*10)-180)+" "+str((i*10)-180)+"
"+str(float(data[val+36-j])*multi)+"\n"

    points = points[:-2]
    #remove carriage return as \n is not a single character as there is no formatting in python strings

```

```

elif Code == 1:
    for k in range(0,len(data)):
        data[k] = str( (float(data[k])-mini)*KJ)

    points = ""
    for i in range(0,37):
        for j in range(0,37):
            val = i*37
            if i%2 == 0:
                points = points + "\t\t\t\t" + str(j*10-180)+" "+str(i*10-180)+"
"+str(float(data[val+j])*multi)+"\n"
            else:
                points = points + "\t\t\t\t" + str(j*10-180)+" "+str(i*10-180)+"
"+str(float(data[val+36-j])*multi)+"\n"

    points = points[:-2]

    lines1 = "#horisontal"
    lines2 = "#vertical"

    for i in range(0,37):
        val = i*37
        lines1 = lines1 + "\t\t\t\t"
        for j in range(0,37):
            lines1 = lines1 + str(val + j)+" "

        lines1 = lines1 + "-1,\n"

    for i in range(0,37):

        lines2 = lines2 + "\t\t\t\t"
        for j in range(0,37):
            val = j*37
            lines2 = lines2 + str(val + i) + " "

        lines2 = lines2 + "-1,\n"

    lines2 = lines2[:-2]

elif Code == 2:
    for k in range(0,len(data)):
        data[k] = str( (float(data[k])-mini)*KJ)

    points = ""
    for i in range(0,37):
        for j in range(0,37):
            val = i*37
            if i%2 == 0:
                points = points + "\t\t\t\t" + str(j*10-180)+" "+str(i*10-180)+"
"+str(float(data[val+j])*multi)+"\n"
            else:
                points = points + "\t\t\t\t" + str(j*10-180)+" "+str(i*10-180)+"
"+str(float(data[val+36-j])*multi)+"\n"

    points = points[:-2]

    triangles = ""

```

```

        for i in range(0,36):

            for j in range(0,36):#both anti

                triangles = triangles + "\t\t" + str((i*37) + j) + "," + str((i*37) + j + 1) + "," +
str(((i+1)*37) + j) + ",-1,\n"

                triangles = triangles + "\t\t" + str(((i+1)*37) + j + 1) + "," + str(((i+1)*37) + j) + "," +
+ str((i*37) + j+1) + ",-1,\n"

            triangles = triangles[:-2]

        else:
            print "Code Option Selected is not valid\n"
            exit()

#file names and opens file
if Code == 0:
    print "Creating file output points wrl\n"
    text_file3 = open(input[0:-4]+"_output_points.wrl","w")

elif Code == 1:
    print "Creating file output lines wrl\n"
    text_file3 = open(input[0:-4]+"_output_lines.wrl","w")

elif Code == 2:
    print "Creating file output surface wrl\n"
    text_file3 = open(input[0:-4]+"_output_surface.wrl","w")

text_file3.write("#VRML V2.0 utf8\n")
text_file3.write("Background\n")
text_file3.write("{\n")
text_file3.write("\tskyColor 0 0 0\n")
text_file3.write("\tgroundColor 0 0 0\n")
text_file3.write("}\n")
text_file3.write("Shape\n")
text_file3.write("{\n")
text_file3.write("\tappearance Appearance\n")
text_file3.write("\t{\n")
text_file3.write("\t\tmaterial Material\n")
text_file3.write("\t\t{\n")
text_file3.write("\t\t\t#emissiveColor 1.0 1.0 0.0\n")
text_file3.write("\t\t}\n")
text_file3.write("\t}\n")

if Code ==0:
    text_file3.write("\tgeometry PointSet\n")

elif Code == 1:
    text_file3.write("\tgeometry IndexedLineSet\n")

elif Code == 2:
    text_file3.write("\tgeometry IndexedFaceSet\n")

text_file3.write("\t{\n")
text_file3.write("\t\tcoord Coordinate\n")
text_file3.write("\t\t{\n")
text_file3.write("\t\t\tpoint\n")
text_file3.write("\t\t\t{\n")
text_file3.write(points+"\n")
text_file3.write("\t\t\t}\n")
text_file3.write("\t\t}\n")

```

```

if Code == 1 :
    text_file3.write("\t\tcoordIndex\n")
    text_file3.write("\t\t{\n")
    text_file3.write(lines1 + lines2 + "\n")
    text_file3.write("\t\t}\n")

if Code == 2 :
    text_file3.write("\t\tcoordIndex\n")
    text_file3.write("\t\t{\n")
    text_file3.write(triangles + "\n")
    text_file3.write("\t\t}\n")
    text_file3.write("\t\ttsolid FALSE\n")

text_file3.write("\t\tcolor Color\n")
text_file3.write("\t\t{\n")
text_file3.write("\t\t\tcolor\n")
text_file3.write("\t\t\t{\n")
for k in range(0,len(colours)):
    text_file3.write("\t\t\t\t" + str(colours[k])+",\n")
text_file3.write("\t\t\t}\n")
text_file3.write("\t\t}\n")

if Code == 1 :
    text_file3.write("\t\tcolorIndex\n")
    text_file3.write("\t\t{\n")
    text_file3.write(lines1 + lines2 + "\n")
    text_file3.write("\t\t}\n")
    text_file3.write("\t\tcolorPerVertex TRUE\n")

if Code == 2 :
    text_file3.write("\t\tcolorIndex\n")
    text_file3.write("\t\t{\n")
    text_file3.write(triangles + "\n")
    text_file3.write("\t\t}\n")
    text_file3.write("\t\tcolorPerVertex TRUE\n")

text_file3.write("\t}\n")
text_file3.write("}\n")
text_file3.close()

elif Type == 2:

    if Code == 0:
        for k in range(0,len(data)):
            data[k] = str( (float(data[k])-mini)*KJ)

        points = ""
        for i in range(0,37):
            for j in range(0,37):
                val = i*37
                if i%2 == 0:
                    points = points + str((j*10)-180)+" "+str((i*10)-180)+"
"+str(float(data[val+j])*multi)+", "
                else:
                    points = points + str((j*10)-180)+" "+str((i*10)-180)+"
"+str(float(data[val+36-j])*multi)+", "

            points = points[:-1]

        elif Code == 1:
            for k in range(0,len(data)):
                data[k] = str( (float(data[k])-mini)*KJ)

            points = ""

```



```

        for i in range(0,37):
            for j in range(0,37):
                val = i*37
                if i%2 == 0:
                    points = points + str(j*10-180)+" "+str(i*10-180)+"
"+str(float(data[val+j])*multi)+", "
                else:
                    points = points + str(j*10-180)+" "+str(i*10-180)+"
"+str(float(data[val+36-j])*multi)+", "

            points = points[:-1]

            lines1 = ""
            lines2 = ""

            for i in range(0,37):
                val = i*37
                for j in range(0,37):
                    lines1 = lines1 + str(val + j)+" "

                lines1 = lines1 + "-1\n"

            for i in range(0,37):

                for j in range(0,37):
                    val = j*37
                    lines2 = lines2 + str(val + i) + " "

                lines2 = lines2 + "-1"

elif Code == 2 or Code == 3:
    for k in range(0,len(data)):
        data[k] = str( (float(data[k])-mini)*KJ)

    points = ""
    for i in range(0,37):
        for j in range(0,37):
            val = i*37
            if i%2 == 0:
                points = points + str(j*10-180)+" "+str(i*10-180)+"
"+str(float(data[val+j])*multi)+", "
            else:
                points = points + str(j*10-180)+" "+str(i*10-180)+"
"+str(float(data[val+36-j])*multi)+", "

        points = points[:-1]

    triangles = ""

    for i in range(0,36):
        for j in range(0,36):

            triangles = triangles + str((i*37) + j) + " " + str((i*37) + j + 1) + " " + str(((i+1)*37) +
j) + " -1,"

        for j in range(0,36):

            triangles = triangles + str(((i+1)*37) + j + 1) + " " + str(((i+1)*37) + j) + " " +
str((i*37) + j+1) + " -1,"

```

```

        triangles = triangles[:-1]

else:
    print "Code Option Selected is not valid\n"
    exit()

if Code == 0:
    print "Creating file output points x3d\n"
    text_file3 = open(input[0:-4]+"_output_points.x3d","w")

elif Code == 1:
    print "Creating file output lines x3d\n"
    text_file3 = open(input[0:-4]+"_output_lines.x3d","w")

elif Code == 2:
    print "Creating file output surface x3d\n"
    text_file3 = open(input[0:-4]+"_output_surface.x3d","w")

elif Code == 3:
    print "Creating file output surface h3d\n"
    text_file3 = open(input[0:-4]+"_output_haptic_surface.h3d","w")

text_file3.write("<X3D>\n")
text_file3.write("<Scene>\n")
text_file3.write("<Group>\n")
text_file3.write("<Transform scale = '0.05 0.05 0.05' >\n")
text_file3.write("<Group>\n")
text_file3.write("<Transform translation = '-180.0 -180.0 0.0' >\n")
text_file3.write("<Shape DEF = 'Surface'>\n")
if Code == 3 :
    text_file3.write("<Appearance>\n")
    text_file3.write("<SmoothSurface stiffness = '0.2' />\n")
    text_file3.write("</Appearance>\n")
else:
    text_file3.write("<Appearance />\n")

if Code == 0:

    text_file3.write("<PointSet>\n")
    text_file3.write("<Color color = """)
    for k in range(0,len(colours)-1):
        text_file3.write(str(colours[k])+",")
    text_file3.write(str(colours[len(colours)-1])+"" />\n")

    text_file3.write("<Coordinate point = \n")
    text_file3.write(points+" ' />\n")
    text_file3.write("</PointSet>\n")

elif Code == 1:

    text_file3.write("<IndexedLineSet coordIndex = ' "+lines1 + lines2 +" ' colorPerVertex = 'true'
containerField = 'geometry' >\n")
    text_file3.write("<Coordinate point = \n")
    text_file3.write(points+" ' />\n")

    text_file3.write("<Color color = """)
    for k in range(0,len(colours)-1):
        text_file3.write(str(colours[k])+",")
    text_file3.write(str(colours[len(colours)-1])+"" />\n")
    text_file3.write("</IndexedLineSet>\n")

elif Code == 2 or Code == 3:

    text_file3.write("<IndexedFaceSet coordIndex = ' "+ triangles +" ' colorPerVertex = 'true'
normalPerVertex = 'true' solid ='false' ccw ='true' containerField = 'geometry' >\n")

```

```
text_file3.write("<Coordinate point = '\n")
text_file3.write(points+" ' />\n")
```

```
text_file3.write("<Color color = ""
for k in range(0,len(colours)-1):
    text_file3.write(str(colours[k])+",")
text_file3.write(str(colours[len(colours)-1])+" ' />\n")
text_file3.write("</IndexedFaceSet>\n")
```

```
text_file3.write("</Shape>\n")
text_file3.write("</Transform>\n")
text_file3.write("<Transform translation = '-180.0 180.0 0.0' >\n")
text_file3.write("<Shape USE = 'Surface' />\n")
text_file3.write("</Transform>\n")
text_file3.write("<Transform translation = '180.0 -180.0 0.0' >\n")
text_file3.write("<Shape USE = 'Surface' />\n")
text_file3.write("</Transform>\n")
text_file3.write("<Transform translation = '180.0 180.0 0.0' >\n")
text_file3.write("<Shape USE = 'Surface' />\n")
text_file3.write("</Transform>\n")
text_file3.write("</Group>\n")
text_file3.write("</Transform>\n")
text_file3.write("</Group>\n")
text_file3.write("</Scene>\n")
text_file3.write("</X3D>\n")
```

```
text_file3.close()
print "File creation complete\n"
```